Silvia Weigand, BSc

Petrological investigation of the Surna Nappe, Scandinavian Caledonides, Sør-Trøndelag, Norway

Mastes's Thesis

Thesis prepared for the degree of
Master of Science

submitted at

Graz University of Technology

Supervisor

Ao.Univ.-Prof. Mag. Dr.rer.nat., Christoph Hauzenberger

NAWI Graz Geozentrum
Petrology & Geochemistry

Graz, September 2016

STATUTORY DECLERATION

I declare that I have authored this thesis independently, that I have not used other than the declared sources/resources, and that I have explicitly marked all material which has been quoted either literally or by content from the used source. The file uploaded in TUGRAZonline is identically with the here presented Master's thesis.

_____ _____

Date Signature

…for my parents

and Rasputin…

DANKSAGUNG

An dieser Stelle möchte ich mich bei all jenen bedanken die mich während meines Studiums begleitet und unterstützt haben, und zum Gelingen der hier vorliegenden Arbeit beigetragen haben.

Mein größter Dank gilt meinen Betreuern, einerseits Christoph Hauzenberger (Karl-Franzens-Universität Graz) welcher mir bei jeglichen petrologischen und analytischen Fragenstellungen eine große Unterstützung war, und Deta Gasser (Geological Survey of Norway) für Anliegen in Bezug auf Regionale Geologie, Geländearbeit und Interpretation.

Karl Ettinger und Jürgen Neubauer und seien ebenfalls an dieser Stelle erwähnt für ihre Betreuung an der Mikrosonde und Rasterelektronenmikroskop.

Ganz besonders möchte ich mich bei meinen Studienkollegen, insbesondere Philip, Christian, Dominik, Fede, Simon, Sara, Isa, Doria, Marlene, Anna, Kathi, Karin, Dragan, Sebastian und Ruth bedanken für die unzähligen Stunden des gemeinsamen Lernens und diskutieren und der wahrscheinlich besten Zeit des Lebens. Außerdem Corni, Tina und Seema für ihre unendliche Geduld und ihren nie aufhörenden Glauben an mich.

Zu guter Letzt möchte ich mich bei meinen Eltern, meiner Familie und Lore bedanken, die während meiner gesamten Studienzeit immer hinter mir standen und mich in jeder Lebenslage unterstützt haben. Danke.

Table of Content

ABSTRACT

The Seve Nappe Complex, mainly outcropping and investigated in Sweden, comprises relics of Ordovician HP and UHP metamorphic rocks, which were overprinted by upper amphibolite facies metamorphism and anataxis during the Silurian. In Norway, in the hinterland of the Caledonian orogen, rocks of the Surna and Blåhø nappes are generally correlated with the Seve Nappe Complex. However, no detailed metamorphic studies are available from these units, in order to compare them with the Seve Nappe Complex. The Surna and Blåhø nappes are located between the oceanic–derived Støren nappe and the continentally-derived Sætra nappe. Due to a strong post-Caledonian extensional and transtensional overprint and the close proximity to the MTFC (Møre-Trøndelag Fault Complex, a prominent post-Caledonian strike-slip fault complex), investigations of the early metamorphic history of the Surna and Blåhø nappes are challenging. In this contribution we present the results of a petrological and geochemical study of the Surna Nappe, from a ca. 10 km wide transect across this nappe west of Trondheim in Norway. The unit is lithologically very heterogenous, comprising of garnet – amphibole - mica-schists, garnet-quartz mica-schists, amphibolites with tonalitic layers, calc-silicates rocks, as well as pegmatites. Geochemically whole rock compositions vary from ultrabasic to acidic, but a clear distinction between metavolcanic and metasedimentary origin of the lithologies is not always straightforward. Garnet occurs in several lithologies and is used along with clinopyroxene, plagioclase and biotite for conventional geothermobarometry. Additionally, Zr-in-rutile, garnet-biotite and garnet-amphibole thermometers were applied. PT calculations from 25 different samples reveal PT conditions of 10 to 16 kbar and 600 to 700°C. The elevated phengite content in muscovite (Si up to 3.28 p.f.u.) in a few samples may indicate a high pressure evolution of these rocks. Garnet zoning patterns and results from thermodynamic modeling indicate a regional metamorphic prograde PT path reaching upper amphibolite to lower eclogite facies conditions. While no typical eclogite facies mineral assemblages in investigated metabasic rocks from the Surna Nappe are found, PT calculations from more intermediate and acidic lithologies however indicate that they have experienced elevated pressures up to lower eclogite facies conditions at some point, supporting the possible correlation with rocks of the less - overprinted Seve Nappe Complex in Sweden.

Keywords: Caledonides, Surna Nappe, Seve Nappe Complex, Eclogitefacies

KURZFASSUNG

Der Seve Nappe Complex ist primär in Schweden aufgeschlossen und untersucht und besteht aus Relikten von ordovizischen HP und UHP Gesteine welche amphibolitfaziell überprägt wurden und im Silur eine Migmatisierung erlebten. In Norwegen, im Hinterland des kaledonischen Orogens werden die Gesteine der Surna und Blahø Decke mit dem Seve Nappe Complex korreliert. Jedoch existiert keine detaillierte metamorphe Untersuchung dieser Einheiten um eine eindeutige Zuordnung zum Seve Nappe Complex treffen zu können.

Die Surna und Blahø Decke liegen zwischen der ozeanisch Støren Decke und der kontinentalen Sætra Decke. Durch eine post-kaledonische extensionale und transtensionale Überprägung und durch die Nähe zur MTFC (Møre-Trøndelag Fault Complex, ein post-kaledonischer strike-slip Fault Complex) sind Untersuchungen der frühen metamorphen Geschichte der Surna und Blahø Decke anspruchsvoll.

Die vorliegende Arbeit präsentiert eine petrologische und geochemische Studie über die Surna Decke, westlich von Trondheim, Norwegen. Die lithologisch stark heterogene Decke besteht aus Granat-Hornblende Glimmerschiefer, Granat-Quarz Glimmerschiefer, Amphiboliten mit tonalitischen Lagen, kalksilikatischen Gesteinen und Pegmatiten. Geochemisch variiert die Zusammensetzung von ultrabasisch zu sauer und eine Unterscheidung von metavulkanischen und metasedimentären Ursprungs der Gesteine ist nicht eindeutig. Granat kommt in fast allen Lithologien vor, und wurde mit Plagioklas, Clinopyroxen und Glimmer mittels konventioneller Geobarometrie für eine Druckabschätzung herangezogen. Außerdem wurde mittels Granat-Biotit, Zr-in-Rutil und Granat-Amphibole Geothermometern eine Temperaturevaluierung von insgesamt 25 unterschiedlichen Proben durchgeführt. Die Ergebnisse liegen zwischen 10 – 16 kbar und 600 – 700 °C. Erhöhte Phengitegehalte in Hellglimmern (Si 3.28/11O) weisen auf eine eventuelle Hochdruck Entwicklung der Gesteine hin. Granatprofile und thermodynamische Modellierung ausgewählter Proben zeigen einen prograden PT Pfad mit peak Bedingungen welche der unteren Eklogitfazies entsprechen. Diese Ergebnisse der hier vorliegenden Arbeit sprechen aufgrund der ähnlichen metamorphen Geschichte für eine Korrelation der Surna Decke mit dem Seve Nappe Complex.

INTRODUCTION

The widely accepted division of the Scandinavian Caledonides into four allochthons by Gee et al., 1985 was a useful tool over the past decades for understanding this complex, far-traveled, laterally wide ranging, Paleozoic orogen and its Archaean and Proterozoic footwall units. Since the investigation and analytical methods progressed, this simple and rigid model became impractical (Corfu et al., 2014). Since the Caledonian nappe pile is better preserved in the Swedish part of the Caledonides, the focus of research was concentrated there. In the hinterland within Norway, these nappes are thinned out, and highly deformed and overprinted by strike-slip and extensional tectonics related to the post-Caledonian Møre-Trøndelag Fault Complex (MTFC), the Høybakken detachment and the opening of the Atlantic Ocean (see Figure 1). Consequently, the lithological, structural, petrological and geochronological evolution of the Norwegian Caledonian nappes and their relation to the Caledonian nappe pile in Sweden is far from completely understood.

This work presents a petrological and geochemical study of the Surna Nappe, located in Sør-Trøndelag, Norway, where lithological, structural and tectonostratigraphic knowledge is present, but yet lacks in petrological, geochemical and geochronological information (Gee et al., 1985). Consequently, there is a lack of understanding if the Surna Nappe can be correlated with the far better known Seve Nappe Complex in Sweden.

Due to the position of the Surna Nappe between the oceanic Støren Nappe and the continental Sætra Nappe, a correlation to the Seve Nappe Complex is favored (see Figure 1). Also the similar lithologies, such as high-grade mica schists, amphibolite and foliated pegmatitic felsic veins, which were found in both units, suggest a relationship (Grimmer et al., 2015; Roberts & Gee, 1985 & Kontny et al., 2012). However high-pressure rocks as found in the Seve Nappe Complex (described by Andréasson et al., 1985, Kolnowska et al., 2013 and Majka et al., 2013) are so far not described from the Surna Nappe.

This study presents a detailed petrological and geochemical investigation of the Surna Nappe, in order to contribute to the ongoing understanding of the geodynamic evolution of the Norwegian part of the Caledonides. Therefore, a combination of analytical methods such as conventional geothermobarometry, a detailed geochemical data set of major and trace elements and thermodynamic modelling were used to reconstruct the metamorphic history of the Surna Nappe.

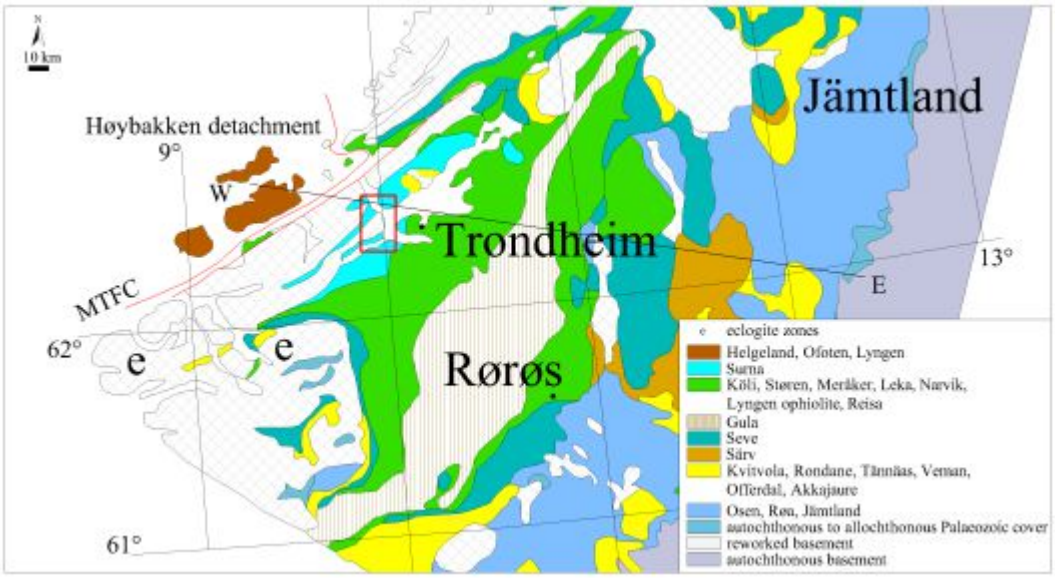

Figure 1 Geological map showing the southern part of the Central Segment within the Caledonian orogen (modified after Corfu et al., 2014). The study area is indicated by a red rectangle, with the corresponding cross-section after Gee et al., 2010 (see **Figure 4**).

GEOLOGICAL BACKGROUND

The Scandinavian Caledonides

The Scandinavian Caledonides are subject of research since many decades, and extend for about 1800 km from north to south and vary up to 300 km in width (Figure 2). They are the product of a continent-continent collision that occurred in the Paleozoic, resulting in the formation of many thrust complexes, of which the higher ones show several hundred kilometers of displacement (Gee et al., 1985, Roberts & Gee, 1985 and Roberts 2003). Gee et al., 1985 introduced a widely used and accepted subdivision of the entire orogeny into four major allochthon complexes: the Lower, Middle, Upper and Uppermost Allochthons. Subjacent to these, there are parautochthonous units and an autochthonous sedimentary cover overlaying Archaean and Proterozoic crystalline rocks of the Fennoscandian Shield (Roberts, 2003). The Lower and Middle Allochthons are correlated with Baltoscandian Platform and margin successions, which were deposited in the Late Proterozoic and Early Paleozoic. These greenschist facies continental and shelf rise successions also contain slivers of crystalline basement. Superimposed, the Upper Allochthon consists mainly of low grade volcanics and volcano-clastic sedimentary rocks derived from island-arc, back-arc and fore arc ocean floor settings from within the Iapetus ocean (Gee et al., 1985, Roberts, 2003). The Uppermost Allochthon is primary composed of rocks derived from the Laurentia margin (Stephens & Gee, 1985, Roberts et al., 2007).

Since its introduction, the simple model of four major allochthons has received revisions and critics. One of the major modifications, suggested by Andréasson & Gee, 2008, was the reassignment of the Seve Nappe Complex of Sweden to the Middle Allochthon, instead of the Upper Allochthon. The original assignment was based on the essentially different metamorphic grade of the Seve Nappe Complex (then Upper Allochthon) from the subjacent Svärv Nappes of the Middle Allochthon. However, the Köli Nappe Complex overlaying the Seve Nappe Complex also shows a markedly different metamorphic grade compared to the Seve Nappe Complex, (e.g., Roberts & Stephens 2000), and is assumed to have an exotic origin from the Iapetus ocean, including fossil evidence pointing towards an origin of at least parts of these nappes close to the Laurentian margin (Robinson & Roberts, 2008).Therefore, the Seve Nappe Complex seems to have a particular history different from the under- and overlaying units.

In addition to these uncertainties regarding the affinity of major nappe complexes to one or the other allochthon, the simple allochthon model does not account for the complex setting

of passive margins, the presence of microcontinents and volcanic or non-volcanic margins. The involved Baltica, Iapetus and Laurentia terranes seem to be insufficient to describe the wide-ranging sources of the different nappe systems (Corfu et al., 2014a). Evidence for the presence of more than the former mentioned terranes is given for instance by Cocks & Torsvik, 2002, who demonstrate that the Caledonian margin of Baltica probably moved from high southern latitude (~60°) in the Late Neoproterozoic to an equatorial position in the Silurian, when united Baltica- Avalonia collided with Laurentia. The indicated travel path gives various opportunities for Baltica to face and capture different elements of Siberia-, Gondwana- and or ocean derived units and also a possible counter-clockwise rotation. The model became too rigid for an 1800 km long orogen with along - strike variations and does not consider polyphase deformation and out-of-sequence thrusting (Corfu et al., 2014). Due to the aforementioned reasons Corfu et al., 2014 separated the orogen into three different segments: the southern, central and northern segments with each its characteristics (see Figure 3Figure 2).

The central segment (see Figure 3) is of special interest for the current thesis, since a cross-section from Jämtland (Sweden) in the east, to Trøndelag (Norway) in the west, shows a nearly complete section through the Caledonian tectonostratigraphy (see Figure 4). In general, all tectonic units are thicker and better preserved in the eastern Swedish parts, and thin or wedge-out westwards, in Trøndelag, Norway (Gee et al., 1985). Additionally, the NE-SW-trending Møre-Trøndelag Fault Complex (MTFC) has a crucial geometrical influence in the Trondheim region, overprinting earlier thrust geometries (Corfu et al., 2014, Seranne 1992, Osmunden et al., 2006). One key task therefore is to trace the better-known Swedish tectonostratigraphy into the more heavily overprinted hinterland of the orogeny in Trøndelag (Robinson et al., 2008, Gee et al., 2010). Since the Seve Nappe Complex and correlative units are the topic of the current work, they are described in more detail in the following.

The Seve Nappe Complex in Sweden

Roberts & Gee, 1985 described the Seve Nappe Complex and correlatives as basal units of the Upper Allochthon, containing high-grade psammitic schists, gneisses, amphibolites and migmatites. In some localities, there are retrograde eclogites present (Andréasson et al., 1985, Kolnowska et al., 2013, Majka et al., 2013, Brueckner & Roermund, 2004). Rb-Sr and U-Pb ages revealed a complex evolution and indicate early Caledonian ages for this high grade metamorphism (Reymer et al., 1980, Claesson, 1981, Root & Corfu 2012).

In the Jämtland-Västerbotten region the Seve Nappe Complex is subdivided into Lower, Middle and Upper Seve nappes (Grimmer et al., 2015). The Upper Seve nappe is composed of a several hundred meters thick mylonitic garnet mica schist succession with interbedded amphibolites and ultramafic rocks (Kontny et al., 2012). Additionally, foliated pegmatitic felsic veins, up to 0.5m thick, can be followed along strike as foliation-parallel beds in mica schists and amphibolites (Grimmer et al., 2015). The Middle Seve nappe is made up of garnet-kyanite mica schists and of pyroxene-garnet bearing metabasites and migmatites (Brueckner & van Roermund, 2007, Majka et al., 2014). Root & Corfu, 2012 dated two discrete high-pressure metamorphic events of Ordovician age (482 $\pm$ 1 Ma respectively 446 $\pm$ 1 Ma) both on eclogites with corresponding P/T conditions of 25 kbar/ 650 – 700 °C by Majka et al., 2013. Felsic segregations with a migmatitic amphibolite crystallized at 436 $\pm$ 2 Ma. Pegmatites cross-cutting a prevalent Caledonian foliation yield 428 - 430 Ma (Ladenberger et al., 2013). Grimmer et al., 2015 presented evidence for a Silurian extrusions wedge with mantle rooted shear zones in the Swedish part of Scandianvian Caledonides, indicating an early stage of exhumation of (U)HP rocks.

Potential correlative of the Seve Nappe Complex in Norway: the Surna Nappe west of Trondheim

There are several occurrences of similar rocks in the hinterland of Norway that have been correlated with the Seve Nappe Complex (e.g. Figure 3). One of these occurrences is located west of Trondheim city in South-Trøndelag county and is the topic of this thesis (see Figure 1).

Peacey, 1963 did some initial petrological and deformation-history studies in the area investigated in this thesis, which has been correlated with the Seve Nappe Complex based on lithological similarities and tectonostratigraphic position (Gee et al. 1985, Corfu et al. 2014). The name Gangåsvann Group was introduced, and a short characterization of the lithology was given, in particular garnet-hornblende-mica schists with sheets or lenses of trondhjemite were described. The name was adopted by Johnsen, 1979 who did slight modifications in the regional mapping and tectonostratigraphic classifications. His Sjuråsen and Gangåsvann Groups consist mainly of mica schists and amphibolites. The major lithology Johnsen, 1979 described is garnet-biotite schist containing quartz, feldspar, biotite and porphyroblastic garnets. The

amphibolites were described as nearly black, fine-grained and with a pronounced schistosity. They also contain epidote, garnet, biotite and chlorite.

Krill, 1985 was the first one who defined the Surna Nappe, overlying the Blåhø Nappe in the northern Oppdal district. The main difference between the Blåhø and Surna nappes is the common presence of trondhjemite intrusions in the latter, which cut an early schistosity in amphibolite and schist of the Surna Nappe (Krill, 1985, Johnsen, 1979). Finally, Kollung, 1990 assigned the rocks of the Sjuråsen and Gangåsvann Groups to the Surna Nappe. Already Gee et al., 1985, and later Robinson & Roberts, 2008 and Corfu et al., 2014 correlated the various mica schist units (Blåhø, Surna, Skjøtingen Nappe) in the Norwegian Caledonides on a bigger scale with the Seve Nappe Complex. Robinson & Roberts, 2008 described a representative outcrop from the Surna Nappe as consisting of metamorphic rocks with a south-dipping foliation, composed of garnet – amphibolite, diopside – epidote amphibolite. An early tectonic foliation is cut by deformed pegmatites. The pegmatites probably belong to the same group of pegmatites which Trucker et al., 2004 dated to 431 ±2.9 Ma and 422 ±1.8 Ma, respectively. The results suggest that the peak high- grade metamorphism of the Surna Nappe occurred before ca. 430 Ma, 25 – 30 m.y. before peak Scandian metamorphism of the subadjacent basement at 400 – 395 Ma (Robinson & Roberts, 2008). Hacker & Gans, 2005 published a not well-documented P/T estimate from a sample of the Surna Nappe indicating 9 kbar/625 °C and a $^{40}Ar/^{39}Ar$ muscovite cooling age of 404 Ma.

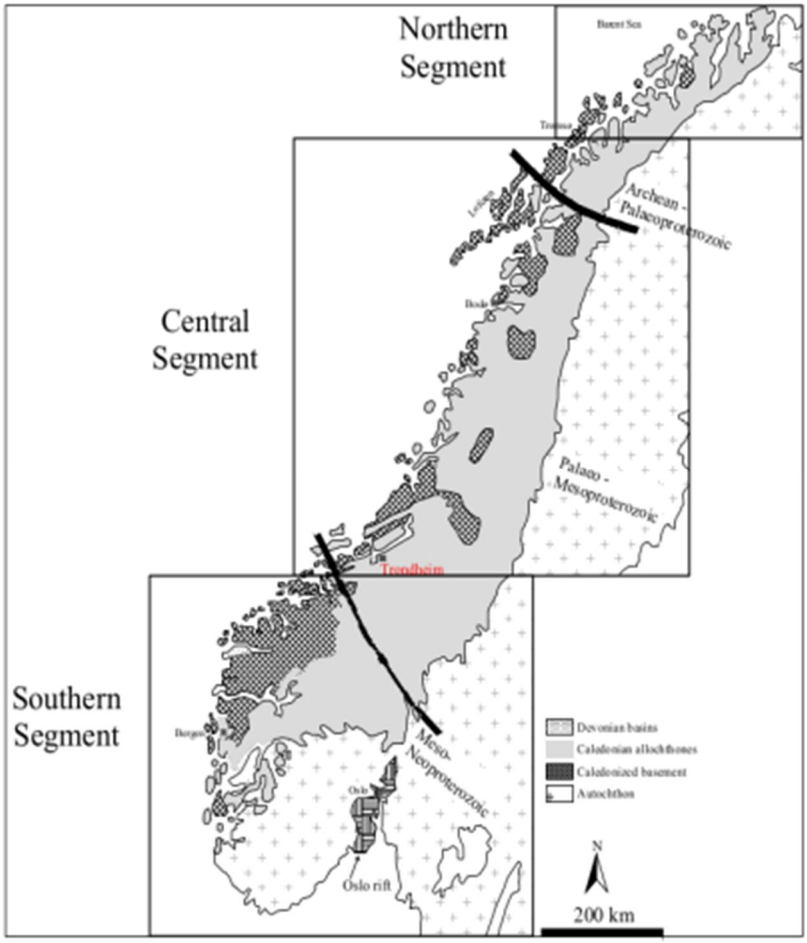

Figure 2 Simplified tectonostraigraphic map of Scandinavian Caledonides after Gee et al., 1985, with alternative subdivision after Corfu et al., 2014.

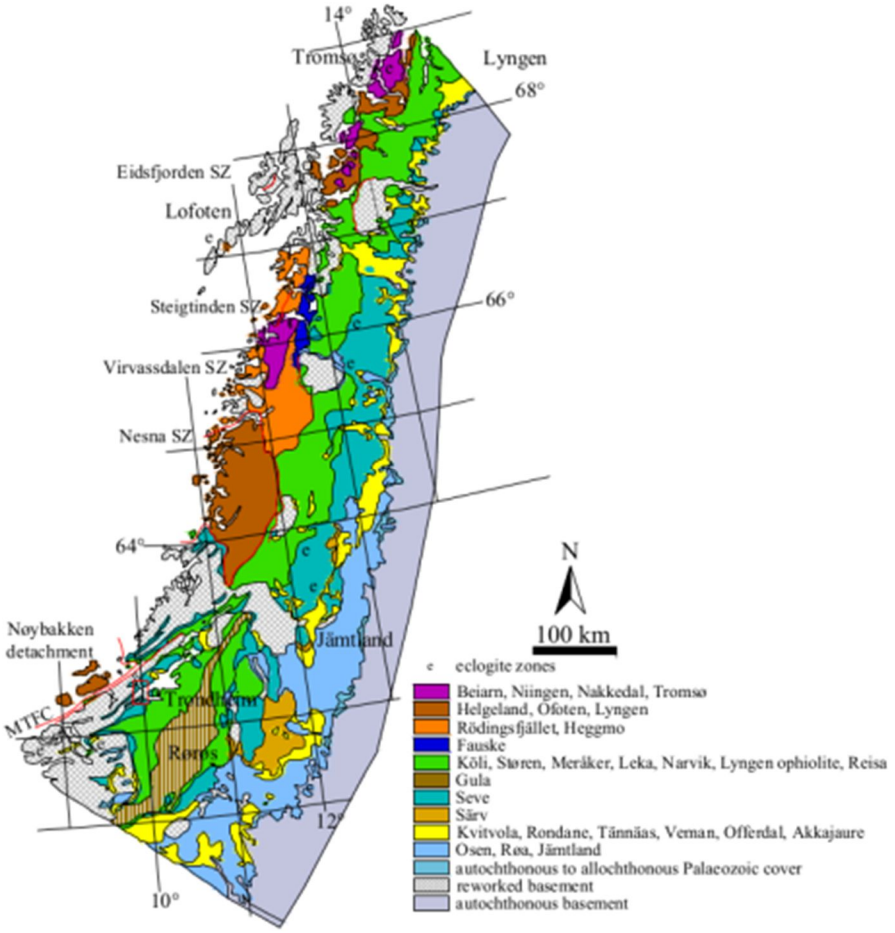

Figure 3 Geological framework of the southern part of central segment after Corfu et al., 2014, adapted from Gee et al., 1985. The red box west of Trondheim corresponds to the study area. Corfu et al., 2014 stated the latter on a bigger scale as part of Seve Nappe Complex. MTFC Møre Trøndelag fault complex, SZ shear zone.

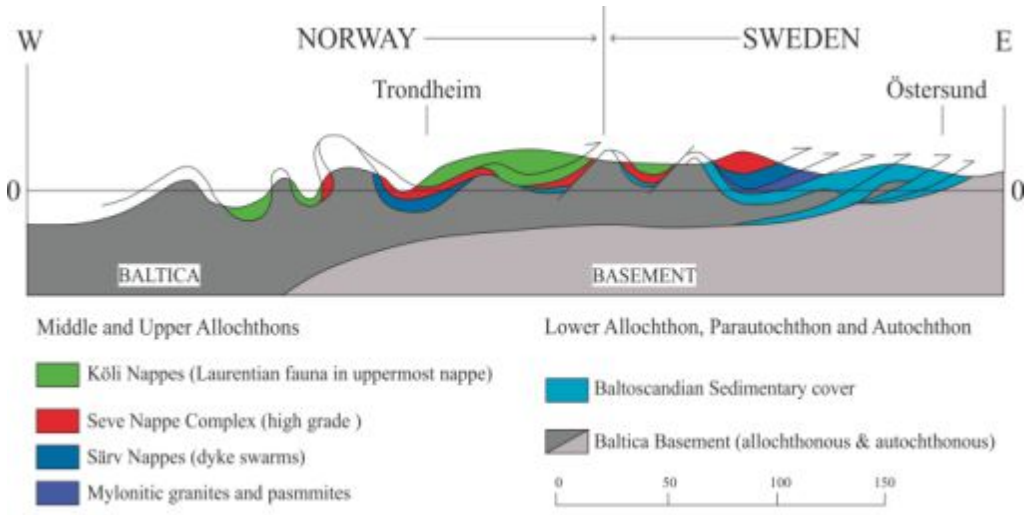

Figure 4 Schematic cross section through the Central Scandinvian Caledonides, after Gee et al., 2010. Vertical exaggeration times five, for profile location see **Figure 1**.

METHODS

Fieldwork was conducted in autumn 2014, in order to collect representative samples for further petrological analysis. 82 samples were collected in the field. In addition, 23 samples were provided by the Geological Survey of Norway (NGU), collected in 2012 and 2013, resulting in 105 hand pieces in total.

Electron microprobe and scanning electron analysis

All samples were prepared as polished thin sections and then investigated by a combination of transmitted and reflected light microscopy. At the University of Graz (Austria), Department of Petrology and Geochemistry, quantitative mineral chemical analyses were performed on representative carbon coated thin sections, using a JEOL-JSM-6310 scanning electron microscope equipped with a LINK ISIS energy dispersive system (measurement time for energy dispersive elements 100 sec), and a MICROSPEC wavelength dispersive system (measurement time for wavelength dispersive elements 20 sec on peak position, and 10 sec/10 sec on background), University of Graz (Austria) at the Institute of Earth Science (for used standards see Table 1). In addition, quantitative analyses and 2D chemical mappings were performed with a JEOL JXA-8200 electron microprobe at the UZAG EUGEN F. STUMPFL Electron Microprobe Laboratory (University of Leoben, University of Graz, and Graz University of Technology). For used standards see Table 2. The measurement time on the peak position of elements was 20 seconds and 10 seconds / 10 seconds on the background. Measuring conditions for both devices were 15 kV acceleration voltage and ~ 6 (SEM) and 12 (EPMA) nA beam current, with ~ 1 µm beam diameter. Mineral formulas were calculated with the program PET (Petrological Elementary Tool), version 7 (Dachs, 1998). Mineral abbreviations were used after Whitney & Evans, 2001.

Conventional geothermobarometry

Selected mineral compositions were calculated with the program PET (Petrological Elementary Tool), version 7 (Dachs, 1998), and the multi-equilibrium application winTWQ by Berman, 1991, version 2.3, database version 2.32 (DEC06.DAT for mineral data and DEC06.SLN for mineral solution data). Samples containing amphibole, version 1.02 of winTWQ was used (JUN92.GSC, JUN9.SLN).

Whole rock analysis and thermodynamic modelling

For whole rock composition approximately 100 g of 69 samples were crushed and prepared as fused glass disks (1.0 gr sample + 7.0 gr di-Lithiumtetraborate). Major and trace elements were determined by using the wavelength dispersive fluorescence spectrometer (WDXRF) Bruker Pioneer S4, at Institute of Earth Science, University of Graz (Austria). Whole rock data was plotted and processed by using the R language software package GCDkit (Geochemial Data Toolkit) version 3 (Janoušek et al., 2013). Thermodynamic phase equilibrium calculations were performed with the program Perplex_X by Connolly, 2005 version 6.7.3, with the revised hp04ver.dat thermodynamic dataset from Holland & Powell, 1998.

Table 1 Standards for SEM analysis.

Element	Standard	Location	Source/donor	Reference
K, Si, Al	Adular		Naturhistorisches Museum Vienna	
Ca, Ti	Titanite	Rundner Oberland	Collection, ETH-Zürich	Wark 1998 (SBMQ)
Mn	Rhodonite		Evans	
Fe, Mg	Garnet (Pyrope-Almandine)	Gore Mountain, Adirondaks, New York	U.C. Berkeley (S.E. Evans)	Levin, GSA Bull, 1960, 519-565
Cr	Chromite		U.S. Geol. Survey	Analyst J.J. Dinnin
Na, Al, Si: for Pap	Albite		Naturhistorisches Museum Vienna	
Na for Cpx	Jadeite	Clear Creek, California		G. Ernst
Si, Al: for Garnet	Almandine	Southern France		European Journal of Mineralogy 1995, 7, 187-96
Cl	Anacamite		Naturhistorisches Museum Vienna	
F	synthetic F-Phlogopite		Bucher Basel	Analyst Evans

Table 2 Standards for EPMA analysis.

Element	Standard	Location	Source/donor	Reference
Na, Al, Si	Albite			
Cl	Anatomite		Collection of the Naturhistorisches Museum Vienna	
	Tychite	Danbury Mine, San Benito Co, California	U. C. Berkeley Collection (B. Evans)	Frondel and Ito 1957 Bull Dep Geol U Col Vol. 5, p. 149-153 and 331-381
Cr	Chromite (Cr-Al-Si)		U.S. Geol. Survey	Analyst J.J. Dinnin
Mg, Fe, Si, Al	Garnet (Pyrope-Almandine)	Gore Mountain, Adirondaks, New York	U. C. Berkeley (S.E. Evans)	Levin, GSA Bull, 1960, 519-565
Si, Ca, Mg	Diopside		Ingersoll	Analyst Ingersoll
F, K, Mg	synthetic F-Phlogopite		Bucher-Basel	Analyst Evans
Mn	Rhodonite		Evans	
Fe, Al, Mg, Si	Almandine		New York State, USA	
Ba, Ba	Sanidin	Hohenfels, Germany		
Ti	Rutile		Atomergic Chemicals Corp., USA	
Zr	Cubic Zirconia			
F	F-Topaz	Schneckstein		
Ca	Plagioclase			
Cr, Ni, Fe	Mn-Cr-Ni			
Na	Jadeite	China		

FIELD SETTING

The majority of samples presented in this study were collected from the Surna Nappe, located in the communities of Skaun and Orkdal, Sør-Trøndelag (Norway). The sample area is predominately situated along Trondheimsfjord respectively Orkdalsfjord, and extents from Furuvik in the east to Orkdal in the west and south, and Trongen in the north. The entire region is dominated by upright folds, which become thinner towards NW. The Surna Nappe is characterized by a flat extensional foliation. 105 hand pieces were sampled from six different lithologies. Figure 5 illustrates sample locations, Appendix A & Appendix B provide information on GPS coordinates of sampled localites, as well as a petrographic summary on investigated samples. Sample which have been investigated by the scanning electron microscope or the electron microprobe are shown in Figure 6. N.d. is designated for not determined and b.d.l. for below detection limit in the following.

The Surna Nappe is composed of (a) garnet – hornblende – mica schist, (b) garnet – quartz - mica schist, (c) amphibolite, (d) tonalitic layer (e) calc-silicate rock and (f) pegmatite:

(a) The major lithology present in the Surna Nappe is garnet – hornblende – mica schist. These rocks appear as fresh, blocky, dark grey, fine - grained and weakly to strongly foliated schists (see Figure 7A). Macroscopic red garnets are resistant to weathering and sometimes accumulate in quartz - and feldspar - rich domains or roddings, but also in the mafic groundmass (see Figure 7B & C). The size of garnet is ranging from 2 mm to 20 mm. Beside garnet, clinozoisute also forms large crystals, up to 2 mm in size.

(b) Garnet - quartz - mica schist is found close to the Støren Nappe in the east, and also in the proximity of the Sætra Nappe in the west. Garnet, muscovite and biotite are the main constituents, whereas amphibole is rarely present. Due to the high aboundance of garnet in certain samples (14SW04, 14SW05, 14SW06, 14SW16) some of these rocks can be defined as garnet- mica fels.

(c) Two different types of amphibolite are observed: fine-grained microcrystalline amphibolitic schist (type I) found in the vicinity of the Støren Nappe, and as coarse-grained amphibole gneiss (type II). Both are dark grey with macroscopic red irregular garnets scattered in the second type (see Figure 14B). In the field amphibolite is characterized by the occurrence of concordant

tonalitic layers (see ad (d)) with diffuse contacts (see Figure 14A), and pegmatites forming boudins (see (f)).

(d) Tonalitic layers with a thickness of up to 2m are parallel to the foliation of their host amphibolite (see Figure 18A & B). They are fine-grained, and can be distinguished in the field by their variations in greyscale color.

(e) Calc-silicate rock is rare and occurs in layers of up to 1m in thickness. These greenish and white rocks with a granoblastic fabric have macroscopic garnets and clinopyroxene.

(f) Pegmatite is found in amphibolite and garnet – hornblende mica schist throughout the Surna Nappe. They mainly occur in boudins, and also cut an older fabric. The thickness varies from approximately 0.1 m to 3 m (see Figure 25A).

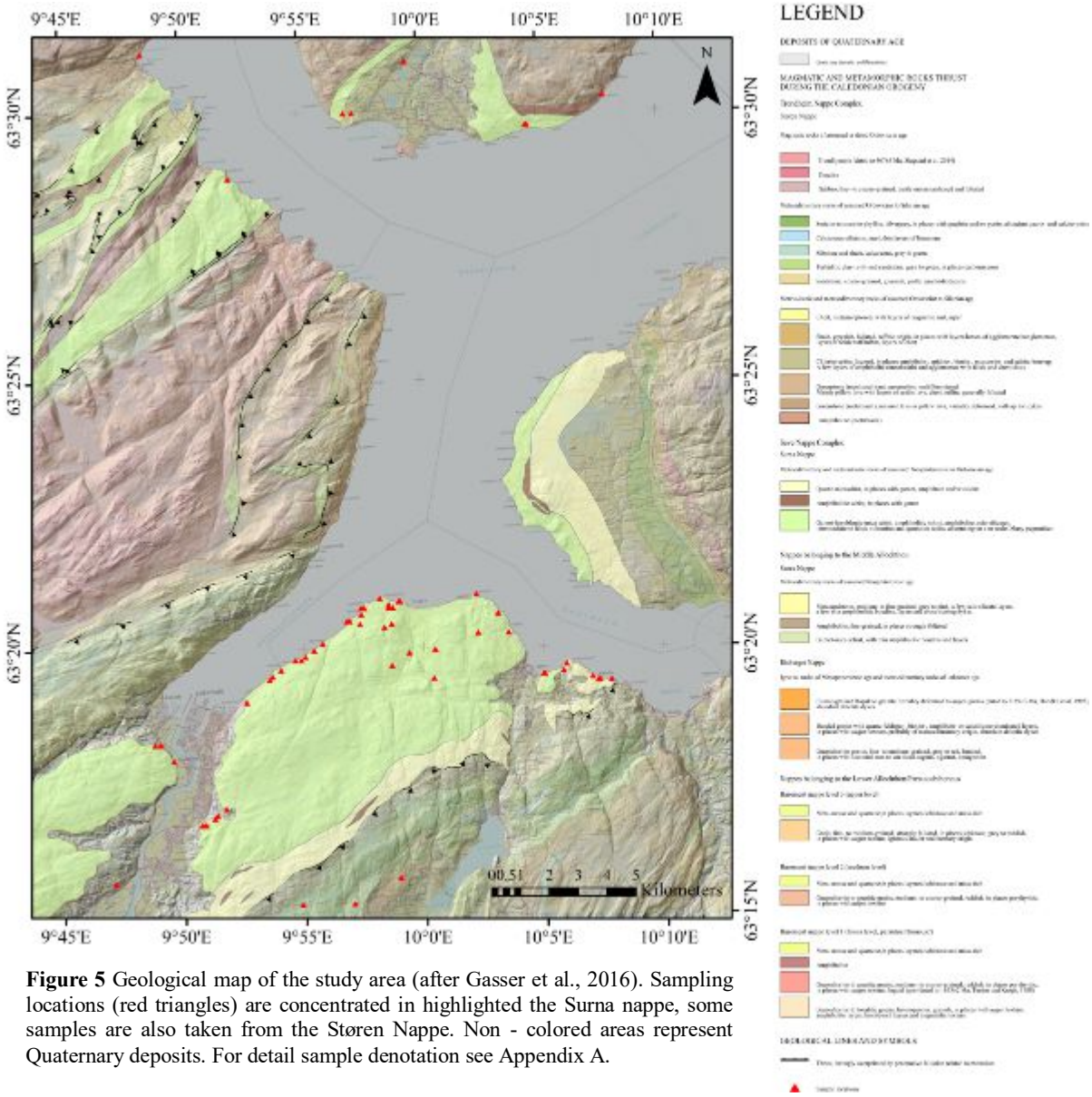

Figure 5 Geological map of the study area (after Gasser et al., 2016). Sampling locations (red triangles) are concentrated in highlighted the Surna nappe, some samples are also taken from the Støren Nappe. Non - colored areas represent Quaternary deposits. For detail sample denotation see Appendix A.

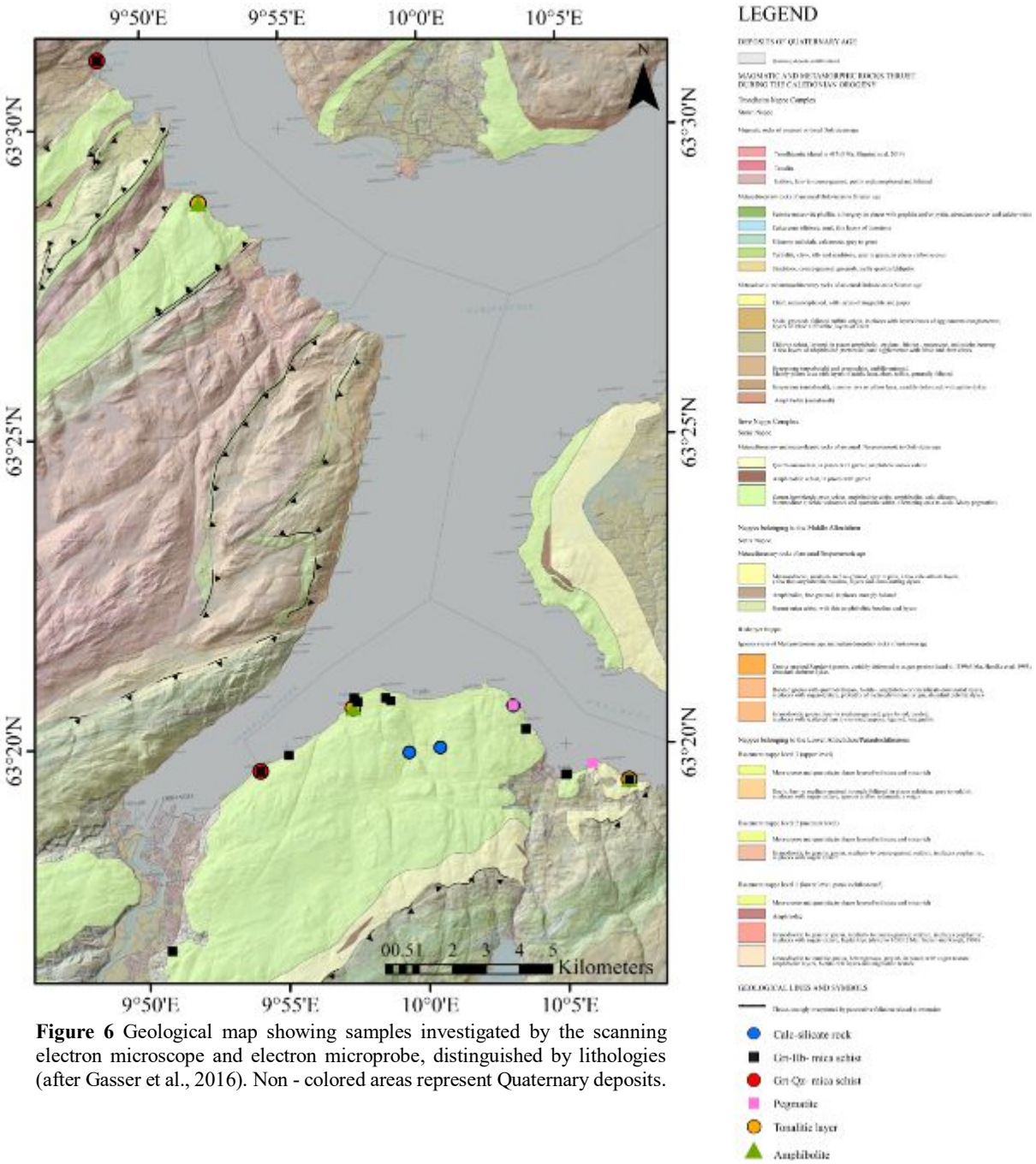

Figure 6 Geological map showing samples investigated by the scanning electron microscope and electron microprobe, distinguished by lithologies (after Gasser et al., 2016). Non - colored areas represent Quaternary deposits.

PETROGRAPHY AND MINERAL CHEMISTRY

GARNET-HORNBLENDE MICA SCHIST

The mineral assemblage mainly consists of garnet ± hornblende ± clinozoisite porphyroblasts, which rarely show an euhedral habitus, enveloped in a schistose matrix of fine-grained quartz, biotite, white mica, plagioclase, epidote and minor alkali feldspar. Chlorite and calcite appear as secondary phases. Rutile, apatite, titanite, allanite, zircon, tourmaline, ilmenite, pyrite, chalcopyrite and iron-oxides are present as accessory phases. The fabric varies from a weakly developed schistosity (gneissose structure) to a clear schistose structure (see Figure 7D, E & F).

Subhedral to anhedral garnet porphyroblasts, vary in size and can reach ~ 20mm in diameter. Many are highly fractured and show common mineral inclusions of quartz, biotite, rutile, plagioclase, amphibole, clinozoisite, chlorite, epidote, ilmenite, pyrite, zircon and allanite. Rutile inclusions are often restricted to garnet rims but are also found in the matrix. Frequently, garnet comprises a reaction rim decomposing to biotite, amphibole and chlorite. The garnet composition varies considerably between samples and is $Alm_{31-76}Grs_{4-45}Prp_{3-35}Sps_{0-16}$ (see Table 3). Biotite inclusions in garnet are enriched in MgO (16.14 wt%) and depleted in Fe^{2+} (11.52 wt%), compared to matrix biotite (14.58 wt% and 13.07 wt%, respectively). Overall, 27 garnet compositional profiles reveal that only a few samples show distinct zoning patterns (see Figure 8A). Xsps is typically bell-shaped, with maximum values of 0.11 in core regions; Xalm and Xprp are increasing towards the rim from 0.59 to 0.67 and from 0.1 to 0.23, respectively. Xgrs is increasing from core to rim (0.1 to 0.2). The majority of compositional profiles indicate fairly homogenous chemistry with weak zoning at the rims as shown in Figure 8B. The element distribution map of Y is characterized by a remarkable oscillatory growth zoning (see Figure 8F).

Green and brown amphiboles appear with moderately developed growth faces in the vicinity of garnet and form sharp grain boundaries (see Figure 7E & F). According to the nomenclature of Leake et al., 1997 all amphiboles from this lithology are characterized as calcic amphiboles, and classified as tschermakite, magnesiohornblende and pargasite (Fe^{3+} calculated after Leake et al., 1997) as illustrated in Figure 9. Although they are optically homogeneous, the rims are slightly depleted in Na_2O (1.69 wt%), compared to the cores (2.25 wt%), and vice versa. Contrary behavior is observed for ferrous iron, where the core has lower values (11.14

wt%) than the rim (13.70 wt%, see Table 4). Inclusions of plagioclase have compositions of $Ab_{76-87}An_{13-23}Or_{0-1}$. No clear difference to matrix plagioclase is observed. White mica inclusions reveal a significant difference in TiO_2 values (0.29 wt%), compared to matrix white mica (0.92 wt%). Biotite inclusions in amphibole are slightly depleted in FeO and MgO (13.8 wt% and 14.35 wt%, respectively) in contrast to matrix biotite (14.65 wt% and 15.05 wt%, respectively). The $Mg/(Mg+Fe^{2+})$ ranges from 0.483 to 0.804. Rutile is abundant, and is mainly enclosed in amphibole rims (see Figure 7F).

White mica represents one of the main constituents in the matrix. Individual white mica platelets of, up to ~ 2000 µm in size show perfectly developed basal cleavage (see Figure 7F). If not present as idiomorphic crystal and part of the stable paragenesis, they are intergrown with biotite and amphibole or indicate a reaction relationship with garnet. In samples which experienced higher deformation rates, white mica and biotite are distorted around garnet and form oriented bands parallel to the schistosity (see Figure 7D). Equilibrium with amphibole is observed. The Xna component of muscovite is between 0.13 and 0.28 and the phengite content is in the range of 3.11 – 3.25Si/11 O (see Table 5). Sample 98820 contains paragonite with 13.0 mol% muscovite. The margarite component is negligible.

Red-brownish biotite is observed in two modifications: mainly as alteration product of garnet and amphiboles, or as primary phase in the matrix, forming flakes up to 1500 µm in size (see Figure 7D & H). Zircon and allanite are common inclusions in biotite and form pleochroic halos. Matrix biotite is typically enriched in TiO_2 (3.09 wt%), other than biotite adjacent to garnet (TiO_2 = 0.71 wt%). Overall $Mg/(Mg/Fe^{2+})$ ratios range from 0.50 to 0.73, where highest values are observed in matrix biotite. The F content varies between 0.20 and 0.33 wt% (see Table 5).

Plagioclase, up to ~ 600µm in size, is besides quartz and mica the main rock – forming mineral (see Figure 7G). Locally plagioclase replaces garnet or is enclosed in garnet and amphibole. Polysynthetic twinning and irregular grain shape are common. Matrix plagioclase indicates general higher Xab content than plagioclase adjacent to garnet (0.86 and 0.74, respectively) (see Table 6). The majority of plagioclase is classified as oligoclase (see Figure 10 and Table 6). Fine - grained sericite occasionally forms rims around plagioclase.

Clinozoisite forms elongated crystals with euhedral to anhedral grain shapes (see Figure 7G). The porphyroblasts are poikiloblastic and enclose biotite, quartz, epidote and apatite. In

some samples clinozoisite represents the main constitute of porphyroblasts. Rims are slightly enriched in ferric iron in contrast to the core (1.68 wt% respectively 1.35 wt%, see Table 6).

Acicular, retrograde light green chlorite occurs in the vicinity of garnet and amphibole (see Figure 7H). XFe ranges from 0.29 (adjacent to garnet) to 0.38 (matrix). Chlorite adjacent to biotite reveals higher FeO values than chlorite in contact to garnet (14.45 wt% and 12.90 wt%, respectively).

Quartz is a major constituent of the matrix, but also the main enclosed in garnet. Undulatory extinction in coarser grains is common. Grain boundaries are straight to highly sutured, and recrystallization of small grains around bigger ones is frequent.

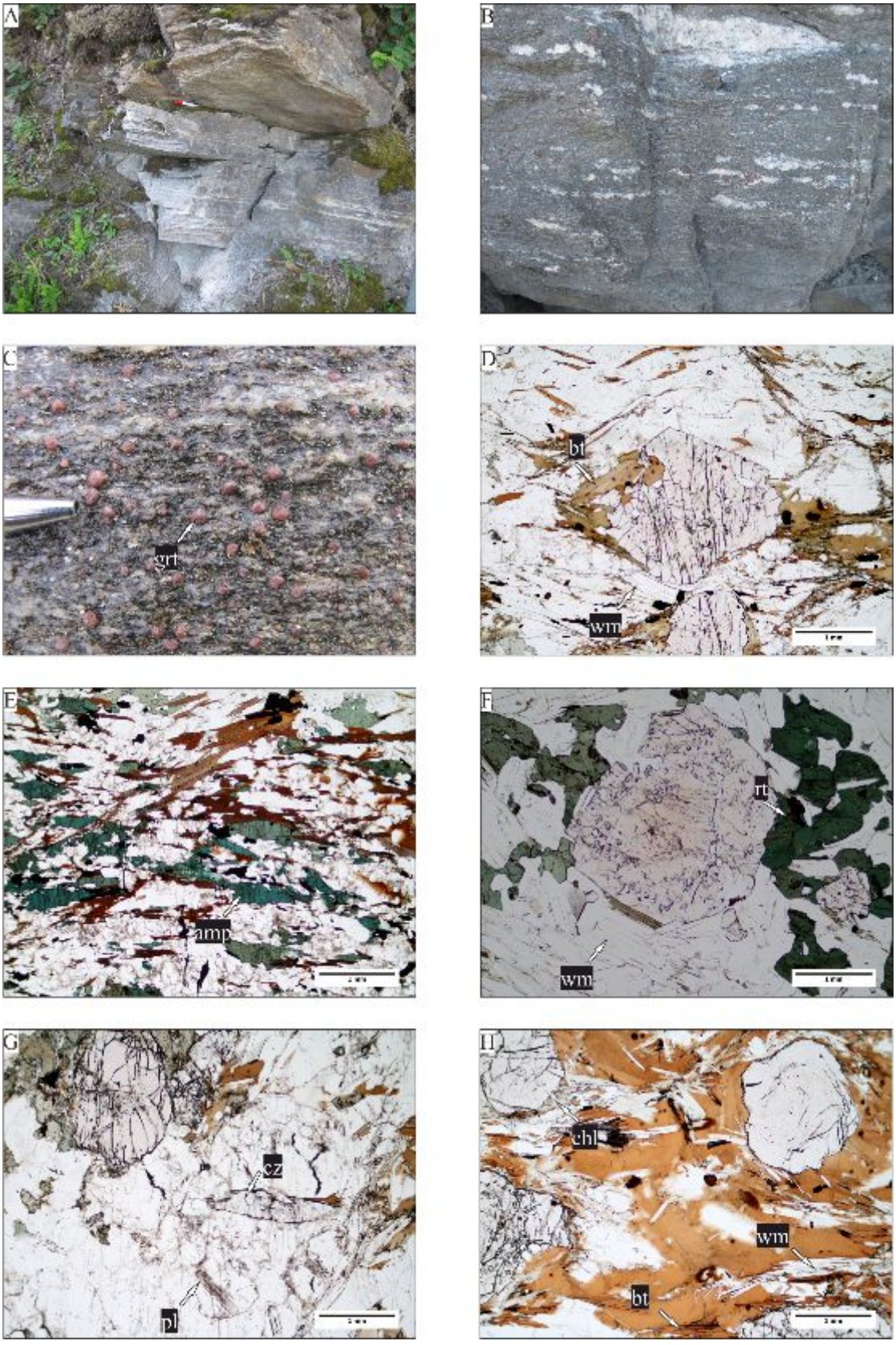

Figure 7 Field setting and microphotographs of garnet – hornblende mica schist (A-H). (A) Typical outcrop situation indicating the fine grained schistose structure, sample 14SW01&02. (B) Macroscopic garnets frequently accumulated in quartz-rich domains, sample 14SW18. (C) Massive garnet accumulation pointing out the high weathering resistance of garnet, sample 14SW37&38. (D) Schistose structure type with idiomorphic garnet, sample 14SW52. (E) More retrograde schistose structure type, sample 14SW29. (F) Gneissose structure type indicating Mn – rich core of poikiloblastic garnet and dark green hornblende and rutile, sample 14SW18. (G) Idiomorphic clinozoisite, sample 98814. (H) Biotite-rich garnet – hornblende mica schist, were latter represents the main constituent of the matrix, sample 98817.

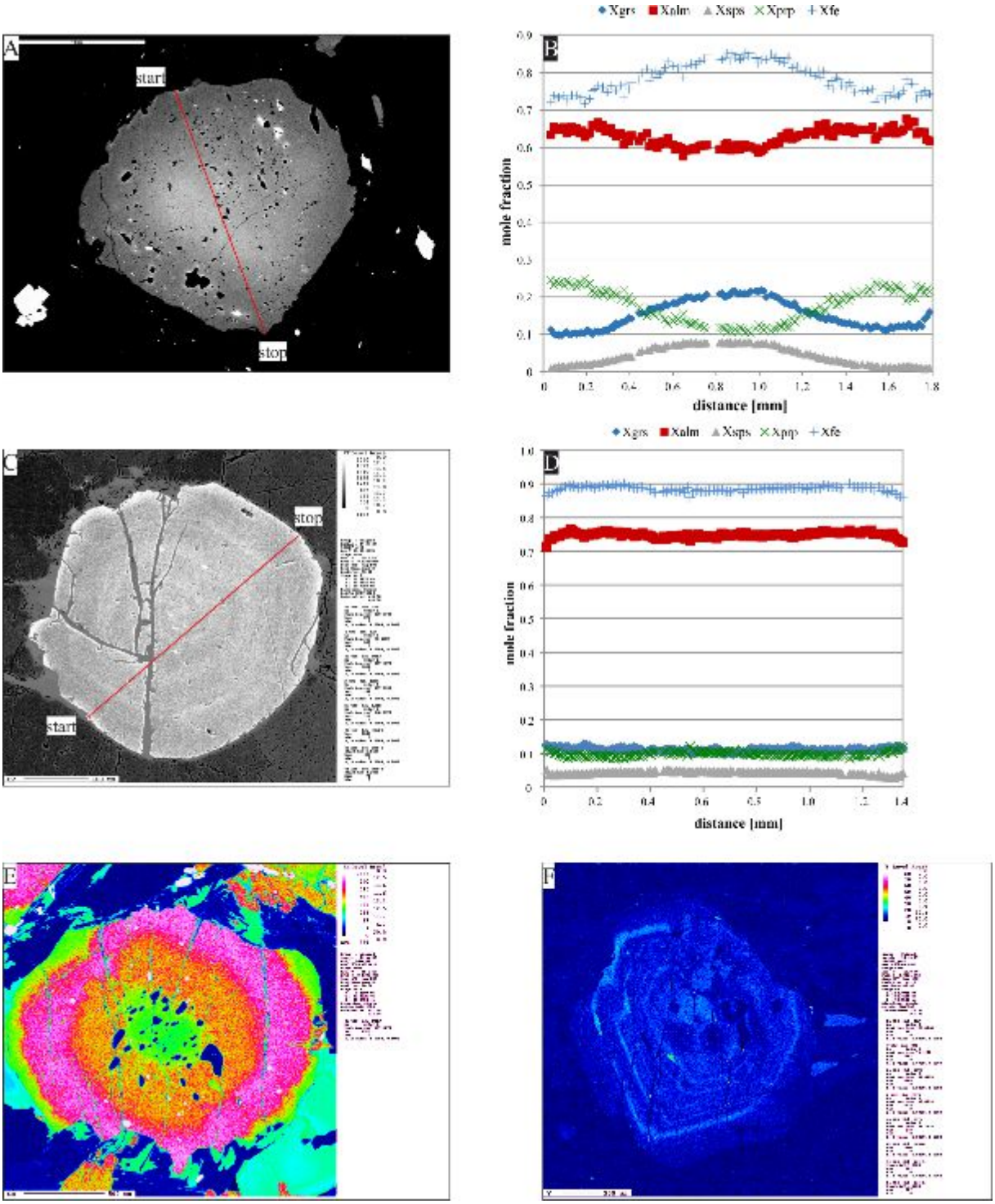

Figure 8 BSE images, compositional garnet profiles and element distribution maps of garnet in garnet - hornblende mica schist (A-F). BSE image (A) and corresponding compositional profile (B) type I, sample 98806, show a distinct zoning pattern where Xsps is typically bell-shaped and maximum value of 0.11 in core region; Xalm and Xprp are increasing towards the rims from 0.59 to 0.67 and from 0.1 to 0.23, respectively. Xgrs is decreasing from rim to core (0.2 – 0.1), with an increase again at the outermost rim to 0.15. BSE image (C) and corresponding compositional profile (D) of type II sample, 14SW27, which represents the majority of samples indicate a fairly homogenous composition with weak zoning at the rims. (E) Element distribution map of Ca, sample 14SW66, where the core and outermost rim are enriched in Ca. (F) Element distribution map of Y, sample 14SW27 with oscillatory enriched realms of Y.

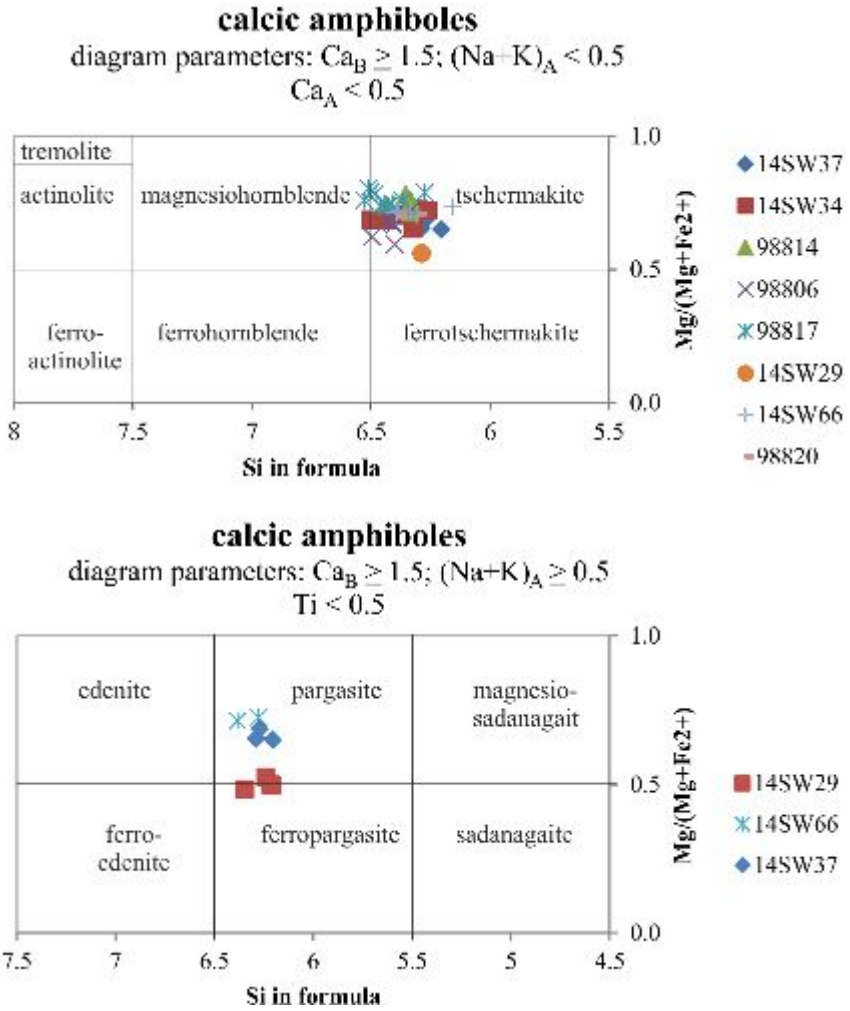

Figure 9 Classification of amphiboles in garnet – hornblende mica schist after Leake et al., 1997. Amphiboles from all samples can be classified as calcic amphiboles with the majority plotting in the tschermakite field. Amphiboles from three samples can be classified as pargasite respectively ferropargasite because of higher $(Na+K)_A$ values.

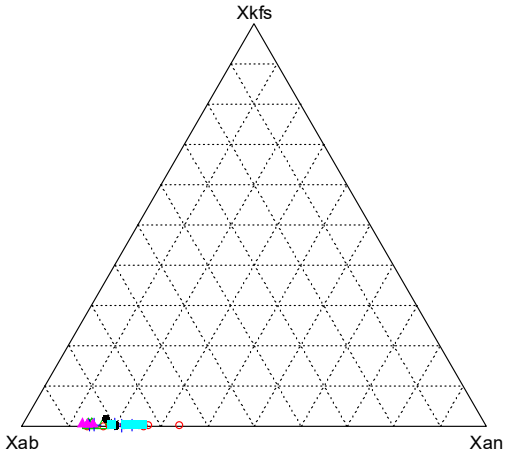

Figure 10 Ternary plot of feldspar in garnet – hornblende mica schist. In total 50 measurements of eight different samples plot all in the field of oligoclase and andesine.

Table 3 Representative composition of garnet in garnet - hornblende mica schist.

Sample	14SW18	14SW18	14SW27	14SW27	14SW52	14SW52	14SW66	14SW66	98S06	98S06
Mineral	grt-rim	grt-core	grt-rim	grt-core	grt-rim	grt-core	grt-rim	grt-core	grt-rim	grt-core
SiO2	37.57	37.32	37.76	37.82	37.87	37.69	38.72	38.84	37.52	36.69
TiO2	b.d.l.	b.d.l.	b.d.l.	b.d.l.	b.d.l	b.d.l	b.d.l	b.d.l.	b.d.l.	b.d.l.
Al2O3	21.17	20.32	21.60	21.65	21.87	21.67	21.50	21.38	22.22	21.04
Cr2O3	b.d.l.	b.d.l.	b.d.l.	b.d.l.	b.d.l	b.d.l	b.d.l.	b.d.l.	b.d.l.	0.14
FeO	29.56	27.75	31.93	31.60	31.34	31.23	22.59	21.23	30.12	27.54
MnO	1.21	4.84	1.34	1.13	0.45	0.76	0.51	1.48	0.66	3.36
MgO	3.99	2.61	3.15	3.25	5.77	3.75	4.51	3.61	5.95	2.89
CaO	6.13	6.97	4.29	4.20	2.72	4.88	11.87	13.15	3.45	7.19
Total	**99.93**	**99.81**	**100.07**	**99.65**	**99.98**	**99.98**	**99.64**	**99.69**	**99.91**	**98.85**
Si per 12 O	2.971	2.983	3.003	3.011	2.975	2.988	3.010	3.024	2.941	2.949
Ti	0	0	0	0	0	0	0	0	0	0
Al	1.973	1.915	2.024	2.032	2.027	2.025	1.970	1.962	2.053	1.993
Cr	0	0	0	0	0	0	0	0	0	0.009
Fe3+	0.081	0.106	0	0	0.026	0	0.033	0	0.060	0.092
Fe2+	1.874	1.749	2.124	2.109	2.035	2.071	1.466	1.383	1.914	1.759
Mn	0.081	0.328	0.091	0.076	0.030	0.051	0.034	0.098	0.044	0.229
Mg	0.470	0.311	0.373	0.385	0.676	0.443	0.523	0.419	0.695	0.346
Ca	0.545	0.597	0.365	0.358	0.229	0.414	0.984	1.097	0.289	0.619
cations	**7.995**	**7.989**	**7.980**	**7.966**	**7.998**	**7.992**	**7.991**	**7.983**	**7.997**	**7.996**
Xgrs	0.135	0.167	0.110	0.109	0.092	0.122	0.247	0.268	0.089	0.173
Xalm	0.631	0.586	0.719	0.720	0.685	0.695	0.488	0.461	0.651	0.596
Xsps	0.027	0.110	0.031	0.026	0.010	0.017	0.011	0.033	0.015	0.078
Xprp	0.158	0.104	0.126	0.132	0.228	0.149	0.174	0.140	0.236	0.117
Xfe	0.799	0.849	0.851	0.845	0.751	0.824	0.737	0.767	0.734	0.836

Table 4 Representative composition of amphibole in garnet - hornblende mica schist.

Sample	14SW29	14SW29	14SW34	14SW34	14SW66	14SW66	98S06	98S06	98S17	98S17
Mineral	amp-rim	amp-core	amp-rim	amp-core	amp-rim	amp-core	amp-rim	amp-core	amp-rim	amp-core
SiO2	41.26	40.75	44.10	43.64	44.29	44.50	43.74	44.29	44.68	45.80
TiO2	0.79	0.70	0.59	0.72	0.67	0.57	0.48	0.84	0.47	0.80
Al2O3	13.59	13.13	15.39	16.01	15.14	14.92	15.9.	15.72	15.81	14.88
Cr2O3	b.d.l.	b.d.l.	b.d.l.	0.13	b.d.l	b.d.l	b.d.l	b.d.l.	0.14	b.d.l.
FeO	20.04	20.29	13.07	11.97	11.59	12.13	13.70	12.20	11.29	10.18
MnO	0.35	0.30	b.d.l.	b.d.l.	b.d.l	b.d.l	b.d.l	b.d.l.	b.d.l.	b.d.l.
MgO	8.31	8.71	12.12	12.22	11.99	12.17	10.80	11.21	12.34	13.42
CaO	9.74	9.90	9.96	10.16	10.90	10.99	11.19	10.32	9.76	9.91
Na2O	2.04	2.17	2.07	2.48	2.22	2.09	1.69	2.23	..91	1.89
K2O	0.81	0.67	0.55	0.63	0.90	0.81	0.39	0.51	0.40	0.35
F	0.30	0.28	0.28	0.18	b.d.l	b.d.l	0.32	0.36	0.13	0.28
Cl	b.d.l.	b.d.l.	b.d.l.	b.d.l.	b.d.l	b.d.l	b.d.l.	b.d.l.	b.d.l.	b.d.l.
Total	**97.06**	**96.90**	**98.13**	**98.14**	**97.70**	**98.18**	**97.42**	**97.58**	**96.93**	**97.61**
Si per 23 O	6.245	6.173	6.339	6.262	6.382	6.381	6.399	6.404	6.412	6.500
Ti	0.090	0.080	0.064	0.078	0.075	0.061	0.053	0.091	0.051	0.085
Al(IV)	1.750	1.830	1.670	1.740	1.620	1.620	1.600	1.580	1.590	1.500
Al(VI)	0.640	0.510	0.930	0.970	0.950	0.900	1,140	1.110	1.080	0.990
Cr	0	0	0	0.015	0	0	0	0	0.016	0.006
Fe3+	0.648	0.787	0.551	0.424	0.362	0.436	0.186	0.258	0.471	0.468
Fe2+	1.888	1.784	1.017	1.073	1.034	1.018	1.480	1.217	0.884	0.740
Mn	0.045	0.068	0	0	0	0	0	0	0	0
Mg	1.882	1.967	2.593	2.614	2.575	2.602	2.187	2.417	2.640	2.839
Ca	1.580	1.607	1.532	1.562	1.685	1.689	1.754	1.599	1.501	1.507
Na	0.599	0.637	0.576	0.690	0.620	0.581	0.479	0.625	0.551	0.520
K	0.156	0.129	0.101	0.115	0.165	0.148	0.073	0.044	0.073	0.063
F	0.150	0.130	0.130	0.180	0	0	0.150	0.120	0.060	0.170
Cl	0	0	0	0	0	0	0	0	0	0
cations	**15.523**	**15.542**	**15.363**	**15.483**	**15.464**	**15.436**	**15.355**	**15.395**	**15.249**	**15.218**

Table 5 Representative compositions of bioite and white mica in garnet – hornblende mica schist.

Sample	14SW29	14SW52	14SW52	14SW66	14SW66	98820	14SW52	14SW52	98817	98820
Mineral	bt-matrix	bt-adjacent to grt	bt-matrix	bt-adjacent to grt	bt-matrix	bt-matrix	wm-inclusion in grt	wm-matrix	wm-matrix	wm-adjacent to grt
SiO2	35.81	38.49	37.14	38.07	37.71	39.17	47.54	48.87	48.89	46.77
TiO2	3.09	1.78	1.66	1.30	1.30	1.26	1.13	0.87	0.87	0.23
Al2O3	14.84	17.46	18.40	17.64	17.45	17.39	32.84	31.10	31.67	29.78
Cr2O3	b.d.l.	n.d.	n.d.	b.d.l.	b.d.l.	b.d.l.	n.d.	n.d.	0.15	b.d.l.
FeO	20.17	16.55	14.73	14.10	14.57	11.32	1.54	1.73	1.30	0.67
MnO	0.16	b.d.l.	b.d.l.	b.d.l.	b.d.l.	b.d.l.	b.d.l.	b.d.l.	b.d.l.	b.d.l.
MgO	11.69	12.67	13.49	14.88	15.05	17.05	1.60	2.35	2.17	b.d.l.
CaO	b.d.l.	b.d.l.	b.d.l.	b.d.l.	b.d.l.	b.d.l.	b.d.l.	b.d.l.	b.d.l.	0.50
Na2O	0.12	0.27	0.23	0.16	0.14	0.29	1.05	0.88	1.26	6.72
K2O	9.45	9.41	9.72	9.28	9.29	9.28	9.45	9.69	9.32	1.46
F	0.42	b.d.l.	b.d.l.	b.d.l.	b.d.l.	2.10	b.d.l.	b.d.l.	b.d.l.	b.d.l.
Cl	0.11	b.d.l.	b.d.l.	b.d.l.	b.d.l.	b.d.l.	b.d.l.	b.d.l.	b.d.l.	b.d.l.
Total	**95.86**	**96.64**	**95.37**	**95.43**	**95.49**	**97.86**	**95.15**	**95.49**	**95.63**	**96.13**
Si per 11 O	2.753	2.831	2.757	2.803	2.786	2.832	3.158	3.236	3.225	2.973
Ti	0.179	0.099	0.092	0.072	0.072	0.069	0.056	0.043	0.043	0.011
Al	1.345	1.514	1.609	1.531	1.517	1.482	2.571	2.427	2.462	2.981
Cr	0	n.d.	n.d.	0	0	0	n.d.	n.d.	0.008	0
Fe3+	0	0	0	0	0	0	0	0	0	0
Fe2+	1.297	1.018	0.915	0.868	0.9	0.684	0.086	0.096	0.072	0.086
Mn	0.010	0	0	0.002	0.005	0	0	0	0	0
Mg	1.340	1.390	1.493	1.634	1.656	1.838	0.158	0.232	0.213	0
Ca	0	0	0	0	0	0	0	0	0	0.034
Na	0.018	0.038	0.034	0.023	0.020	0.041	0.135	0.113	0.161	0.828
K	0.927	0.883	0.920	0.872	0.875	0.856	0.807	0.819	0.784	0.118
F	0.100	0	0	0	0	0.920	0	0	0	0
Cl	0.010	0	0	0	0	0	0	0	0	0
cations	**7.869**	**7.773**	**7.820**	**7.805**	**7.828**	**7.802**	**6.965**	**6.966**	**6.968**	**6.981**
Xmg	0.508	0.577	0.620	0.653	0.648	0.729				
Xk							0.856	0.879	0.880	0.125
Xna							0.144	0.121	0.120	0.875

Table 6 Representative composition of feldspars and clinozoisite in garnet - hornblende mica schist.

Sample	14SW34	14SW34	14SW37	98814	98817	98811	98811	98814	98814
Mineral	pl-adjacent to amp	pl-matrix	pl-matrix	pl-matrix	pl-inclusion in amp	czo-rim	czo-core	czo-rim	czo-core
SiO2	64.72	59.45	64.53	64.45	64.69	40.22	40.73	41.11	39.83
TiO2	n.d.	n.d.	n.d.	b.d.l.	b.d.l.	b.d.l.	b.d.l.	b.d.l.	b.d.l.
APO3	22.43	25.49	22.26	22.40	21.86	33.13	33.75	33.30	33.25
Fe2O3	b.d.l.	b.d.l.	b.d.l.	b.d.l.	b.d.l.	1.68	1.35	1.54	1.38
MnO	n.d.	n.d.	n.d.	b.d.l.	b.d.l.	b.d.l.	b.d.l.	b.d.l.	b.d.l.
MgO	n.d.	n.d.	n.d.	b.d.l.	b.d.l.	b.d.l.	b.d.l.	b.d.l.	b.d.l.
CaO	3.06	7.12	2.99	3.52	2.91	23.69	23.96	23.42	23.86
Na2O	10.33	7.72	10.01	9.23	9.93	b.d.l.	b.d.l.	b.d.l.	b.d.l.
K2O	b.d.l.	b.d.l.	b.d.l.	0.33	0.09	b.d.l.	b.d.l.	b.d.l.	b.d.l.
Total	**100.54**	**99.78**	**99.79**	**99.93**	**99.48**	**98.72**	**99.79**	**99.27**	**98.32**
Si per 8/12.5 O	2.837	2.655	2.847	2.842	2.858	3.015	3.017	3.058	3.006
Ti	0	0	0	0	0	0	0	0	0
Al	1.159	1.342	1.157	1.164	1.138	2.927	2.947	2.911	2.958
Fe3+	0	0	0	0	0	0.095	0.075	0.086	0.078
Mn	0	0	0	0	0	0	0	0	0
Mg	0	0	0	0	0	0	0	0	0
Ca	0.144	0.341	0.141	0.166	0.138	1.903	1.902	1.867	1.929
Na	0.878	0.668	0.856	0.789	0.851	0	0	0	0
K	0	0	0	0.019	0.005	0	0	0	0
cations	**5.018**	**5.006**	**5.001**	**4.980**	**4.990**	**7.940**	**7.941**	**7.922**	**7.971**
Xab	0.859	0.662	0.859	0.810	0.856				
Xan	0.141	0.338	0.141	0.170	0.139				
Xkfs	0.000	0.000	0.000	0.020	0.005				

GARNET – QUARTZ - MICA SCHIST

The mineral assemblage typically consists of quartz, biotite, white mica and garnet. Minor constituents are chlorite, calcite, plagioclase and clinozoisite/epidote. The key distinction to garnet – hornblende mica schist is the common lack of amphibole. Accessory phases are apatite, zircon, pyrite, iron-oxides, rutile, ilmenite, allanite, titanite, sylvine and chalcopyrite. Quartz and micas are building up the matrix in which garnets are interbedded, to varying degree.

Subhedral, highly fractured garnet is up to 5mm in size, with two distinct textural appearances (see Figure 11A - D): coarse – grained poikiloblastic garnet (type I) and smaller garnet crystals scattered in the matrix (type II). Inclusions of ilmenite, biotite, plagioclase, white mica, epidote and apatite are common in type I. Veins are filled with ilmenite and Fe-oxides. Garnet cores show a different color than rims (see Figure 11A). Average garnet composition is $Alm_{42-84}Sps_{2-31}Grs_{4-28}Prp_{4-21}$ (see Table 7). The two textural garnet types show also differences in chemical compositional profiles: Type I garnet indicates a distinct decrease of Xsps (0.3 to 0.09) and Xgrs (0.2 to 0.1) towards the rim (Figure 12A-D). Xalm and Xprp show a contrary behavior. Smaller type II garnet (see Figure 12E & F) reveal an almost homogenous composition, with an increase of Xprp from 0.1 to 0.2 from the core to rim, Xalm shows an opposite trend. Xsps is typically bell-shaped (Figure 12E - F).

Brown biotite represents a major constituent of this lithology and forms platelets of up to 2 mm in size with a basal cleavage (see Figure 11C & D). Retrograde formed biotite is also found at garnet rims (see Figure 11H). The $Mg/(Mg+Fe^{2+})$ ratio ranges from 0.43 – 0.59 and highest values are found in biotite adjacent to garnet (see Table 8). Matrix – biotite is Ti-rich (3.19 wt%) compared to biotite adjacent to garnet (2.39 wt%).

Along with quartz band biotite, plateltes of white mica represent the matrix (see Figure 11A - D). Since K/(K+Na) ranges from 0.86 to 0.97 and Na/(Na+K) from 0.04 to 0.14, white mica is classified as muscovite. The phengite content varies from 3.10 to 3.22 Si/11O, where maximum values are reached when in vicinity to garnet (see Table 8).

Deformed plagioclase is part of the matrix. In garnet-mica fels, however plagioclase is missing. Single grains can reach up to 500 µm in size. Highest CaO values are found adjacent to garnet (8.15 wt%) as shown in Table 9. Figure 13 illustrates the ternary plot of plagioclase measurements with an average composition of $Ab_{60-77}An_{21-39}Kfs_{1-2,}$ being classified as oligoclase and andesine.

Chlorite is found as inclusions in garnet or as alteration product of biotite (see Figure 11E - H). The $Mg/(Mg+Fe^{2+})$ ratio is 0.50 (see Table 9).

Quartz shows undulatory extinction and forms grains of up to 2mm in size. Sample 14SW28 (see Figure 11G) reveals a more schistose fabric, although quartz crystals are significantly smaller.

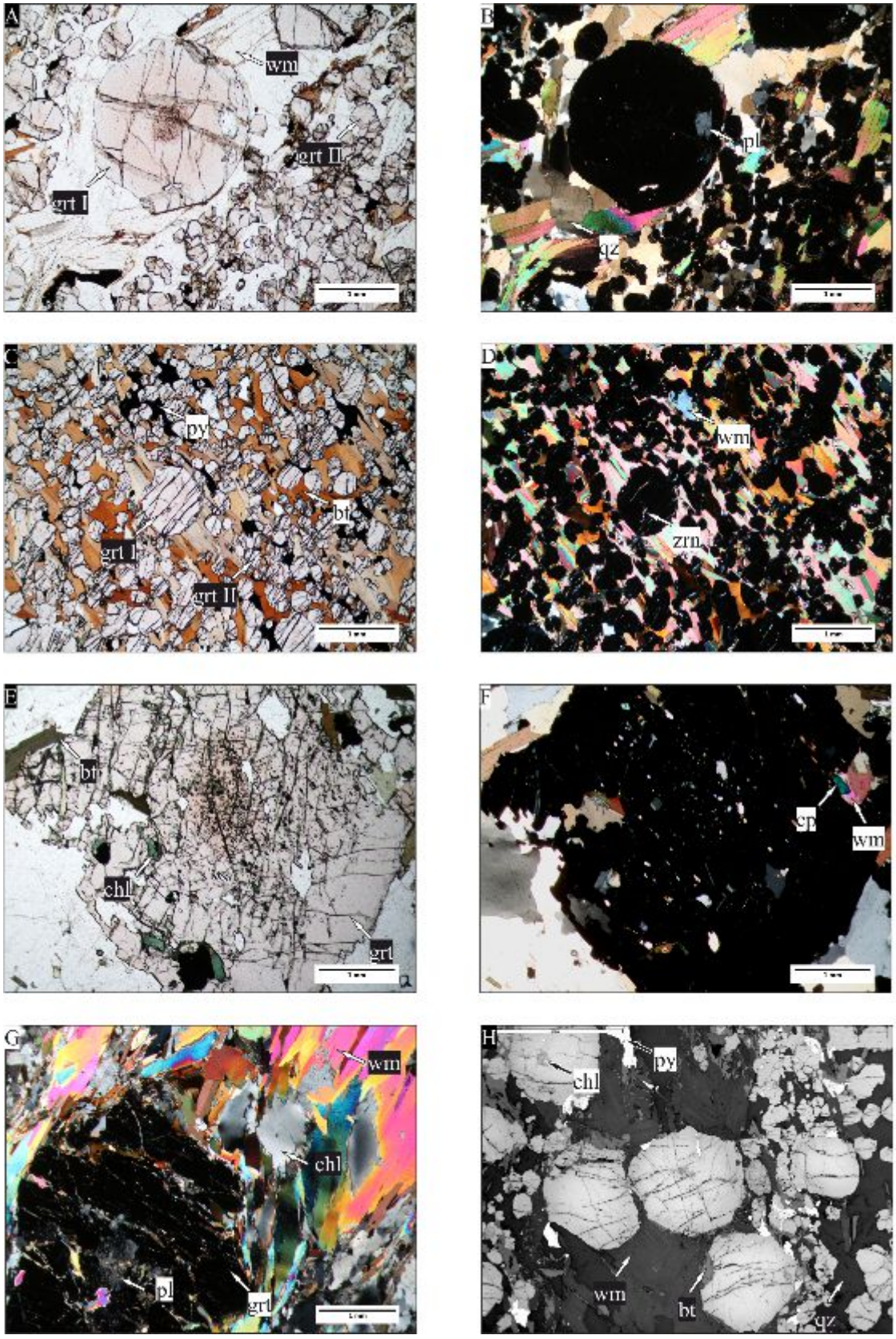

Figure 11 Photomicrographs and BSE images of garnet-quartz mica schist (A-H). (A) Sample 14SW06 with highlighted texturally different types of garnet and reddish core region. (B) Sample 14SW06, (crossed nicols): plagioclase inclusions in garnet. (C) More biotite rich sample with massive occurrence of two textural garnet types again in two textural types, sample 14SW05. (D) Sample 14SW05, (crossed nicols): white mica is less frequent. (E) Chlorite inclusions at rims of garnet, crossed nicols, sample 14SW16. (F) Epidote and white mica inclusions in garnet, sample 14SW16. (G) Matrix - white mica and chlorite, in vicinity of highly fractured garnet, sample 14SW28. (H) BSE image of sample 14SW06 with chlorite inclusions in garnet core and biotite replacing garnet rims.

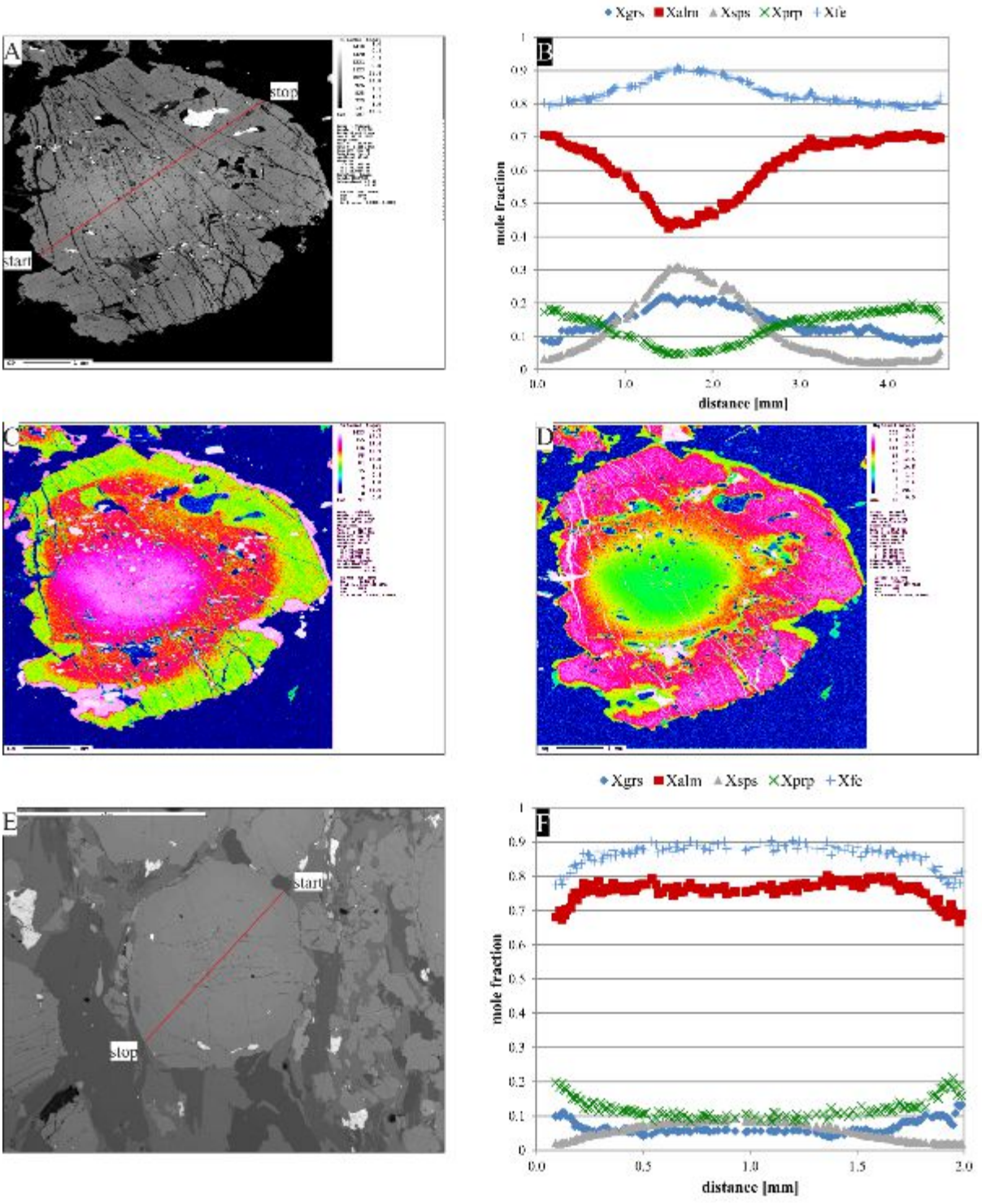

Figure 12 BSE image, compositional profile and element distribution map of garnet in garnet – quartz mica schist (A-F). (A) BSE image, sample 14SW16. (B) Compositional profile with significant chemical zoning, reflected an enrichment of Xsps (0.09 to 0.3) and Xgrs (0.1 to 0.2) from rim to core and contrary behavior of Xalm (0.7 to 0.3) and Xprp (0.2 to 0.05), sample 14SW. 16 (C) Element distribution map of Ca and (D) Mg support the compositional profile, sample 14SW16. (E) BSE image of second textural occurrence of garnet, sample 14SW06. (F) Compositional profile with bell-shaped trend of Xsps, a slight decrease of Xprp and Xgrs from rim to core and increase in Xalm from rim to core, sample 14SW06.

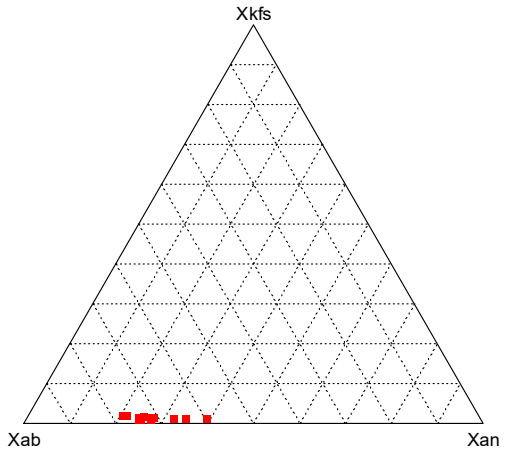

Figure 13 Ternary plot of feldspar in garnet – quartz mica schist. Nine measurements from sample 14SW28 classified as oligoclase and andesine.

Table 7 Representative composition of garnet in garnet – quartz mica schist.

Sample	14SW06	14SW06	14SW06	14SW16	14SW16	14SW16	14SW28	14SW28	14SW28
Mineral	grt-rim	grt-core	grt-transition	grt-rim	grt-core	grt-transition	grt-rim	grt-core	grt-transition
SiO2	37.97	36.35	37.73	36.20	36.07	36.86	37.05	36.85	36.69
TiO2	b.d.l.	b.d.l.	b.d.l.	b.d.l.	b.d.l.	b.d.l.	b.d.l.	b.d.l.	b.d.l.
Al2O3	20.74	19.58	21.04	21.79	20.47	21.10	21.16	20.93	20.62
Cr2O3	b.d.l.	b.d.l.	b.d.l.	b.d.l.	b.d.l.	b.d.l.	b.d.l.	b.d.l.	b.d.l.
FeO	31.97	36.54	32.56	32.80	20.57	30.62	33.58	33.78	33.41
MnO	1.01	3.53	0.99	1.45	12.83	3.15	2.36	3.38	3.41
MgO	4.46	1.56	4.63	4.26	1.19	3.71	1.65	1.25	1.83
CaO	4.21	1.70	3.34	2.98	7.03	4.22	3.91	3.52	3.50
Na2O	n.d.	n.d.	n.d.	b.d.l.	b.d.l.	b.d.l.	n.d.	n.d.	n.d.
K2O	n.d.	n.d.	n.d.	b.d.l.	b.d.l.	b.d.l.	n.d.	n.d.	n.d.
Total	**100.36**	**99.26**	**100.29**	**99.48**	**98.16**	**99.66**	**99.71**	**99.71**	**99.46**
Si per 12 O	3.002	2.992	2.985	2.892	2.951	2.944	2.994	2.995	2.981
Ti	0	0	0	0	0	0	0	0	0
Al	1.932	1.899	1.962	2.051	1.974	1.986	2.015	2.005	1.975
Cr	0	0	0	0	0	0	0	0	0
Fe3+	0.061	0.106	0.064	0.171	0.118	0.131	0	0	0.046
Fe2+	2.052	2.409	2.091	2.020	1.289	1.914	2.270	2.296	2.224
Mn	0.068	0.246	0.066	0.098	0.889	0.213	0.162	0.233	0.235
Mg	0.526	0.191	0.546	0.507	0.145	0.442	0.199	0.151	0.222
Ca	0.357	0.150	0.283	0.255	0.616	0.361	0.339	0.307	0.305
Na	n.d.	n.d.	n.d.	0	0	0	n.d.	n.d.	n.d.
K	n.d.	n.d.	n.d.	0	0	0	n.d.	n.d.	n.d.
cations	**7.998**	**7.993**	**7.997**	**7.994**	**7.982**	**7.991**	**7.979**	**7.987**	**7.988**
Xgrs	0.119	0.050	0.095	0.089	0.210	0.123	0.114	0.103	0.102
Xalm	0.683	0.804	0.700	0.701	0.439	0.653	0.764	0.769	0.745
Xsps	0.023	0.082	0.022	0.034	0.302	0.073	0.055	0.078	0.079
Xprp	0.175	0.064	0.183	0.176	0.049	0.151	0.067	0.051	0.074
Xfe	0.796	0.927	0.793	0.799	0.899	0.812	0.919	0.938	0.909

Table 8 Representative composition of biotite and white mica in garnet – quartz mica schist.

Sample	14SW06	14SW06	14SW28	14SW28	14SW06	14SW06	14SW06	14SW28	14SW28	14SW28
Mineral	bt - matrix	bt-adjacent to grt	bt-vicinity of grt	bt-adjacent to grt	wm-matrix	wm-vicinity of grt	wm-vicinity of grt	wm-adjacent to grt	wm-matrix	wm-adjacent to grt
SiO2	37.23	37.37	35.89	35.03	47.34	46.58	47.82	46.53	47.40	46.07
TiO2	1.54	1.65	3.19	2.39	1.09	1.62	0.95	1.02	1.01	0.67
Al2O3	17.84	17.73	16.49	18.12	31.86	31.80	30.86	30.58	30.71	32.15
Cr2O3	b.d.l.	b.d.l.	b.d.l.	b.d.l.	b.d.l	b.d.l.	b.d.l.	b.d.l.	b.d.l.	b.d.l.
FeO	16.31	15.9	17.86	21.29	1.40	1.78	1.76	3.93	3.66	3.77
MnO	b.d.l.	b.d.l.	0.40	0.16	b.d.l	b.d.l.	b.d.l.	b.d.l.	b.d.l.	b.d.l.
MgO	12.54	12.72	11.05	9.06	1.85	1.87	2.19	1.70	2.06	1.33
CaO	b.d.l.	b.d.l.	b.d.l.	b.d.l.	b.d.l	b.d.l.	b.d.l.	b.d.l.	b.d.l.	b.d.l.
Na2O	0.30	0.23	0.08	0.11	0.89	0.94	0.92	0.33	0.30	0.38
K2O	8.84	9.07	9.62	9.72	9.89	9.79	9.95	11.00	10.95	11.04
F	0.40	0.37	0.40	0.18	0.16	0.18	0.21	0.14	b.d.l.	b.d.l.
Cl	b.d.l.	b.d.l.	b.d.l.	b.d.l.	b.d.l	b.d.l.	b.d.l.	b.d.l.	b.d.l.	b.d.l.
Total	**95.00**	**95.04**	**94.98**	**96.06**	**94.48**	**94.56**	**94.66**	**95.23**	**96.09**	**95.41**
Si per 11 O	2.790	2.800	2.747	2.684	3.180	3.140	3.210	3.163	3.177	3.117
Ti	0.090	0.090	0.184	0.138	0.060	0.080	0.050	0.052	0.051	0.034
Al	1.580	1.570	1.488	1.636	2.520	2.530	2.440	2.450	2.426	2.563
Cr	0	0	0	0	0	0	0	0	0	0
Fe2+	1.020	1.000	1.143	1.364	0.080	0.100	0.100	0.223	0.205	0.213
Mn	0	0	0.026	0.010	0	0	0	0	0	0
Mg	1.400	1.420	1.261	1.035	0.190	0.190	0.220	0.172	0.206	0.134
Ca	0	0	0	0	0	0	0	0	0	0
Na	0.040	0.030	0.012	0.016	0.120	0.120	0.120	0.043	0.039	0.050
K	0.850	0.870	0.940	0.950	0.850	0.840	0.850	0.954	0.936	0.953
F	0.190	0.170	0.190	0.090	0.070	0.070	0.090	0.060	0	0
Cl	0	0	0	0	0	0	0	0	0	0
cations	**7.770**	**7.780**	**7.801**	**7.833**	**7.000**	**7.000**	**6.990**	**7.057**	**7.040**	**7.064**
Xmg	0.578	0.588	0.525	0.431						
Xk					0.880	0.872	0.878	0.957	0.960	0.950
Xna					0.120	0.128	0.122	0.043	0.040	0.050

Table 9 Representative composition of feldspar and chlorite in garnet – quartz mica schist.

Sample	14SW28	14SW28	14SW28	14SW28	14SW28	14SW28	14SW28	14SW28	14SW28
Mineral	pl-matrix	pl-matrix	pl-matrix	pl-matrix	pl-adjacent to grt	pl-adjacent to grt	pl-inclusion in grt	chl-adjacent to grt	chl-adjacent to grt
SiO2	63.20	61.83	59.81	63.68	61.28	58.16	59.21	24.98	25.47
TiO2	n.d.	n.d.	n.d.	n.d.	n.d	n.d.	n.d.	0.12	b.d.l.
Al2O3	23.31	23.37	25.20	22.71	24.80	26.16	25.77	20.13	20.36
Fe2O3	b.d.l.	b.d.l.	b.d.l.	b.d.l.	b.d.l.	b.d.l.	b.d.l.	0	0
FeO	0	0	0	0	0	0	0	27.62	24.83
MnO	n.d.	n.d.	n.d.	n.d.	n.d	n.d.	n.d.	0.52	0.51
MgO	n.d.	n.d.	n.d.	n.d.	n.d	n.d.	n.d.	14.13	15.41
CaO	4.53	5.22	6.63	4.45	5.90	8.15	7.37	0.11	b.d.l.
Na2O	9.34	8.71	7.58	8.87	8.68	6.82	7.53	0.07	b.d.l.
K2O	0.35	0.21	0.19	0.33	0.22	0.19	0.19	b.d.l.	b.d.l.
F	n.d.	n.d.	n.d.	n.d.	n.d	n.d.	n.d.	b.d.l.	0.18
Cl	n.d.	n.d.	n.d.	n.d.	n.d	n.d.	n.d.	b.d.l.	b.d.l.
Total	**100.73**	**99.34**	**99.41**	**100.04**	**100.88**	**99.48**	**100.07**	**87.68**	**86.76**
Si per 8/14 O	2.782	2.761	2.677	2.813	2.704	2.613	2.642	2.679	2.714
Ti	n.d.	n.d.	n.d.	n.d.	n.d	n.d.	n.d.	0.010	0
Al	1.209	1.230	1.329	1.182	1.290	1.385	1.355	2.544	2.557
Fe3+	0	0	0	0	0	0	0	0	0
Fe2+	0	0	0	0	0	0	0	2.477	2.212
Mn	n.d.	n.d.	n.d.	n.d.	n.d	n.d.	n.d.	0.047	0.046
Mg	n.d.	n.d.	n.d.	n.d.	n.d	n.d.	n.d.	2.259	2.448
Ca	0.214	0.250	0.318	0.211	0.279	0.392	0.352	0.013	0
Na	0.797	0.754	0.658	0.760	0.743	0.594	0.651	0.015	0
K	0.020	0.012	0.011	0.019	0.012	0.011	0.011	0	0
F	n.d.	n.d.	n.d.	n.d.	n.d	n.d.	n.d.	0	0.060
Cl	n.d.	n.d.	n.d.	n.d.	n.d	n.d.	n.d.	0	0
cations	**5.022**	**5.007**	**4.993**	**4.985**	**5.028**	**4.995**	**5.011**	**10.044**	**9.977**
Xab	0.773	0.742	0.667	0.768	0.719	0.596	0.642		
Xan	0.208	0.246	0.322	0.213	0.270	0.393	0.347		
Xkfs	0.019	0.012	0.011	0.019	0.012	0.011	0.011		
Xmg								0.477	0.525

AMPHIBOLITE

The mineral assemblage in both, the fine-grained and coarse-grained amphibolites is made up of amphibole, garnet, plagioclase, quartz, clinozoisite, epidote, biotite, chlorite, minor white mica, calcite, rutile and titanite. Accessory pyrite, apatite, zircon, allanite, ilmenite, pyrrhotite, and pentandite are also present.

Based on the textures, two amphibolite types are distinguished: type I amphibolite is rare and shows a clear schistosity defined by aligned amphiboles and quartz. Outstanding are chlorite nests of up to 1000 µm in width (see Figure 14C). Veins are filled with calcite and fine-grained chlorite while garnet is missing. Rutile and idiomorphic titanite are prominent accessories.

Type II amphibolite is more common and mainly distinguished by a gneissouse structure and the presence of garnet (see Figure 14E&F). Amphibole, plagioclase and fine-grained quartz are representing the matrix.

Green to brown amphibole, up to 2mm in size, is sub- to anhedral. Only a few amphibole inclusions in garnet have an euhedral grain shape. Inclusions of biotite (up to 2 mm in length), rutile, apatite and epidote are in equilibrium with garnet and plagioclase (see Figure 14E & F). After Leake et al., 1997, the amphiboles belong to the calcic amphibole group and can be classified as Mg-hornblende, tschermakite and pargasite (see Figure 16). The $Mg/(Mg+Fe^{2+})$ ratio varies between 0.532 and 0.817. The grains are in general chemically homogenous within one sample, only idiomorphic grains locally show a slight zoning (see Table 10 for representative chemical analyses).

Plagioclase forms irregularly shaped grains with up to 700µm in size, and is in addition to amphibole and quartz, part of the matrix and equilibrium mineral assemblage (see Figure 14E & F). Again, in amphibolitic schists, plagioclase is aligned parallel to the schistosity, whereas in the gneissouse samples plagioclase shows hypidiomorphic crystals. The average composition is in the range of $Ab_{63-93}An_{6-37}Kfs_{0-7}$, thus the majority is classified as oligoclase (see Figure 17). No significant chemical difference can be observed between matrix plagioclase and adjacent grains to garnet or inclusion plagioclase (see Table 12).

Sub- to anhedral garnet porphyroblast of up to 2.5 mm in diameter, are frequntly fractured, but also occur as small fragments within the matrix. Clinozoisite, titanite, quartz, biotite, chlorite and amphibole are common inclusions. Typical chemical compositions are

shown in Table 12. Helicitic growth of chlorite and rutile – ilmenite inclusions are restricted to the core regions corresponding to the change in chemical composition and Y – enrichment (see Figure 14G & Figure 15D). A garnet chemical compositional profile reveals a weak zoning at the rims (depletion of Xalm from 0.7 to 0.6 and enrichment of Xgrs from 0.1 to 0.2, see Figure 15). The average garnet composition is $Alm_{59-72}Grs_{10-21}Prp_{13-21}Sps_{1-4}$.

Biotite is rare and mainly a reaction product of amphibole and garnet (see Figure 14D). Certain platelets form sharp grain boundaries with amphibole, indicating equilibrium between those two minerals (see Figure 14G). The $Mg/(Mg+Fe^{2+})$ ratio is around 0.65. A slight enrichment of Xmg in matrix biotite is observed in sample 14SW03 (0.69). TiO_2 and F contens have average values of 1.44 wt% and 0.26 wt%, respectively. Highest values are found in biotite enclosed in amphibole (2.11 wt% TiO_2 and 0.34 wt% F, respectively). Table 11 shows representative compositions of biotite.

Chlorite, in type I amphibolite is part of the stable mineral assemblage, and is found as fine-grained aggregate but also as idiomorphic grains with up to 1000 µm in size (see Figure 14C). No difference in chemical composition between rim and core is noticed. The $Fe^{2+}/(Fe^{2+}+Mg)$ ratio is 0.25 (see Table 11). In type II amphibolite chlorite is present as secondary product of amphibole, biotite and garnet, and commonly intergrown with these grains.

White mica is confined to a few samples, mainly located in the matrix and shows clear plane cleavage in individual platelets of up to with 700 µm in size. Equilibrium between amphibole and white mica is observed (see Figure 14D). Na/(Na+K) is between 0.14 and 0.17. 3.18 Si/11 O is the average phengite content (see Table 11).

Rutile, up to 1 mm (see Figure 14H) is found at rims of garnet and amphibole, but occurs also in the matrix and shows exsolutions of ilmenite.

Figure 14 Field setting and microphotographs of amphibolite (A-H). (A) "Orkanger road cut"- outcrop illustrating the prominent wavy pegmatites within amphibolites. (B) Garnet accumulation, sample 14SW60. (C) Type I amphibolite with parallel nicols, indicating a clear schistosity chlorite nests, sample 14SW03. (D) Type II amphibolite with parallel nicols and peak paragenesis consisting of white mica, amphibole, garnet and plagioclase and rutile, sample 14SW09. Type II amphibolite with parallel (E) and crossed nicols (F) with gneissose texture, sample 14SW09. (G) Rare garnet with snowball pattern, sample 14SW22. (H) Rutile grains 1mm in size, sample 14SW22.

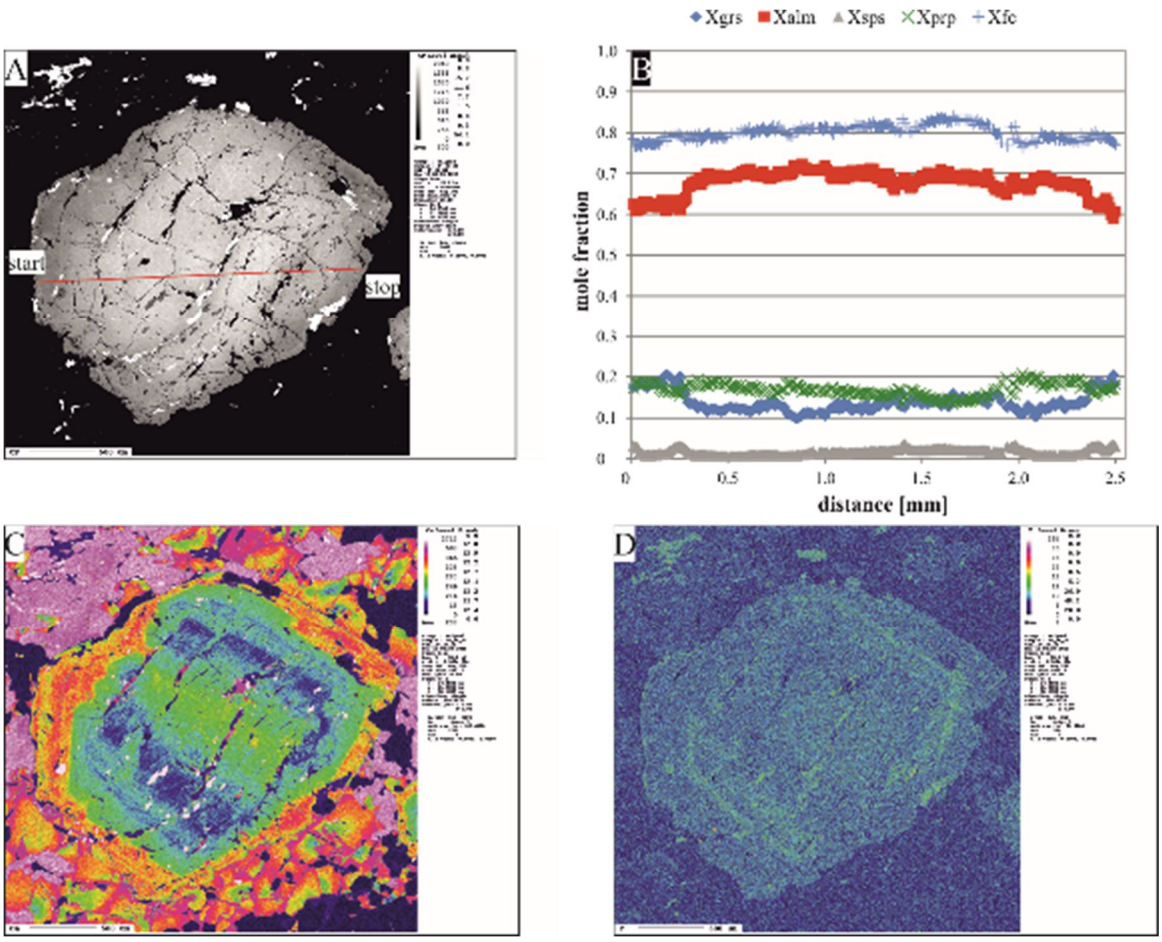

Figure 15 BSE images, compositional garnet profiles and element distribution maps of Ca and Y from garnet in amphibolite (A-D). (A) Helitic growth of inclusions is not continuous from core to rim. (B) Xgrs and Xalm indicate a chemical difference towards the rim, whereas Xprp and Xsps behave more constant throughout the profile. (C) Increase of Xgrs is also reflected in the element distribution map were enrichment is observed at the rim. (D) Distinct Y enrichment is found at the same location where the helitic growth pattern of inclusions ends.

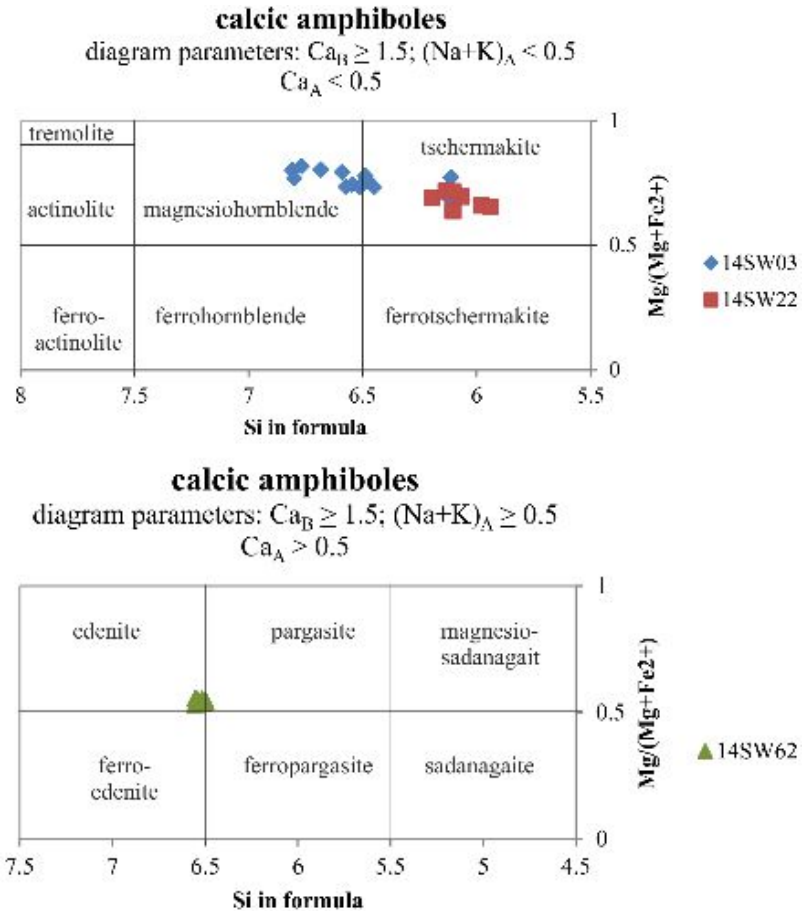

Figure 16 Classification of amphiboles in amphibolite after Leake et al., 1997. Sample 14SW03 and 14SW22 plot in the field of magnesiohornblende and tschermakite, respectively. Amphiboles in sample 14SW62 contain higher Na_2O values and can therefore be classified as pargasite/edenite.

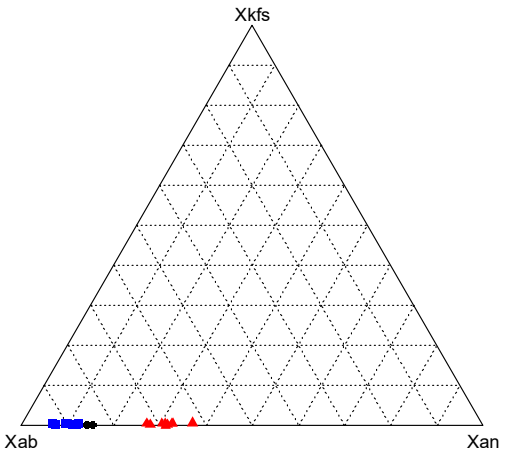

Figure 17 Ternary plot of feldspars in amphibolite. 23 Measurements in three samples reveal albite-rich feldspar, only sample 14SW22 contains a higher anorthite component. Black circles-sample 14SW03, blue squares-sample 14SW66, red triangles-sample 14SW22.

Table 10 Representative composition of amphibole in amphibolite.

Sample	14SW03	14SW03	14SW03	14SW03	14SW22	14SW22	14SW62	14SW62	14SW62	14SW62
Mineral	amp-rim	amp-core	amp-rim	amp-core	amp-adjacent to grt	amp-core	amp-rim	amp-core	amp-rim	amp-core
SiO2	47.45	46.12	43.07	43.55	43.14	42.25	43.32	43.48	43.32	43.09
TiO2	0.28	0.48	0.52	0.51	0.40	0.47	b.d.l.	b.d.l.	b.d.l.	1.03
Al2O3	13.16	13.51	18.58	18.87	17.08	16.37	13.11	12.95	13.60	13.48
Cr2O3	0.16	0.27	0.29	0.29	b.d.l.	b.d.l.	b.d.l.	b.d.l.	b.d.l.	b.d.l.
FeO	9.08	8.51	9.70	9.13	14.06	14.34	14.92	14.51	14.81	14.68
MnO	0.17	0.17	b.d.l.	0.13	b.d.l.	b.d.l.	b.d.l.	b.d.l.	b.d.l.	b.d.l.
MgO	14.71	14.44	12.16	12.78	11.88	11.94	9.66	9.83	9.15	9.51
CaO	10.93	11.27	11.32	11.15	10.70	10.41	10.66	10.95	10.51	10.39
Na2O	2.00	2.16	2.44	2.50	1.05	1.39	2.22	2.12	2.06	2.48
K2O	0.29	0.22	0.24	0.23	0.44	0.39	0.80	0.66	0.92	0.95
F	b.d.l.	0.16	0.18	0.10	n.d.	n.d.	b.d.l.	b.d.l.	b.d.l.	b.d.l.
Cl	0.09	b.d.l.	b.d.l.	b.d.l.	n.d.	n.d.	b.d.l.	b.d.l.	b.d.l.	b.d.l.
Total	**98.27**	**97.31**	**98.50**	**99.24**	**98.75**	**97.56**	**94.72**	**94.50**	**94.37**	**95.61**
Si per 23 O	6.683	6.589	6.120	6.112	6.134	6.102	6.543	6.552	6.554	6.497
Ti	0.030	0.052	0.056	0.051	0.043	0.051	0	0	0	0.117
Al(IV)	1.310	1.410	1.880	1.890	1.870	0.890	1.460	1.450	1.450	1.500
Al(VI)	0.870	0.870	1.230	1.230	0.990	1.900	0.880	0.850	0.980	0.900
Cr	0.018	0.030	0.033	0.032	0	0	0	0	0	0
Fe3+	0.301	0.207	0.217	0.281	0.677	0.714	0.114	0.059	0.058	0.068
Fe2+	0.761	0.810	0.935	0.792	0.995	1.019	1.77.	1.769	1.816	1.783
Mn	0.020	0.021	0	0.015	0	0	0	0	0	0
Mg	3.088	3.076	2.576	2.674	2.517	2.571	2.176	2.209	2.064	2.138
Ca	1.649	1.725	1.723	1.677	1.630	1.611	1.726	1.767	1.704	1.678
Na	0.546	0.598	0.672	0.680	0.289	0.390	0.649	0.620	0.603	0.726
K	0.052	0.040	0.044	0.041	0.081	0.072	0.154	0.127	0.177	0.183
F	0	0.070	0.080	0.040	0	0	0	0	0	0
Cl	0.020	0	0	0	0	0	0	0	0	0
cations	**15.330**	**15.428**	**15.486**	**15.477**	**15.226**	**15.320**	**15.473**	**15.403**	**15.406**	**15.590**

Table 11 Representative composition of chlorite, biotite and white mica in amphibolite.

Sample	14SW03	14SW03	14SW03	14SW03	14SW22	14SW22	14SW62	14SW03	14SW03	14SW03
Mineral	chl-adjacent to amp, core	chl-rim	chl-core	bt-matrix	bt-matrix	bt-matrix	bt-inclusion in amp	wm-matrix	wm-matrix	wm-matrix
SiO2	27.76	27.88	28.30	38.44	38.09	38.79	38.79	49.17	48.37	48.92
TiO2	b.d.l.	b.d.l.	b.d.l.	1.23	1.27	1.21	1.75	0.60	0.49	0.59
Al2O3	22.06	22.65	22.61	17.57	17.00	17.30	16.50	33.26	32.85	32.88
Cr2O3	0.25	0.16	0.16	0.18	0.02	0	0.07	0.61	0.42	0.38
FeO	14.44	13.50	13.64	12.73	14.76	14.64	14.67	1.09	0.90	1.08
MnO	b.d.l.	b.d.l.	b.d.l.	b.d.l.	0.02	0.05	0.02	b.d.l.	b.d.l.	b.d.l.
MgO	23.07	24.19	24.17	15.96	15.95	15.87	13.57	1.96	1.95	2.00
CaO	b.d.l.	b.d.l.	b.d.l.	b.d.l.	0.07	0.05	0.00	b.d.l.	b.d.l.	b.d.l.
Na2O	b.d.l.	b.d.l.	b.d.l.	0.10	0.30	0.27	0.27	1.25	1.25	1.11
K2O	b.d.l.	b.d.l.	b.d.l.	8.69	7.89	8.41	9.17	9.89	9.52	9.86
F	0.12	0.17	b.d.l.	0.16	0.16	0.23	0.32	b.d.l.	0.09	0.10
Cl	n.d.	b.d.l.	b.d.l.	n.d.	0.02	0.01	0.02	n.d.	n.d.	n.d.
Total	**87.70**	**88.55**	**88.88**	**95.06**	**95.65**	**96.83**	**94.75**	**97.74**	**95.94**	**96.92**
Si per 14/11 O	2.747	2.719	2.743	2.815	2.798	2.814	2.867	3.180	3.182	3.197
Ti	0	0	0	0.068	0.070	0.066	0.098	0.029	0.024	0.029
Al	2.573	2.604	2.583	1.516	1.472	1.479	1.453	2.535	2.547	2.528
Cr	0.020	0.012	0.012	0.010	0.001	0	0.004	0.031	0.022	0.040
Fe3+	0	0	0	0	0	0	0	0	0	0
Fe2+	1.195	1.101	1.106	0.780	0.906	0.889	0.916	0.055	0.050	0.059
Mn	0	0	0	0	0.001	0.003	0.007	0	0	0
Mg	3.403	3.517	3.492	1.742	1.746	1.716	1.51.	0.189	0.191	0.195
Ca	0	0	0	0	0.005	0.001	0	0	0	0
Na	0	0	0	0.014	0.042	0.038	0.039	0.154	0.172	0.140
K	0	0	0	0.812	0.748	0.779	0.874	0.816	0.799	0.821
F	0.040	0.050	0	0.08	0.038	0.052	0.076	0	0	0.040
Cl	n.d.	0	0	n.d.	0.002	0.001	0.002	n.d.	n.d.	n.d.
cations	**9.938**	**9.953**	**9.936**	**7.757**	**7.789**	**7.788**	**7.763**	**6.989**	**6.987**	**7.004**
Xmg/k	0.740	0.762	0.759	0.691	0.658	0.659	0.623	0.811	0.823	0.851
Xfe/ma	0.260	0.238	0.241	0.309	0.342	0.341	0.377	0.189	0.177	0.148

Table 12 Representative composition of garnet and feldspar in amphibolite.

Sample	14SW22	14SW22	14SW30	14SW30	14SW30	14SW06	14SW22	14SW22	14SW62	14SW62
Mineral	grt-rim	grt-core	grt-core	grt-rim	grt-core	pl-adjacent to amp	pl-matrix	pl-adjacent to grt	pl-matrix	pl-matrix
SiO2	37.74	36.97	38.32	38.54	38.52	64.16	60.43	60.51	66.13	67.40
TiO2	0.23	b.d.l.	b.d.l.	b.d.l.	b.d.l.	n.d.	n.d.	n.d.	n.d.	n.d.
Al2O3	21.05	20.78	21.45	21.51	21.59	23.05	25.23	24.80	21.06	20.20
Cr2O3	b.d.l.	b.d.l.	b.d.l.	b.d.l.	b.d.l.	n.d.	n.d.	n.d.	n.d.	n.d.
FeO	28.66	32.51	26.63	27.04	27.24	n.d.	b.d.l.	b.d.l.	b.d.l.	b.d.l.
MnO	0.97	0.76	1.27	1.49	1.84	n.d.	n.d.	n.d.	n.d.	n.d.
MgO	4.11	3.91	5.18	5.02	4.88	n.d.	n.d.	n.d.	n.d.	n.d.
CaO	6.99	4.55	6.23	6.85	6.46	3.37	6.70	6.22	2.35	1.36
Na2O	b.d.l.	b.d.l.	b.d.l.	b.d.l.	b.d.l.	9.52	7.73	7.86	10.37	11.02
K2O	b.d.l.	b.d.l.	b.d.l.	b.d.l.	b.d.l.	b.d.l.	b.d.l.	b.d.l.	b.d.l.	b.d.l.
Total	**99.75**	**99.48**	**99.38**	**100.78**	**100.93**	**100.10**	**100.07**	**99.39**	**99.89**	**99.98**
Si per 12/8 O	2.983	2.953	2.995	2.994	2.992	2.822	2.683	2.701	2.906	2.950
Ti	0.014	0	0	0	0	n.d.	n.d.	n.d.	n.d.	n.d.
Al	1.961	1.956	1.976	2.000	2.013	1.195	1.320	1.305	1.090	1.042
Cr	0	0	0	0	0	n.d.	n.d.	n.d.	n.d.	n.d.
Fe3+	0.050	0.134	0.083	0.071	0.001	n.d.	0	0	0	0
Fe2+	1.844	2.038	1.658	1.746	1.769	n.d.	0	0	0	0
Mn	0.065	0.051	0.101	0.098	0.121	n.d.	n.d.	n.d.	n.d.	n.d.
Mg	0.484	0.466	0.603	0.581	0.565	n.d.	n.d.	n.d.	n.d.	n.d.
Ca	0.592	0.389	0.522	0.570	0.538	0.159	0.319	0.297	0.110	0.064
Na	0	0	0	0	0	0.812	0.665	0.681	0.884	0.935
K	0	0	0	0	0	0	0	0	0	0
cations	**7.993**	**7.987**	**7.941**	**8.000**	**7.999**	**4.988**	**4.992**	**4.990**	**4.990**	**4.991**
Xalm/alb	0.618	0.692	0.574	0.583	0.591	0.836	0.672	0.692	0.889	0.936
Xgrs/Xan	0.198	0.132	0.181	0.190	0.180	0.164	0.323	0.302	0.111	0.064
Xsps/kfs	0.022	0.017	0.036	0.035	0.040	0	0	0	0	0
Xprp	0.162	0.158	0.209	0.194	0.189					
Xfe	0.792	0.814	0.733	0.750	0.758					

TONALITIC LAYER

The mineral assemblage consists of quartz, plagioclase, garnet, biotite, white mica, minor clinozoisite/epidote, retrograde chlorite, and amphibole. Accessory phases like titanite, apatite, tourmaline and pyrite, chalcopyrite and sphalerite. The porphyroblastic fabric consists of a quartzo-feldspatic matrix with interbedded garnets and scattered epidote, where micas appear as undeformed individual flakes (see Figure 18C & D). Alumosilicates and K-feldspar are missing.

Subhedral poikiloblastic garnet is smaller and more frequent in comparison with former lithologies, with maximum size of 1.5 mm. Inclusions of quartz (which again enclose albite), plagioclase, epidote, biotite and chlorite (see Figure 18E). Alteration to biotite and chlorite at rims is common. Epidote forms sharp adjacent grain boundaries (see Figure 18H). The average composition varies between $Alm_{26-66}Grs_{16-38}$ $Sps_{1-13}Prp_{1-10}$ (see Table 13). Ten compositional profiles, as well as BSE images and element distribution maps indicate a distinct chemical zoning of nearly all garnets investigated in this lithology (see Figure 19). Xsps stays homogeneous throughout the profile or shows bell-shaped form. Xprp is approximately constant and if not, it shows similar behavior as Xgrs. Latter varies from 0.37 in the outermost rim to 0.3 in the core. Xalm is depleted at rims (0.55) and reveals a broad core region of 0.6 mole fraction. The corresponding element distribution map of Ca and Y also support these two distinct zones (see Figure 19C & D & G & H).

Plagioclase forms individual grains with up to 3 mm and represents beside quartz the main constituent of the matrix. Polysynthetic twinning, antiperthites and inclusions of apatite are common (see Figure 18F). Average composition ranges from $Ab_{83-91}An_{8-16}Kfs_{0-1}$. Highest Xan values occur in matrix plagioclase at rims (see Table 14 and Figure 20). The core contains higher CaO values (2.81 wt%) compared to the rim where CaO content is 2.09 wt%. Plagioclase in vicinity of garnet is enriched in CaO (3.33 wt%)

Dark brown biotite is produced as reaction product around garnet rims, forms flakes up to 1mm in the matrix and is part of the stable assemblage. Biotite itself is occasionally decomposed to chlorite. The average Xmg is between 0.42 to 0.50, and highest TiO_2 contents are found in matrix biotite in vicinity of white mica (3.02 wt%), while lowest values (1.58 wt%) are found in matrix biotite of the same sample adjacent to plagioclase (14SW12). Maximum F content is 0.14 wt% in matrix biotite. No significant chemical difference can be observed

between core and rim and also not to grains adjacent to garnet (see Table 15). Highest Cl content is 0.08 wt% and found in biotite adjacent to garnet.

White mica forms euhedral colorless flakes up to 1mm in length, primary in contact with biotite but forms sharp grain boundaries with latter, so equilibrium between those two minerals is assumed (see Figure 18C). Na/(Na+K) shows no distinct variation (0.049-0.056) and all white micas can be classified as muscovite (K/(K+Na) is 0.944 to 0.951). Si/11 O ranges from 3.21 to 3.28 per formula. Representative compositions are shown in Table 15.

Idiomorphic or elongated epidote and clinozoisite, up to 140µm in size, occur frequently as minor constituent in the quartzo-feldspatic matrix but also in the proximity of garnet (see Figure 18E&G). Allanite core within single grains is common. BSE image reveals areas enriched in REE like Ce_2O_3 (0.57 wt%), Nd_2O_3 (0.23 wt%) and La_2O_3 (0.3 wt%) in contrast to depleted realms (Ce_2O_3 0.05 wt%, Nd_2O_3 & La_2O_3 zero). For representative compositions see Table 14).

Dark green to blue rare amphibole with distinct pleochroism forms anhedral grains and is only found in sample 14SW13 and 14SW41 (see Figure 18E) as inclusion in garnet or as alteration product of latter, and also in the matrix. Maximum size is 500 µm and after Leake et al., 1997 amphiboles in tonalitic dikes can be classified as ferropargasite. The $Mg/(Mg+Fe^{2+})$ ratio shows no variability and is 0.48 in average.

Equigranular quartz shows approximately straight grain boundaries und undulatory extinction.

Figure 18 Field setting and microphotographs of tonalitic layer (A-H). (A) "Orkanger road cut" - outcrop with highlighted layer of interest, sample 14SW12, 14SW13 and 14SW14 were taken from this location. (B) Detailed shot of lithology in the field. Overview of mineral assemblage with parallel nicols (C) and crossed nicols (D), sample 14SW12. (E) Sample 14SW41 which contains amphibole, with parallel nicols. (F) Plagioclase, up to 3mm in size with distinct polysynthetic twinning. (G) Indicated idiomorphic epidote. (H) Frequent apatite inclusions in plagioclase.

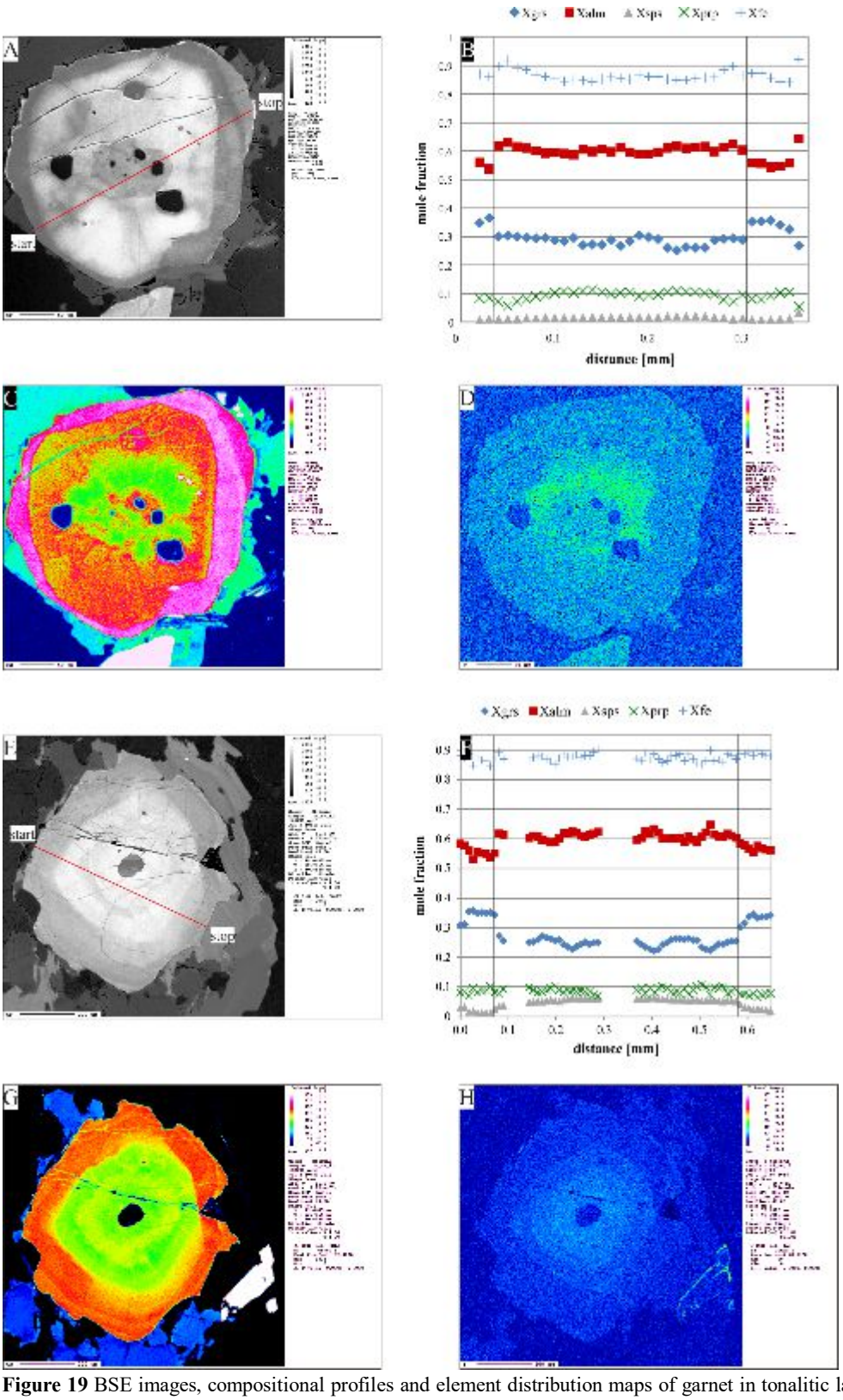

Figure 19 BSE images, compositional profiles and element distribution maps of garnet in tonalitic layer (A-H). (A) BSE image, (B) compositional profile, (C) element distribution map of Ca, and (D) of Y, sample 14SW41. The conspicuous pattern in the BSE image is reflected in the compositional profile at least for the rim, with an increase of Xgrs and decrease of Xalm, also visible in (C). The chemical difference of the core (A) and (D) is not pronounced in the compositional profile. (E) BSE image, (F) compositional profile, (G) element distribution map of Ca, and (H) of Y, sample 14SW12 with chlorite inclusion. Chemical change is reflected in all indicated by an increase of again Xgrs from 0.25 – 0.35 mole fractions and decrease in Xalm.

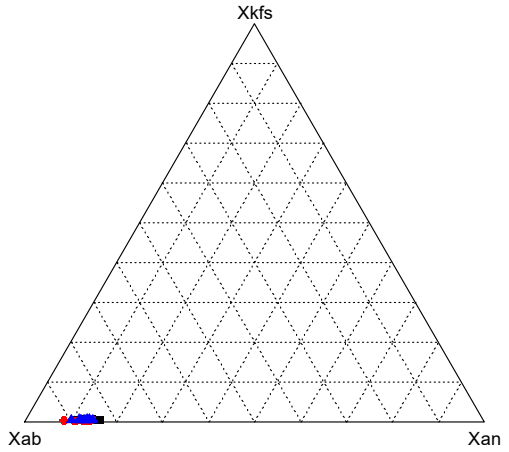

Figure 20 Ternary plot of feldspars in tonalitic layer. All samples can be classified as albite rich plagioclase. Sample 14SW12 red circles, sample 14SW41 black squares, sample 14SW42 blue triangles.

Table 13 Representative composition of garnet in tonalitic layer.

Sample	14SW12	14SW12	14SW12	14SW12	14SW12	14SW41	14SW41	14SW41	14SW42	14SW42
Mineral	grt-rim	grt-core	grt-rim	grt-mantle	grt-core	grt-rim	grt-mantle	grt-core	grt-rim	grt-mantle
SiO2	38.13	37.33	38.15	37.57	37.37	37.70	36.98	37.64	37.73	38.00
TiO2	b.d.l.	b.d.l.	b.d.l.	b.d.l.	b.d.l	b.d.l.	b.d.l.	b.d.l.	b.d.l.	b.d.l.
Al2O3	20.67	20.18	20.89	21.02	20.50	21.30	20.57	20.72	21.11	20.96
Cr2O3	b.d.l.	b.d.l.	b.d.l.	b.d.l.	b.d.l	b.d.l.	b.d.l.	b.d.l.	b.d.l.	b.d.l.
FeO	25.89	27.93	25.42	27.75	28.50	25.10	29.52	28.52	28.99	27.08
MnO	0.66	2.90	0.69	2.37	2.62	0.36	0.65	0.85	0.63	0.57
MgO	2.17	2.50	1.80	2.23	2.19	2.32	1.85	2.89	2.63	2.36
CaO	12.31	8.65	12.57	9.29	8.20	12.87	10.38	9.30	10.14	11.39
Na2O	n.d.	n.d.	n.d	n.d.	n.d.	b.d.l.	b.d.l.	b.d.l.	b.d.l.	b.d.l.
K2O	n.d.	n.d.	n.d	n.d.	n.d.	b.d.l.	b.d.l.	b.d.l.	b.d.l.	b.d.l.
Total	**99.83**	**99.49**	**99.52**	**100.23**	**99.38**	**99.65**	**99.95**	**99.92**	**101.23**	**100.36**
Si per 12 O	3.014	2.987	3.026	2.983	3.001	2.974	2.945	2.979	2.950	2.992
Ti	0	0	0	0	0	0	0	0	0	0
Al	1.925	1.903	1.953	1.967	1.940	1.980	1.931	1.933	1.945	1.945
Cr	0	0	0	0	0	0	0	0	0	0
Fe3+	0.033	0.118	0	0.074	0.051	0.07	0.184	0.096	0.159	0.075
Fe2+	1.679	1.751	1.686	1.768	1.863	1.585	1.782	1.792	1.736	1.708
Mn	0.044	0.197	0.046	0.159	0.178	0.024	0.044	0.057	0.042	0.038
Mg	0.256	0.298	0.213	0.264	0.262	0.273	0.220	0.341	0.307	0.277
Ca	1.042	0.742	1.068	0.790	0.706	1.088	0.886	0.789	0.849	0.961
Na	0	0	0	0	0	0	0	0	0	0
K	0	0	0	0	0	0	0	0	0	0
cations	**7.993**	**7.996**	**7.992**	**8.005**	**8.001**	**7.994**	**7.992**	**7.987**	**7.988**	**7.996**
Xgrs	0.345	0.248	0.354	0.265	0.235	0.366	0.302	0.265	0.289	0.322
Xalm	0.556	0.586	0.560	0.593	0.619	0.534	0.608	0.602	0.592	0.572
Xsps	0.015	0.066	0.015	0.053	0.059	0.008	0.015	0.019	0.014	0.013
Xprp	0.085	0.100	0.071	0.089	0.087	0.092	0.075	0.114	0.105	0.093
Xfe	0.868	0.855	0.888	0.870	0.877	0.853	0.890	0.840	0.850	0.860

Table 14 Representative composition of feldspar and epidote in tonalitic layer.

Sample	14SW12	14SW12	14SW12	14SW41	14SW42	14SW42	14SW12	14SW12	14SW12	14SW12
Mineral	pl-matrix	pl-adjacent to grt	pl-adjacent to wm	pl-matrix	pl-vicinity of grt	pl-matrix	ep-core	ep-rim	ep-rim	ep-adjacent to grt
SiO2	65.76	65.02	65.00	65.24	65.10	65.87	38.04	38.28	38.21	38.08
TiO2	n.d.	n.d.	n.d.	b.d.l.	b.d.l.	b.d.l.	0.24	b.d.l.	b.d.l	0.30
Al2O3	21.80	21.65	21.57	22.58	21.68	21.52	26.21	27.26	26.01	27.34
Fe2O3	n.d.	n.d.	n.d.	b.d.l.	b.d.l.	b.d.l.	10.14	8.76	10.19	8.88
MnO	n.d.	n.d.	n.d.	b.d.l.	b.d.l.	b.d.l.	b.d.l	b.d.l.	b.d.l	b.d.l
MgO	n.d.	n.d.	n.d.	b.d.l.	b.d.l.	b.d.l.	b.d.l	b.d.l.	b.d.l	b.d.l
CaO	2.84	2.21	2.94	3.33	2.82	2.56	23.90	24.23	24.25	24.04
Na2O	10.29	10.24	10.26	9.73	10.40	10.39	b.d.l	b.d.l.	b.d.l	b.d.l
K2O	0.17	0.08	0.16	0.10	0.09	0.11	b.d.l	b.d.l.	b.d.l	b.d.l
Ce2O3	n.d.	n.d.	n.d.	n.d.	n.d.	n.d.	b.d.l	b.d.l.	b.d.l	b.d.l
Nd2O3	n.d.	n.d.	n.d.	n.d.	n.d.	n.d.	b.d.l	b.d.l.	b.d.l	b.d.l
La2O3	n.d.	n.d.	n.d.	n.d.	n.d.	n.d.	b.d.l	b.d.l.	b.d.l	b.d.l
Total	**100.86**	**99.20**	**99.93**	**100.98**	**100.09**	**100.45**	**98.53**	**98.53**	**98.66**	**98.64**
Si per 8/12.5 O	2.872	2.879	2.868	2.845	2.866	2.884	2.971	2.972	2.978	2.959
Ti	n.d.	n.d.	n.d.	0	0	0	0.014	0	0	0.018
Al	1.122	1.130	1.122	1.160	1.125	1.111	2.413	2.494	2.389	2.504
Fe3−	n.d.	n.d.	n.d.	0	0	0	0.596	0.512	0.598	0.519
Mn	n.d.	n.d.	n.d.	0	0	0	0	0	0	0
Mg	n.d.	n.d.	n.d.	0	0	0	0.010	0.008	0.008	0.006
Ca	0.133	0.105	0.139	0.156	0.133	0.120	2.000	2.016	2.025	2.001
Na	0.871	0.879	0.878	0.823	0.888	0.882	0	0	0	0
K	0.009	0.005	0.009	0.006	0.005	0.006	0	0	0	0
Ce3+	n.d.	n.d.	n.d.	n.d.	n.d.	n.d.	0	0	0	0
Nd	n.d.	n.d.	n.d.	n.d.	n.d.	n.d.	0	0	0	0
La	n.d.	n.d.	n.d.	n.d.	n.d.	n.d.	0	0	0	0
cations	**5.007**	**4.998**	**5.016**	**4.990**	**5.017**	**5.003**	**8.004**	**7.997**	**7.998**	**8.007**
Xab	0.860	0.889	0.856	0.836	0.865	0.875				
Xan	0.131	0.106	0.135	0.158	0.130	0.119				
Xkfs	0.009	0.005	0.009	0.006	0.005	0.006				

Table 15 Representative composition of biotite and white mica in tonalitic layer.

Sample	14SW12	14SW12	14SW41	14SW42	14SW42	14SW12	14SW12	14SW12	14SW12	14SW12
Mineral	bt-matrix	bt-adjacent to grt	bt-matrix	bt-matrix	bt-matrix	wm-matrix	wm-vicinity of grt	wm-matrix	wm-matrix	wm-matrix
SiO2	35.92	37.24	36.51	36.60	36.59	48.14	48.22	48.47	48.25	47.76
TiO2	3.00	2.28	1.91	2.50	2.45	0.77	1.07	1.01	0.95	1.02
Al2O3	17.03	16.40	15.87	16.20	16.69	28.76	28.88	29.96	28.97	29.49
Cr2O3	b.d.l.	b.d.l.	b.d.l.	b.d.l.	b.d.l	b.d.l.	b.d.l.	b.d.l.	b.d.l.	b.d.l.
FeO	21.26	21.42	21.95	19.65	19.61	3.55	3.37	3.31	3.34	3.31
MnO	b.d.l.	0.13	b.d.l.	b.d.l.	b.d.l	b.d.l.	b.d.l.	b.d.l.	b.d.l.	b.d.l.
MgO	9.64	9.56	9.98	10.41	10.14	2.02	2.28	2.12	2.37	2.02
CaO	b.d.l.	b.d.l.	b.d.l.	b.d.l.	b.d.l	b.d.l.	b.d.l.	b.d.l.	b.d.l.	b.d.l.
Na2O	0.11	0.07	b.d.l.	0.20	0.19	0.37	0.42	0.38	0.37	0.39
K2O	9.44	9.10	9.53	9.79	9.43	10.59	10.70	10.53	10.71	10.58
F	0.36	0.33	0.14	b.d.l.	b.d.l	0.16	0.88	0.18	b.d.l.	0.19
Cl	0.07	0.08	0.02	b.d.l.	b.d.l	b.d.l.	b.d.l.	b.d.l.	b.d.l.	b.d.l.
Total	**96.83**	**96.61**	**95.91**	**95.35**	**95.1**	**94.36**	**95.82**	**95.96**	**94.96**	**94.76**
Si per 11 O	2.728	2.823	2.799	2.792	2.791	3.280	3.260	3.239	3.261	3.239
Ti	0.171	0.130	0.110	0.144	0.140	0.039	0.054	0.051	0.048	0.052
Al	1.525	1.465	1.434	1.456	1.500	2.309	2.301	2.36	2.308	2.357
Cr	0	0	0	0	0	0	0	0	0	0
Fe3+	0	0	0	0.005	0.001	0	0	0	0	0
Fe2+	1.351	1.358	1.408	1.254	1.251	0.202	0.191	0.185	0.189	0.188
Mn	0	0.008	0	0	0	0	0	0	0	0
Mg	1.092	1.081	1.141	1.184	1.153	0.205	0.230	0.211	0.239	0.204
Ca	0	0	0	0	0	0	0	0	0	0
Na	0.016	0.010	0	0.029	0.028	0.049	0.055	0.049	0.048	0.051
K	0.915	0.880	0.932	0.953	0.918	0.921	0.923	0.898	0.923	0.915
F	0.170	0.160	0.034	0	0	0.070	0.040	0.080	0	0.080
Cl	0.020	0.020	0.003	0	0	0	0	0	0	0
cations	**7.798**	**7.755**	**7.824**	**7.817**	**7.782**	**7.005**	**7.014**	**6.993**	**7.016**	**7.006**
Xmg	0.447	0.443	0.448	0.486	0.480					
Xk						0.949	0.944	0.948	0.951	0.947
Xna						0.051	0.056	0.052	0.049	0.053

CALC-SILICATE ROCK

The dominating minerals are clinopyroxene, clinozoisite/epidote, amphibole, garnet and plagioclase. Minor constitutes are quartz, biotite, titanite, calcite and white mica. Accessory pyrite, apatite, ilmenite, rutile, allanite and zircon are found. The granoblastic fabric is made up of aggregates of garnet, clinopyroxene and clinozoisite/epidote. Figure 21C & D illustrate the typical mineral assemblage.

Colorless to green clinopyroxene is up to 2 mm in size and represents one of the main constituent of this lithology. Occurrence in the vicinity of garnet is common. Grain boundaries are sub- to anhedral and twinning are observed (see Figure 21E). Inclusion minerals are quartz, biotite, amphibole and plagioclase. At the rims clinopyroxene is sometimes replaced by amphibole. Mineral chemical analyses were calculated after Morimoto, 1988 on the base of 4 cations and 6 O and all samples can be can be classified as diopside. Individual grains are inhomogeneous and chemical difference is essentially caused by Na_2O (1.33 wt% respectively 0.86 wt%) as shown in Figure 21B. Xmg ranges from 0.59 tio0.76 and highest values are found at rims. For composition clinopyroxene see Table 16.

Clinozoisite occurs in two textural positions. One forming big anhedral grains with characteristic anormal blue interference color whereas the second appears as small euhedral crystals within the matrix and grey interference color (see Figure 21C & D). First-generation-clinozoisite contains non-orientated ellipsoid and flame - shaped inclusions of quartz (see Figure 21F). Fe_2O_3 is enriched at rims (2.28 wt%) in contrast to core composition (1.69 wt%), see Table 18 for compositions.

Subhedral, poikiloblastic garnet is up to 4mm in diameter and comprises inclusions of quartz, rutile, plagioclase, calcite, titanite, chlorite, clinozoisite and ilmenite. CaO decreases from core to rim from 16.61 wt % to 13.60 wt% and MnO and MgO are increasing slightly from core to rim (1.03 wt% to 1.47 wt% and 0.99 wt% to 2.60 wt%, respectively), for compositions see Table 17. A compositional line exhibits a Grs- and Alm - rich garnet with average composition varying between $Alm_{39-52}Grs_{38-52}Prp_{3-9}Sps_{2-5}$. The BSE image indicates chemical heterogeneity, but no distinct zoning pattern can be observed (see Figure 22).

Brownish biotite is rarely found and if present forms flakes and exhibits clear cleavage. No clear chemical difference can be observed between matrix biotite and biotite adjacent to clinopyroxene, garnet or clinozoisite. Xmg varies between 0.503 to 0.589 and the TiO_2

maximum is 1.83 wt%, found in a grain adjacent to clinopyroxene. Table 18 shows selected compositions of biotite.

Dark green subhedral amphibole occurs in different modifications. In sample 98848 and 98850 amphibole is more common, whereas in sample 14SW36 and 98812 amphiboles is rare and mainly an alteration product of garnet and clinopyroxene. Inclusions are rare and quartz is the main phase found. After Leake et al., 1997 all amphiboles belong to the group of calcic amphiboles, and are classified as ferropargasite, pargasite, magnesiohornblende as illustrated in Figure 24 (Fe^{3+} calculated after Leake et al., 1997). There is a decrease from rim to core in MgO (13.24 wt% to 9.17 wt% and SiO_2 (48.62 wt% to 41.58 wt%) and an increase in Al_2O_3 (6.57 wt% to 15.15 wt%) and Na_2O (0.90 wt% to 2.15wt%). See Table 18 for compositions.

Plagioclase is part of the matrix but also found as inclusion in garnet, clinopyroxene and amphibole. Feldspars in sample 98850 and 14SW36 can be classified as albite rich plagioclase (see Figure 23). Plagioclase inclusions are depleted in CaO in comparison to matrix plagioclase (0.73 wt% to 2.55 wt%) and slightly enriched in Na_2O (10.37 wt% to 11.25 wt%). Scattered antiperthite contains K-feldspars exsolutions which are too small to measure. For compositions see Table 17.

K-feldspar is found as inclusion in chlorite (sample 14SW36) but also scattered in the matrix. K-feldspar in sample 98812 is observed only adjacent to garnet. For compositions see Table 17.

Quartz is found in the matrix and also within clinopyroxene and garnet. The grain size varies and grain boundaries are sutured.

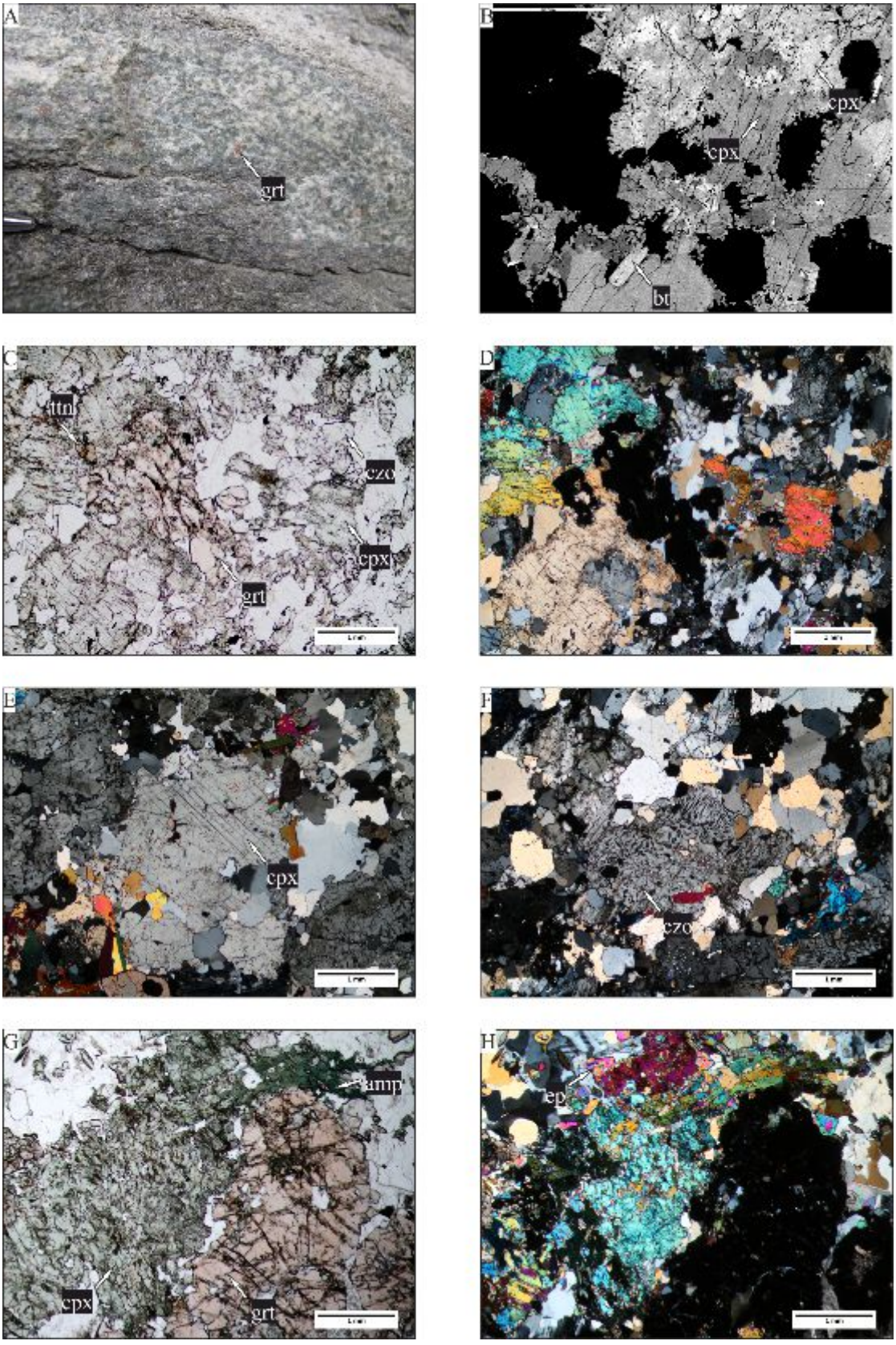

Figure 21 Field setting, photomicrographs and BSE image of calc-silicate rock (A-H). (A) Outcrop situation of calc-silicate rock with macroscopic garnet and clinopyroxene. (B) BSE image of clinopyroxene with chemical inhomogeneity, sample 98812. (C) Overview of mineral assemblage, parallel nicols, sample 14SW36. (D) Overview of mineral assemblage, crossed nicols, sample 14SW36. (E) Sample 98812 with exsolution lamellae of clinopyroxene, crossed nicols. (F) Sample 14SW36 under crossed nicols with anhedral clinozoisite which encloses patchy inclusions of quartz. (G) Amphibole and epidote bearing calc-silicate, parallel nicols, and (H) with crossed nicols, sample 98850.

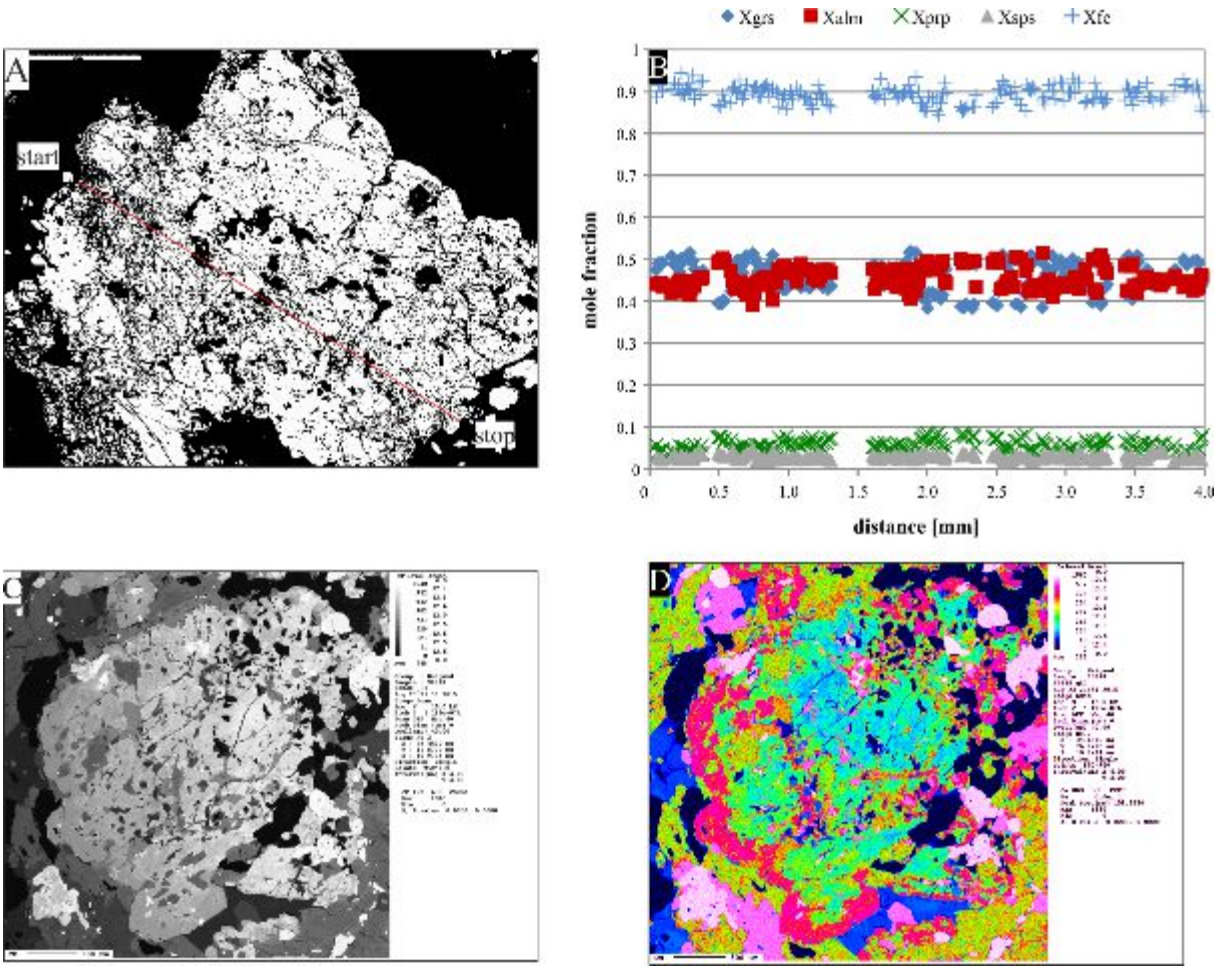

Figure 22 BSE image, compositional profile and element distribution map of garnet in calc-silicate rock (A-D). (A) BSE image indicates chemical inhomogeneity with areas enriched in Xgrs and depleted in Xalm (darker). (B) This imhomogeneity is reflected in the compositional profile, were Xsps and Xprp are constant throughout the profile. Xgrs and Xalm fluctuate between 0.4 and 0.5 mole fraction. BSE image (C) and element distribution map of Ca (D) indicates a diffuse chemical zoning with enriched realms at rims, sample 98848.

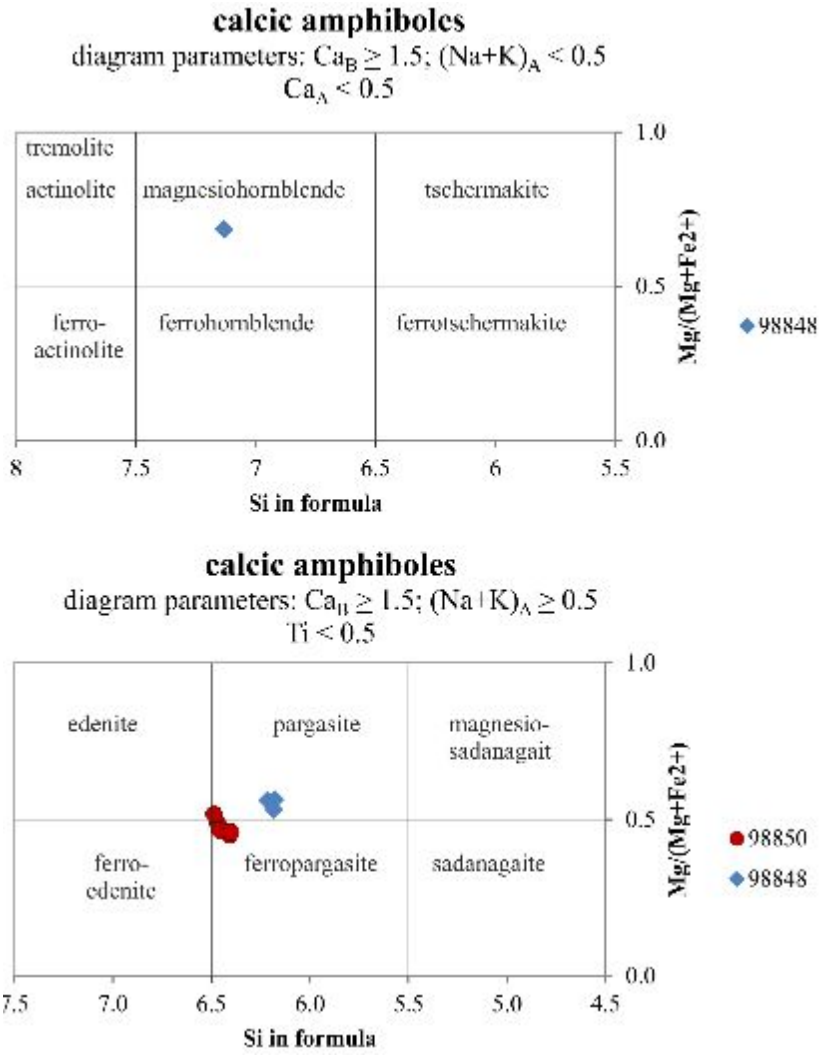

Figure 24 Classification of amphiboles in calc-silicate rock after Leake et al., 1997. The majority of samples plot at the boundary of pargasite and ferropargasite. One measurement of sample 98848, located at the rim of the grain, is depleted in $(Na+K)_A$ and therefore classified as magnesiohornblende.

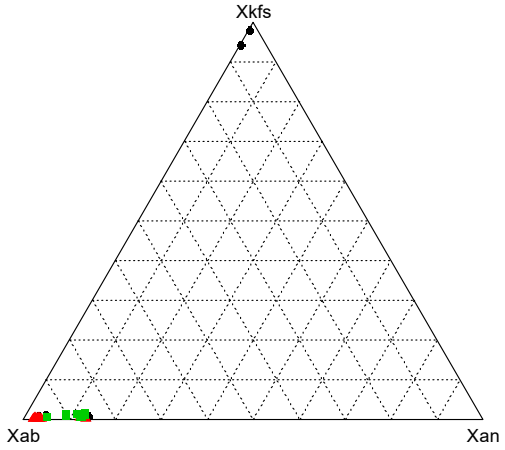

Figure 23 Ternary plot of feldspars in calc-silicate rock. 24 measurements in three samples are illustrated. Feldspars in sample 98812 - black dots- can be classified as orthoclase an oligoclase, sample 98850 - red dots - and sample 14SW36 - green triangles - comprise albite and oligoclase.

Table 16 Representative composition of clinopyroxene in calc-silicate rock.

Sample	14SW36	14SW36	14SW36	98812	98812	98812	98812	98850	98850	98850
Mineral	cpx-core	cpx-rim	cpx-core	cpx-core	cpx-core	cpx-core	cpx-rim	cpx-core	cpx-rim	cpx-rim
SiO2	53.88	53.50	53.82	52.46	53.39	53.51	53.64	52.64	53.13	53.06
TiO2	b.d.l.	b.d.l.	b.d.l.	b.d.l.	b.d.l	b.d.l.	b.d.l.	b.d.l.	b.d.l.	b.d.l.
Al2O3	1.91	1.64	1.54	1.64	1.91	1.93	0.80	1.01	1.51	1.01
Cr2O3	b.d.l.	b.d.l.	b.d.l.	b.d.l.	b.d.l	b.d.l.	b.d.l.	b.d.l.	b.d.l.	b.d.l.
FeO	8.95	8.36	8.40	10.33	9.53	7.90	8.79	11.71	12.05	11.60
MnO	0.25	0.23	0.30	b.d.l.	0.17	0.21	0.24	0.18	0.16	0.20
MgO	12.14	13.56	13.33	11.81	12.39	13.52	12.90	11.67	11.18	11.07
CaO	21.26	22.14	22.04	22.57	21.80	22.56	22.69	21.65	21.22	21.89
Na2O	1.26	0.44	0.65	0.55	1.10	0.65	0.31	0.81	1.12	0.69
Total	**99.65**	**99.87**	**100.08**	**99.36**	**100.29**	**100.28**	**99.37**	**99.67**	**100.37**	**99.52**
Si per 6 O	2.010	1.990	1.990	1.980	1.980	1.980	2.010	1.987	1.991	2.008
Ti	0	0	0	0	0	0	0	0	0	0
Al	0.080	0.070	0.070	0.070	0.080	0.080	0.040	0.045	0.067	0.045
Cr	0	0	0	0	0	0	0	0	0	0
Fe3+	0	0	0	0	0.030	0	0	0.039	0.030	0
Fe2+	0.280	0.260	0.260	0.320	0.270	0.240	0.280	0.331	0.348	0.367
Mn	0.010	0.010	0.010	0	0.010	0.010	0.010	0.006	0.005	0.006
Mg	0.670	0.750	0.740	0.670	0.690	0.750	0.720	0.657	0.625	0.624
Ca	0.850	0.880	0.880	0.910	0.870	0.890	0.910	0.876	0.852	0.887
Na	0.090	0.030	0.050	0.040	0.080	0.050	0.020	0.059	0.081	0.051
cations	**3.990**	**3.990**	**4.000**	**3.990**	**4.010**	**4.000**	**3.990**	**4.000**	**3.999**	**3.988**
Xmg	0.707	0.743	0.739	0.677	0.719	0.758	0.720	0.665	0.642	0.630

Table 17 Representative composition of garnet and feldspar in calc-silicate rock.

Sample	14SW36	98812	98848	98850	14SW36	14SW36	14SW36	98812	98850	98850
Mineral	grt-rim	grt-rim	grt-core	grt-core	kfs-exsolution	pl-matrix	pl-matrix	kfs-adjacent to grt	pl-inclusion in grt	pl-core
SiO2	38.11	38.01	38.22	38.33	64.73	66.00	66.30	65.05	67.54	67.67
TiO2	0.16	0.14	b.d.l	0.32	n.d.	n.d.	n.d.	n.d.	b.d.l	b.d.l.
Al2O3	20.95	21.52	21.31	21.44	18.12	21.55	21.42	17.94	19.87	19.92
Cr2O3	0.14	b.d.l	b.d.l	b.d.l	n.d.	n.d.	n.d.	n.d.	n.d.	n.d.
Fe2O3	0	0	0	0	n.d.	n.d.	n.d.	0.09	b.d.l	b.d.l.
FeO	21.39	19.31	28.33	20.44	n.d.	0	0	0	0	0
MnO	1.78	2.50	1.16	0.91	n.d.	n.d.	n.d.	n.d.	n.d.	n.d.
MgO	1.95	1.30	2.88	1.18	n.d.	n.d.	n.d.	n.d.	b.d.l	b.d.l.
CaO	14.79	17.36	8.97	17.17	b.d.l.	2.66	2.56	b.d.l.	0.51	0.62
BaO	n.d	n.d.	n.d	n.d	0.19	n.d.	n.d.	0.30	b.d.l	b.d.l.
Na2O	n.d.	n.d.	b.d.l	n.d	0.13	10.01	10.08	0.17	11.44	11.64
K2O	b.d.l	b.d.l	b.d.l	b.d.l	16.48	0.27	0.12	16.86	0.10	b.d.l.
Total	**99.27**	**100.14**	**100.87**	**99.79**	**99.65**	**100.49**	**100.48**	**100.41**	**99.46**	**99.85**
Si per 12/8 O	3.010	2.973	2.998	3.002	3.006	2.888	2.897	3.010	2.966	2.963
Ti	0.010	0.008	0	0.019	n.d.	n.d.	n.d.	n.d.	0	0
Al	1.950	1.984	1.970	1.979	0.992	1.111	1.103	0.978	1.029	1.028
Cr	0.010	0	0	0	n.d.	n.d.	n.d.	n.d.	n.d.	n.d.
Fe3	0	0.054	1.832	0	n.d.	n.d.	n.d.	0.003	0	0
Fe2−	1.410	1.209	0.027	1.339	n.d.	0	0	0	0	0
Mn	0.120	0.166	0.077	0.060	n.d.	n.d.	n.d.	n.d.	n.d.	n.d.
Mg	0.230	0.152	0.337	0.138	n.d.	n.d.	n.d.	0	0	0
Ca	1.250	1.455	0.754	1.441	0	0.125	0.120	0	0.024	0.029
Ba	n.d.	n.d.	n.d.	n.d	n.d.	n.d.	n.d.	0.005	0	0
Na	n.d.	n.d.	0	n.d	0.012	0.849	0.854	0.015	0.974	0.988
K	0	0	0	0	0.976	0.015	0.007	0.995	0.006	0
cations	**7.990**	**8.001**	**7.995**	**7.978**	**4.986**	**4.988**	**4.981**	**5.006**	**4.999**	**5.008**
Xgrs/Xab	0.415	0.488	0.251	0.484	0.012	0.858	0.871	0	0.970	0.969
Xalm/Xan	0.469	0.405	0.611	0.046	0.003	0.126	0.122	0.015	0.024	0.028
Xsps/Xkfs	0.039	0.056	0.026	0.020	0.985	0.015	0.007	0.988	0.006	0.003
Xprp	0.076	0.051	0.112	0.450						
Xfe	0.860	0.888	0.074	0.907						

Table 18 Representative composition of amphibole, biotite and clinozoisite in calc-silicate rock.

Sample	98848	98848	98850	98850	98812	98812	98812	98812	98850	98850
Mineral	amp-rim	amp-core	amp-core	amp-core	bt-matrix	bt- adjacent to grt	czo-rim	exo-rim	czo-rim	czo-rim
SiO2	41.52	41.58	43.89	42.47	36.64	36.12	39.51	39.96	39.17	38.71
TiO2	0.72	0.89	0.44	0.64	1.70	0.99	0.24	b.d.l.	0.27	0.22
Al2O3	15.22	15.15	12.10	12.82	16.66	15.92	31.70	32.91	28.17	29.06
Cr2O3	b.d.l.	b.d.l.	b.d.l.	b.d.l.	n.d.	n.d.	n.d.	n.d.	0.13	b.d.l.
Fe2O3	0	0	0	0	0	0	2.28	1.69	7.07	6.77
FeO	15.86	16.68	19.40	19.60	18.37	20.59	0	0	0	0
MnO	b.d.l.	b.d.l.	0.31	0.20	0.21	0.24	b.d.l.	b.d.l.	b.d.l.	b.d.l.
MgO	9.12	9.17	9.34	8.18	13.05	11.69	b.d.l.	b.d.l.	b.d.l.	0.51
CaO	10.52	10.48	10.60	10.52	b.d.l.	b.d.l.	25.13	25.23	22.74	22.79
Na2O	2.35	2.15	1.77	1.70	0.24	0.04	b.d.l.	b.d.l.	b.d.l.	b.d.l.
K2O	1.31	1.36	1.09	1.31	10.35	9.40	b.d.l.	b.d.l.	b.d.l.	b.d.l.
F	b.d.l.	0.16	0.29	0.30	0.32	0.42	n.d.	n.d.	n.d.	n.d.
Cl	0.08	0.03	b.d.l.	b.d.l.	b.d.l.	b.d.l.	n.d.	n.d.	n.d.	n.d.
Total	**96.70**	**97.65**	**99.23**	**98.04**	**97.54**	**95.41**	**98.86**	**99.79**	**97.55**	**98.06**
Si per 23/11/12.5 O	6.215	6.177	6.487	6.404	2.740	2.780	2.990	2.990	3.035	2.985
Ti	0.081	0.099	0.049	0.073	0.100	0.060	0.010	0	0.016	0.013
Al (IV)	1.760	1.800	1.510	1.600						
Al (VI)	0.940	0.860	0.600	0.680	1.470	1.450	2.830	2.900	2.573	2.641
Cr	0	0	0	0	n.d.	n.d.	n.d.	n.d.	0.008	0
Fe3+	1.593	1.575	0.477	0.330	0	0	0.130	0.100	0.412	0.393
Fe2+	0.393	0.497	1.921	2.141	1.150	1.330	0	0	0	0
Mn	0	0	0.039	0.026	0.010	0.020	0	0	0	0
Mg	2.035	2.031	2.058	1.839	1.460	1.340	0	0	0	0.059
Ca	1.687	1.668	1.678	1.748	0	0	2.040	2.020	1.888	1.883
Na	0.682	0.619	0.507	0.497	0.040	0.010	0	0	0	0
K	0.250	0.258	0.206	0.252	0.990	0.920	0	0	0	0
F	0	0.075	0.140	0.140	0.070	0.100	n.d.	n.d.	n.d.	n.d.
Cl	0.020	0.008	0	0	0	0	n.d.	n.d.	n.d.	n.d.
cations	**15.636**	**15.584**	**15.532**	**15.590**	**7.960**	**7.910**	**8.000**	**8.010**	**7.932**	**7.974**
Xmg	0.838	0.803	0.517	0.462	0.559	0.502				

PEGMATITE

Three samples of pegmatites taken from different locations comprise the stable mineral assemblage quartz, plagioclase, white mica, clinozoisite, garnet, minor amphibole, and epidote. Biotite, K-feldspar and alumosilicates are missing or rare. Accessory phases are pyrite, rutile, apatite, titanite and calcite. The fabric varies from a clear fine-grained schistose (sample 14SW32) to a more coarse-grained magmatic texture (sample 14SW35), in which small garnet, clinozoisite and anhedral amphibole are interbedded (see Figure 25).

Scattered, subhedral garnet, up to 2 mm in size, encloses quartz, and rims are decomposed by biotite, and plagioclase. Garnet encloses plagioclase, chlorite and calcite. The composition is $Alm_{33-53}Grs_{32-50}Sps_{4-18}Prp_{0-6}$. Three compositional profiles of garnet from sample 14SW35 reveal almandine- and grossular - rich garnets, whit a rim composition of $Grs_{50}Alm_{36}Sps_{12}Prp_{2}$ and a core composition of $Grs_{40}Alm_{42}Sps_{15}Prp_{4}$. See Figure 26 for detailed description of garnet and Table 19 for representative compositions.

Plagioclase represents the main constituent of the matrix and is up to 3 mm in size. Inclusions of white mica, clinozoisite and amphibole are found (see Figure 25G). The average composition is $Ab_{78-96}An_{4-22}Kfs_{0-1}$ (Figure 27). Enclaves in garnet are depleted CaO (0.79 wt%, respectively) in comparison to matrix plagioclase (2.63 wt%, respectively) as shown in Table 21. Highest Xan values of 0.22 are found in the core of matrix plagioclase and lowest in grains adjacent to white mica (Xan = 0.10).

White mica is aligned parallel to the schistosity in sample 14SW32 (see Figure 25C & D), whereas in sample 14SW35 white mica appears as undeformed flakes up to 1 mm in size (see Figure 25E & F). Beside the textural difference there is also a chemical variation observed between those two samples. K/(K+Na) ranges from 0.96 to 0.98 in sample 14SW35, and is lower (0.78 to 0.89) in sample 14SW32. Phengite content ranges from 3.27 – 3.40 Si/11O in sample 14SW35 and from 3.15 - 3.20 Si/11O in sample 14SW32. See Table 20 for representative compositions.

Green, sub- to anhedral amphibole shows distinct cleavage of 124° and indicates equilibrium with white mica, plagioclase and garnet (see Figure 25C). No chemical zoning of individual grains can be observed. After Leake et al., 1997 amphiboles can be classified as tschermakite. Average Xmg in amphiboles is 0.55.

Sub- to anhedral clinozoisite is found in the matrix but also in vicinity of garnet forming skeletal clusters or even sometimes acicular grain shape (see Figure 25E&G). Also veins between plagioclase grains are filled up with clinozoisite. Grains in vicinity of garnet are enriched in Fe_2O_3 (3.07 wt%) in contrast to matrix crystals (1.85 wt%). See Table 21 for composition.

Quartz shows recrystallized fabric in sample 14SW32 (see Figure 25C & D), in contrast to sample 14SW35, where quartz is not common and forms straight grain boundaries (see Figure 25E & F).

Figure 25 Field setting and microphotographs of pegmatite (A-H). (A) Field setting of sample 14SW35. (B) Prominent felsic pegmatite of fine-grained type. (C) Overview of mineral assemblage, parallel nicols, sample 14SW32. (D) Sample 14SW32, crossed nicols, indicating the recrystallized quartz matrix. (E) Coarse grained type with white mica flakes and clinozoisite in veins of plagioclase crystals, sample 14SW35. (F) Sample 14SW35, crossed nicols. (G) Conspicuous white mica needles in plagioclase, sample 14SW32. (H) Fine-grained anhedral skeleton clinozoisite, sample 14SW35.

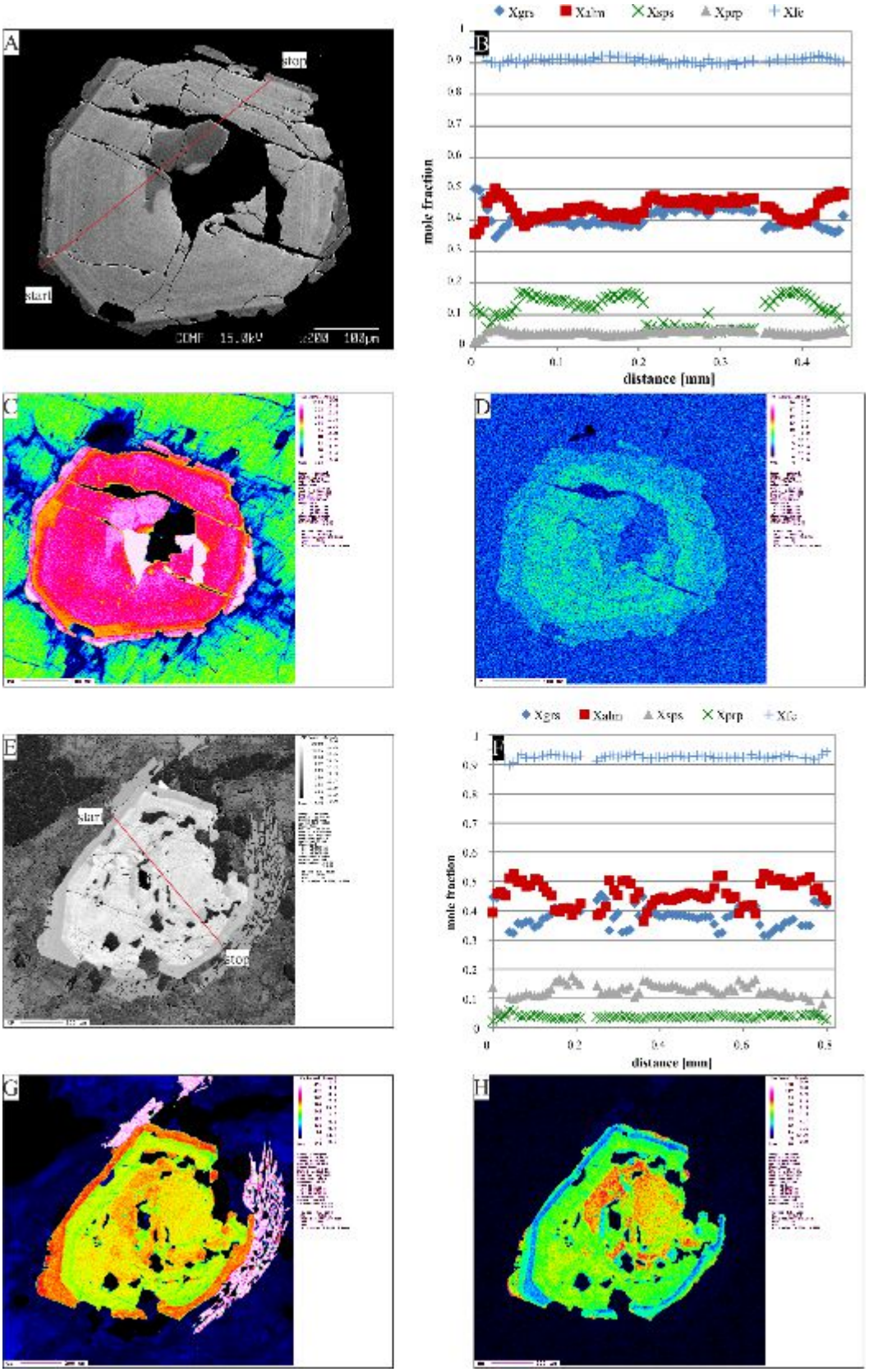

Figure 26 BSE image, composition profiles and element distribution maps of garnet in pegmatite (all images represents sample 14SW35) (A-H). (A) BSE image showing a distinct chemical difference in the outermost rim and again in the core. (B) Compositional profile with Xgrs decreasing from 0.5 to 0.4 from rim to mantle and contrary behavior of Xalm and Xprp, chemical difference of core is reflected in all endmembers and indicates a significant decrease of Xprp (0.15 to 0.05). (C) Element distribution map of Ca, with highest enrichment in core and outermost rim. (D) Element distribution map of Y. (E) BSE image of another garnet grain with again a distinct difference between rim and core. (F) Odd compositional profile with higher Xsps values than Xprp, (G) Element distribution map of Ca shows a distinct enrichment in the outermost core and again in the core. (H) Element distribution map of Mn supporting the trend of compositions profile.

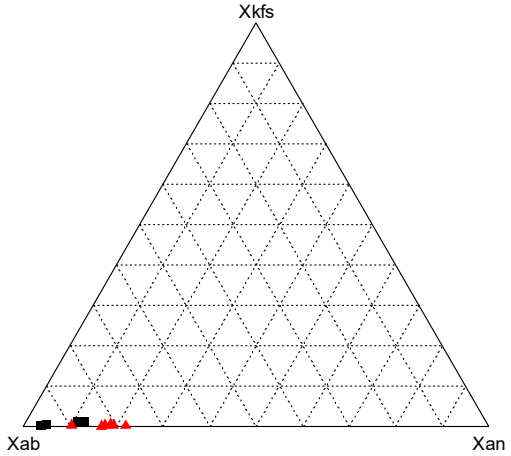

Figure 27 Ternary plot of feldspar in pegmatite. All samples can be classified as albite-rich plagioclase. Red triangles sample 14SW32, black squares sample 14SW35.

Table 19 Representative composition of garnet in pegmatite.

Sample	14SW35	14SW35	14SW35	14SW35	14SW35	14SW35	14SW35	14SW35	14SW35
Mineral	grt-rim	grt-transition	grt-core	grt-rim	grt-transition	grt-core	grt-rim	grt-transition	grt-core
SiO2	38.06	38.08	38.00	38.22	38.00	37.99	37.94	38.20	37.78
TiO2	b.d.l.	b.d.l.	0.50	b.d.l.	b.d.l.	0.50	b.d.l.	b.d.l.	0.38
Al2O3	21.65	21.55	20.82	21.68	21.20	21.05	21.29	21.09	20.71
Cr2O3	b.d.l.	b.d.l.	b.d.l.	b.d.l.	b.d.l.	b.d.l.	b.d.l.	b.d.l.	b.d.l.
FeO	19.18	21.86	20.42	20.89	22.70	19.93	16.97	22.52	20.36
MnO	4.74	1.93	5.64	2.83	4.80	6.36	4.95	4.55	5.80
MgO	0.74	1.05	0.89	0.94	1.04	0.84	0.60	1.36	1.10
CaO	15.26	15.21	13.42	15.80	12.41	13.55	17.56	12.22	14.10
Total	**99.62**	**99.68**	**99.68**	**100.36**	**100.14**	**100.22**	**99.30**	**99.94**	**100.23**
Si per 12 O	3.005	3.002	3.016	2.995	3.004	3.002	3.000	3.023	2.985
Ti	0	0	0	0	0	0	0	0	0
Al	2.014	2.003	1.947	2.003	1.975	1.960	1.983	1.967	1.929
Cr	0	0	0	0	0	0	0	0	0
Fe3+	0	0	0	0	0	0	0.007	0	0.058
Fe2+	1.266	1.441	1.355	1.369	1.501	1.318	1.114	1.491	1.287
Mn	0.317	0.129	0.379	0.188	0.322	0.426	0.331	0.305	0.388
Mg	0.087	0.124	0.105	0.110	0.122	0.099	0.070	0.161	0.130
Ca	1.291	1.284	1.141	1.326	1.051	1.147	1.487	1.036	1.194
cations	**7.980**	**7.983**	**7.943**	**7.991**	**7.975**	**7.952**	**7.992**	**7.983**	**7.971**
Xgrs	0.436	0.431	0.383	0.443	0.351	0.384	0.495	0.346	0.398
Xalm	0.428	0.484	0.455	0.457	0.501	0.441	0.371	0.498	0.429
Xsps	0.107	0.043	0.127	0.063	0.107	0.142	0.110	0.102	0.129
Xprp	0.029	0.042	0.035	0.037	0.041	0.033	0.023	0.054	0.043
Xfe	0.936	0.921	0.928	0.926	0.925	0.930	0.941	0.903	0.908

Table 20 Representative composition of white mica in pegmatite.

Sample	14SW32	14SW32	14SW32	14SW32	14SW32	14SW32	14SW32	14SW32
Mineral	wm-adjacent to pl	wm-matrix	wm-inclusion in pl	wm-matrix	wm-adjacent to amp	wm-matrix	wm-matrix	wm-matrix
SiO2	47.67	48.01	48.49	47.76	48.29	48.75	47.79	48.60
TiO2	0.56	0.69	0.23	0.56	0.68	0.43	0.47	0.36
Al2O3	33.22	32.36	33.14	33.02	32.28	32.96	33.56	33.35
Cr2O3	b.d.l.	b.d.l.	b.d.l.	b.d.l.	b.d.l.	b.d.l.	b.d.l.	b.d.l.
FeO	1.29	1.29	1.12	1.28	1.42	1.29	1.33	1.28
MnO	b.d.l.	b.d.l.	b.d.l.	b.d.l.	b.d.l.	b.d.l.	b.d.l.	b.d.l.
MgO	1.52	1.71	1.72	1.25	2.29	1.9	1.87	1.41
CaO	b.d.l.	b.d.l.	b.d.l.	b.d.l.	b.d.l.	b.d.l.	b.d.l.	b.d.l.
Na2O	1.41	1.41	1.45	1.62	1.32	1.18	1.36	1.67
K2O	9.19	9.16	9.26	8.98	9.17	9.62	9.30	8.75
F	b.d.l.	b.d.l.	b.d.l.	0.18	b.d.l.	0.14	b.d.l.	0.18
Cl	b.d.l.	b.d.l.	b.d.l.	b.d.l.	b.d.l.	b.d.l.	b.d.l.	b.d.l.
Total	**94.86**	**94.63**	**95.41**	**94.65**	**95.45**	**96.27**	**95.68**	**95.60**
Si per 11 O	3.168	3.198	3.198	3.185	3.192	3.198	3.149	3.199
Ti	0.028	0.035	0.011	0.028	0.034	0.021	0.023	0.018
Al	2.602	2.541	2.576	2.595	2.514	2.548	2.606	2.587
Cr	0	0	0	0	0	0	0	0
Fe3+	0	0	0	0	0	0	0	0
Fe2+	0.072	0.072	0.062	0.071	0.078	0.071	0.073	0.070
Mn	0	0	0	0	0	0	0	0
Mg	0.151	0.170	0.169	0.124	0.226	0.186	0.184	0.138
Ca	0	0	0	0	0	0	0	0
Na	0.182	0.182	0.185	0.209	0.169	0.150	0.174	0.213
K	0.779	0.779	0.779	0.764	0.773	0.805	0.782	0.735
F	0	0	0	0.040	0	0.030	0	0.040
Cl	0	0	0	0	0	0	0	0
cations	**6.982**	**6.977**	**6.980**	**6.976**	**6.986**	**6.979**	**6.991**	**6.960**
Xk	0.811	0.811	0.808	0.785	0.821	0.843	0.818	0.775
Xna	0.189	0.189	0.192	0.215	0.179	0.157	0.182	0.225

Table 21 Representative composition of feldspar and clinozoisite in pegmatite.

Sample	14SW32	14SW32	14SW32	14SW32	14SW32	14SW32	14SW35	14SW35	14SW35	14SW35	14SW35
Mineral	czo-adjacent to grt	czo-rim	czo-core	pl-matrix	pl-matrix	pl-matrix	pl-rim	pl-core	pl-rim	pl-adjacent to grt	pl-inclusion in grt
SiO2	39.61	39.41	39.77	63.56	61.79	65.11	65.94	65.28	65.47	65.88	68.61
TiO2	b.d.l.	b.d.l.	b.d.l.	n.d.	n.d.	n.d.	b.d.l.	b.d.l.	b.d.l.	b.d.l.	b.d.l.
Al2O3	31.36	31.22	31.94	22.67	23.54	21.1	21.94	21.60	21.57	21.38	19.80
Fe2O3	3.07	2.32	1.35	n.d.	n.d.	n.d	b.d.l	b.d.l.	b.d.l	b.d.l.	b.d.l
MnO	b.d.l.	b.d.l.	b.d.l	n.d.	n.d.	n.d	b.d.l	b.d.l.	b.d.l.	b.d.l.	b.d.l
MgO	b.d.l	b.d.l.	b.d.l	n.d.	n.d.	n.d	b.d.l	b.d.l.	b.d.l.	b.d.l.	b.d.l
CaO	23.11	24.27	24.39	3.62	4.12	2.21	2.63	2.58	2.63	2.29	0.79
Na2O	b.d.l.	b.d.l.	b.d.l	9.96	9.54	10.74	10.09	10.38	10.47	10.43	11.63
K2O	b.d.l	b.d.l.	b.d.l	b.d.l.	0.07	b.d.l.	b.d.l	b.d.l.	b.d.l.	b.d.l.	b.d.l
Total	**97.15**	**97.22**	**97.95**	**99.81**	**99.06**	**99.16**	**100.60**	**99.84**	**100.14**	**100.08**	**100.82**
Si per N12.5 O	3.038	3.029	3.025	2.813	2.763	2.888	2.876	2.874	2.875	2.890	2.976
Ti	0	0	0	n.d.	n.d.	n.d	0	0	0	0	0
Al	2.835	2.828	2.864	1.183	1.241	1.103	1.128	1.120	1.116	1.105	1.012
Fe3+	0.177	0.134	0.106	n.d.	n.d.	n.d	0	0	0	0	0
Mn	0	0	0	n.d.	n.d.	n.d	0	0	0	0	0
Mg	0	0	0	n.d.	n.d.	n.d	0	0	0	0	0
Ca	1.899	1.999	1.988	0.172	0.197	0.105	0.123	0.122	0.124	0.113	0.036
Na	0	0	0	0.855	0.827	0.924	0.853	0.886	0.891	0.887	0.978
K	0	0	0	0	0.004	0	0	0	0	0	0
cations	**7.949**	**7.99**	**7.983**	**5.023**	**5.032**	**5.020**	**4.980**	**5.002**	**5.006**	**4.995**	**5.002**
Xab				0.833	0.804	0.898	0.874	0.879	0.878	0.887	0.964
Xan				0.167	0.192	0.102	0.126	0.121	0.122	0.113	0.036
Xk/s				0	0.004	0	0	0	0	0	0

GEOCHEMISTRY OF MAJOR AND TRACE ELEMENTS

A whole rock data set of 70 samples from different lithologies of the Surna Nappe is presented in Appendix D. During sample preparation, attention was drawn to use fresh and unaltered samples, since secondary processes (e.g. oxidation, fluid infiltration and resulting element mobilization) influence the whole rock composition. The following investigations provide a broad data set of major and trace elements, of the different lithologies of the Surna Nappe, garnet – hornblende mica schists, amphibolites, and tonalitic layers. Appendix C illustrates sample locations of investigated samples.

GARNET – HORNBLENDE MICA SCHIST

Table 22 shows the average compositions of the major lithologies found in the Surna Nappe. For comparison Table 23 indicates average compositions of peltic and metamorphic rocks, after Miyashiro, 1973. For garnet-hornblende mica schists of the Surna Nappe Al_2O_3, Na_2O and K_2O values are lower than in two-mica schists, CaO, TiO_2 and MgO are higher than average two mica schists. Binary plots of major elements vs. SiO_2 (see Figure 29) reveal a negative correlation for Al_2O_3, MgO and Fe_{tot}. The classification of the protholith, as shown in Figure 28 after Werner, 1987 indicates no clear discrimination between magmatic or sedimentary origin of the protholith.

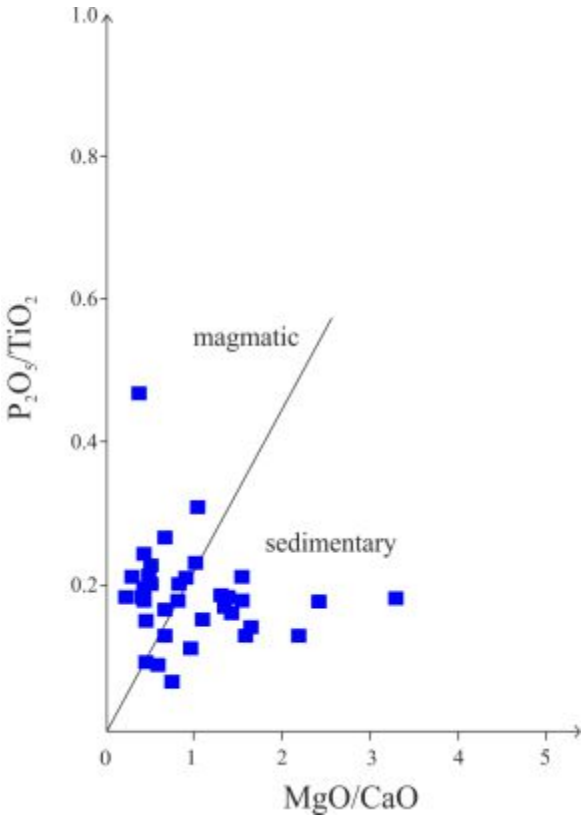

Figure 28 Discrimination diagram between magmatic or sedimentary protolith, after Werner, 1987, with indicate samples of garnet – hornblende mics schist. No clear origin can be determined. Both axes are in wt%.

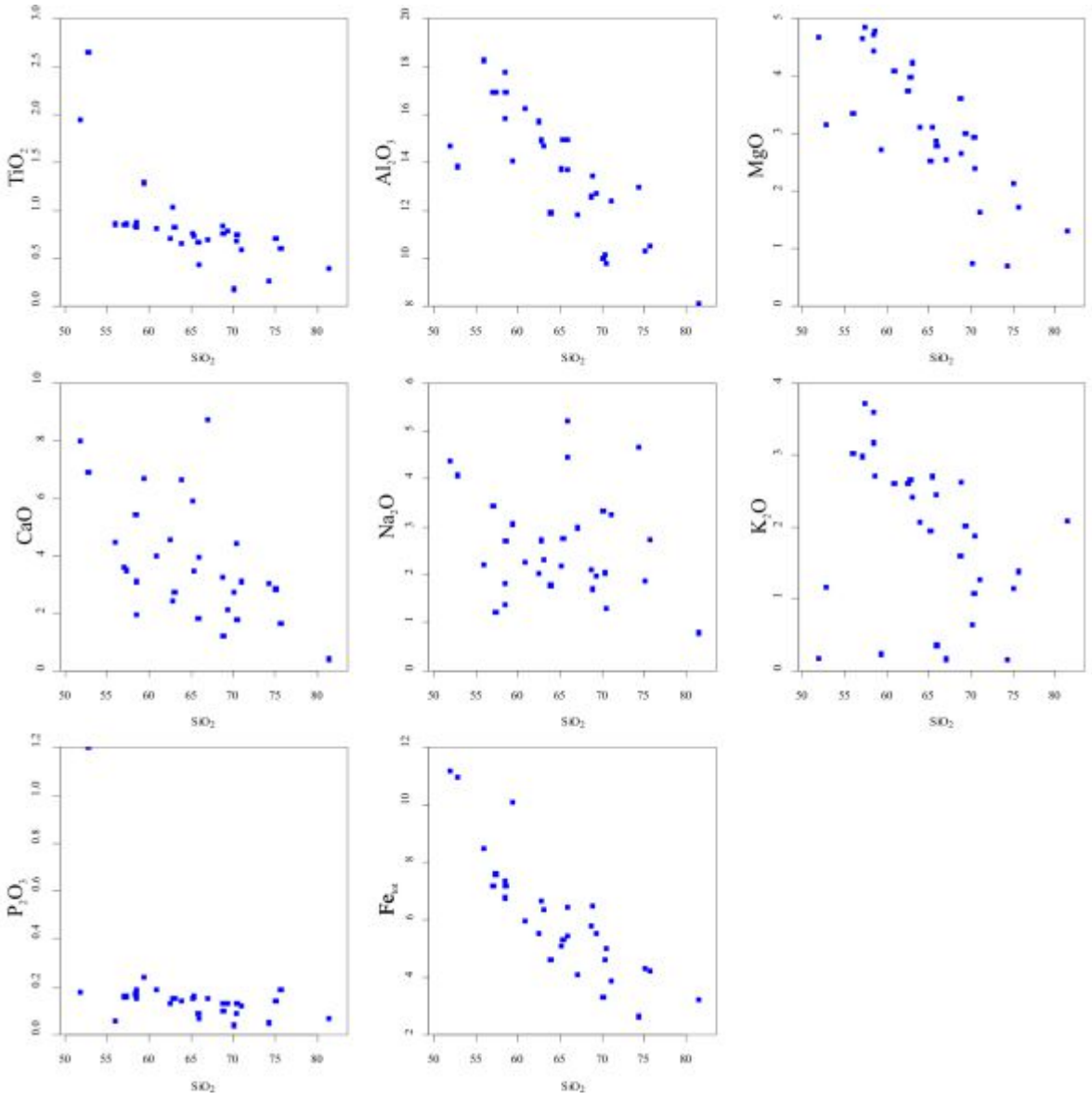

Figure 29 Binary plots of major elements vs. SiO_2, both axes in wt% of garnet – hornblende mica schists. Al_2O_3, MgO and Fe_{tot} indicate a negative correlation with increasing SiO_2 content.

Table 22 Average major and trace elements of garnet-hornblende mica schist, amphibolite and tonalitic layers, Surna Nappe.

Average major and trace elements of different lithologies in the Surna Nappe

	Grt-Hb-mica schist 36 samples	Amphibolite 10 samples	Tonaltic layers 5 samples
Major elements [wt%]	average	average	average
SiO_2	65.56	49.94	71.08
TiO_2	0.79	1.37	0.28
Al_2O_3	13.58	15.87	12.38
Fe_2O_3	6.54	10.92	4.48
MnO	0.09	0.16	0.08
MgO	3.01	5.88	1.05
CaO	3.92	9.94	3.04
Na_2O	2.78	2.82	3.89
K_2O	1.72	0.51	0.76
P_2O_5	0.16	0.20	0.06
LOI	1.08	1.09	0.38
trace elements [ppm]	average	average	average
Ba	265	151	103
Ce	54	71	35
Cr	162	132	50
Cs	28	26	<20
Cu	66	59	61
Ga	19	19	18
Nb	38	<20	38
Nd	38	46	29
Ni	84	66	<20
Pb	22	<20	<20
Rb	63	52	13
Sc	28	27	25
Sr	204	225	227
Th	<20	28	<20
U	<20	<20	<20
V	136	147	159
Y	33	40	29
Zn	83	80	64
Zr	145	184	88

Table 23 Average composition of pelitic and metamorphic rocks, after Miyashiro, 1973.

Average compositions of pelitic rocks of the worlds, after Miyashiro, 1973

	Clays, shales and slates 85 analysis		Phyllites, schists and gneisses 70 analysis	
	average	standard deviation	average	standard deviation
SiO_2	59.93	6.33	63.15	8.94
TiO_2	0.85	0.57	0.79	0.67
Al_2O_3	16.62	3.33	17.35	5.08
Fe_2O_3	3.03	2.08	2.00	1.66
FeO	3.18	1.84	4.71	2.44
MgO	2.63	1.98	2.31	1.82
CaO	2.18	2.54	1.24	0.92
Na_2O	1.73	1.27	1.96	1.06
K_2O	3.54	1.33	3.35	1.31
H_2O	4.34	2.38	2.42	1.53
CO_2	2.31[a]	2.60	0.22[b]	0.22

[a] determined on only 43 analyses

[b] determined in only 19 analyses

Average chemical composition of metamorphic rocks (anhydrous basis), after Miyashiro, 1973

	1	2	3	4	5
	Phyllites	Mica schits	Two-mica schists	Quartzo-feldspatic gneisses	Amphibolites
SiO_2	60.0	64.3	67.7	70.7	50.3
TiO_2	1.1	1.0	-	0.5	1.6
Al_2O_3	20.7	17.5	16.6	14.5	15.7
Fe_2O_3	3.0	2.1	1.9	1.6	3.6
FeO	4.8	4.6	3.4	2.0	7.8
MnO	0.1	0.1	-	0.1	0.2
MgO	2.9	2.7	1.8	1.2	7.0
CaO	1.2	1.9	2.0	2.2	9.5
Na_2O	2.0	1.9	3.1	3.2	2.9
K_2O	4.0	3.7	3.5	3.8	1.1
P_2O_5	0.2	0.2	-	0.2	0.3

1,2,4,5 after Poldervaart, 1955; 3 after Lapadu-Hargues, 1945

AMPHIBOLITE

All amphibolites are ultrabasic to intermediate with SiO_2 values ranging from 41.08wt% to 56.72 wt%. Lost of ignition (LOI) varies from 0.34 to 1.38, except sample 14SW03 which exhibits a high LOI of 5.67 wt%. The majority of amphibolites plot in the field of gabbro and one sample (14SW47) falls into the field of diorite (see Figure 30). Two samples (14SW07 & 14SW09) plot outside of the diagram, due to low content of alkalis as shown in the TAS diagram of Cox et al., 1979. The association to a magmatic trend is vague (see Figure 30A). Amphibolites of the Surna Nappe show slightly lower MgO and higher CaO and K_2O values than average compositions (see Table 22 and Table 23). Figure 31 illustrates the differentiation between ortho- and para-amphibolite after Leake, 1964. Therefore, the Niggli parameters have been calculated as shown in Table 24.

$$mg = \frac{MgO}{FeO + MnO + MgO + Fe_2O_3}$$

The systematic decrease in Niggli mg and increase of Niggli c is associated with magmatic differentiation. All samples plot at the early stage differentiation of basic magmas, indicating no clear trend, but don't fall in the field of the mixtures between pelite – limestone – dolomite. A classification of the magma series based on the ternary AFM diagram after Irvine & Baragar, 1971 is not straightforward (see Figure 30B). Binary plots of major elements vs. MgO (both in wt%) are illustrated in Figure 32. A clear trend is only observed in TiO_2 (negative correlation), which is typical for a tholeiitic fractionation trend.

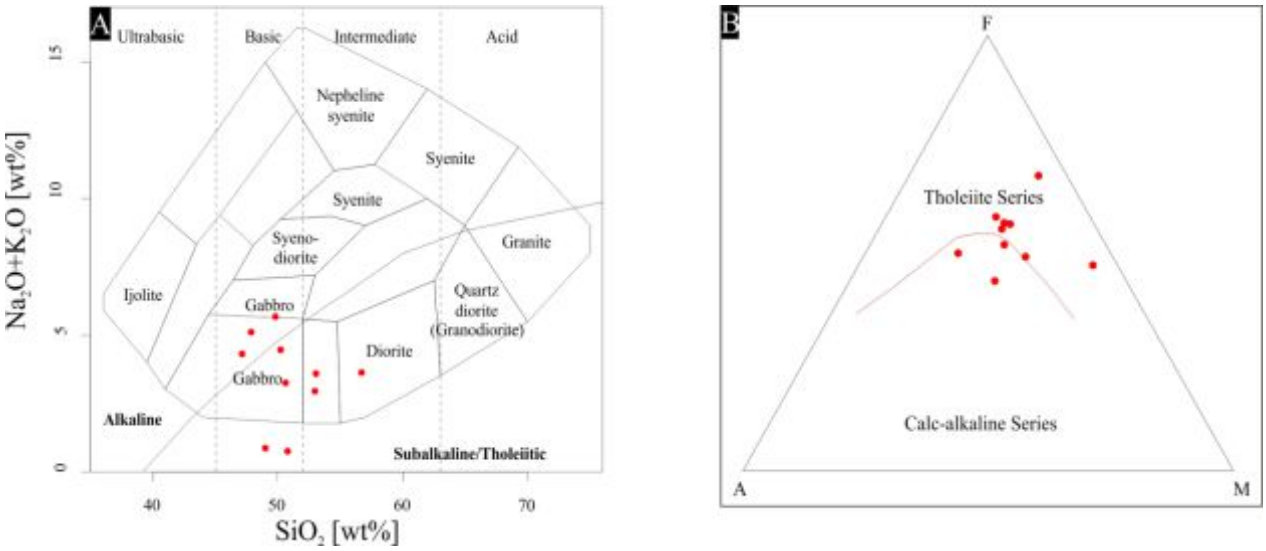

Figure 30 (A) TAS diagram after Cox et al., 1979 with indicated amphibolite samples of the Surna Nappe (red dots). The majority of samples plot in the field of Gabbro, sample 14SW47 can be classified as diorite due to the higher SiO_2 content. (B) Magmatic AFM diagram after Irvine & Baragar, 1971, again of amphibolite (red dots). A differentiation between alkaline and subalkaline/tholeiitic trend is not straightforward. F = Fe_{tot}, M = MgO and A = Na_2O + K_2O.

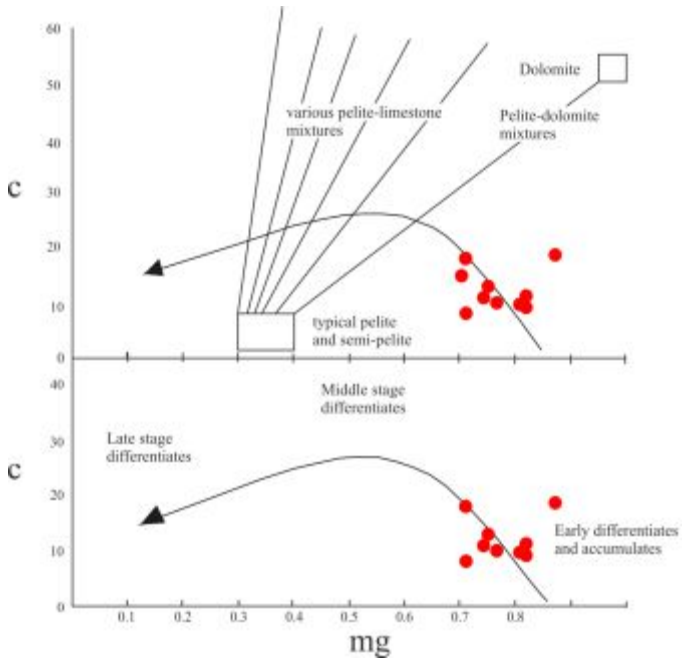

Figure 31 Classification of the amphibolite protolith after Leake, 1964. Arrow represents the trend line of Karroo dolerite. mg = Niggli mg, c = Niggli c. Red dots indicate amphibolites of the Surna Nappe, which plot at the early differentiations stage of basic magmas.

Table 24 Whole rock analysis of amphibolite the Surna Nappe. 10 % Fe_2O_3 is assumed. data and Niggli parameters after Leake et al., 1964.

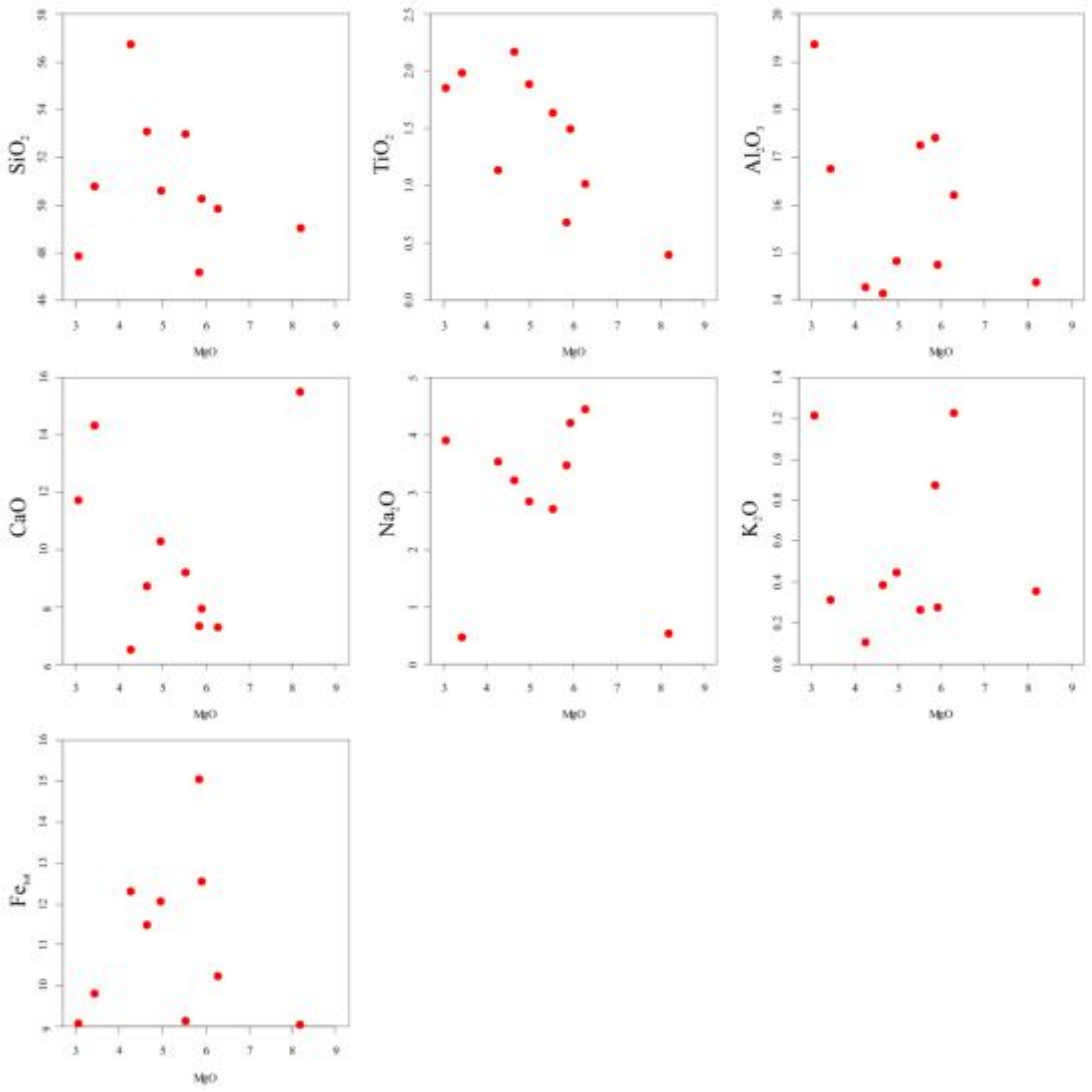

Figure 32 Binary plots of major elements vs. MgO (both axes in wt%) of amphibolites in the Surna Nappe (red dots). A distinct trend is not observed in any major element.

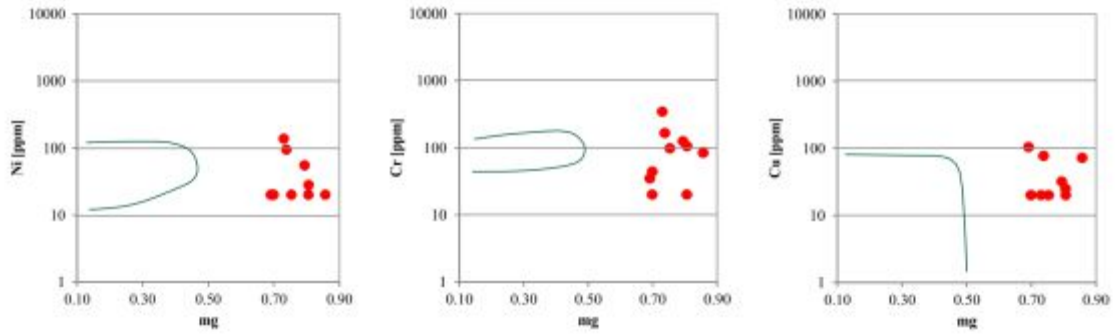

Figure 33 Niggli mg vs Ni, Cr and Cu [ppm] on a logarithmic scale after Leake, 1964 of amphibolites in the Surna Nappe. Green line would enclose pelites. There is no clear positive trend observed as in typical orthoamphibolites recognized, but they don't plot within the field of pelites.

TONALITIC LAYER

Felsic concordant layers in amphibolite clearly of magmatic origin (see Figure 34) and represent tonalitic to granodioritic melt based on the Streckeisen diagram for plutonites, (see Figure 35). The SiO_2 content varies from 67.27 – 75.55 wt%. Binary plots of major elements vs. SiO_2 (see Figure 36) indicate no distinct trend, due to small number of samples.

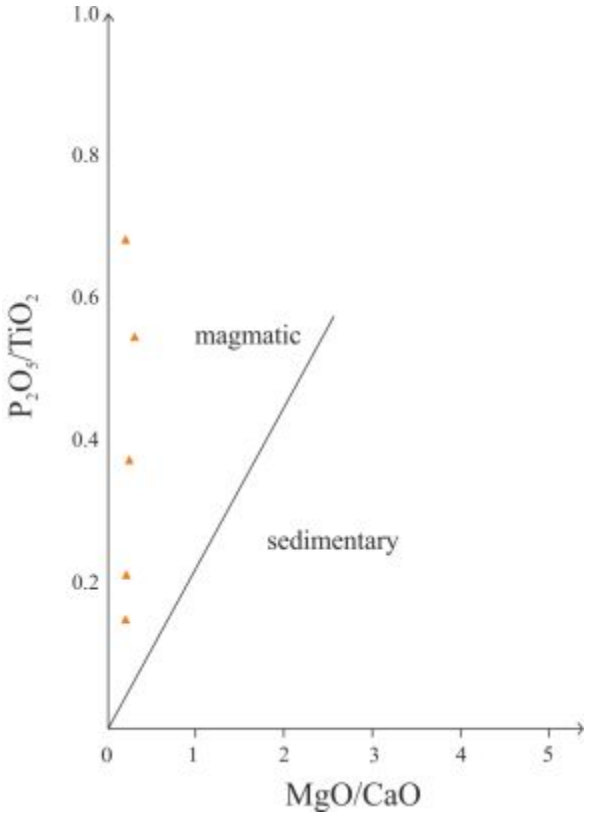

Figure 34 Discrimination diagram between magmatic or sedimentary protolith, after Werner, 1987, with indicate samples of tonalitic layer. All samples have a magmatic origin. Both axes are in wt%.

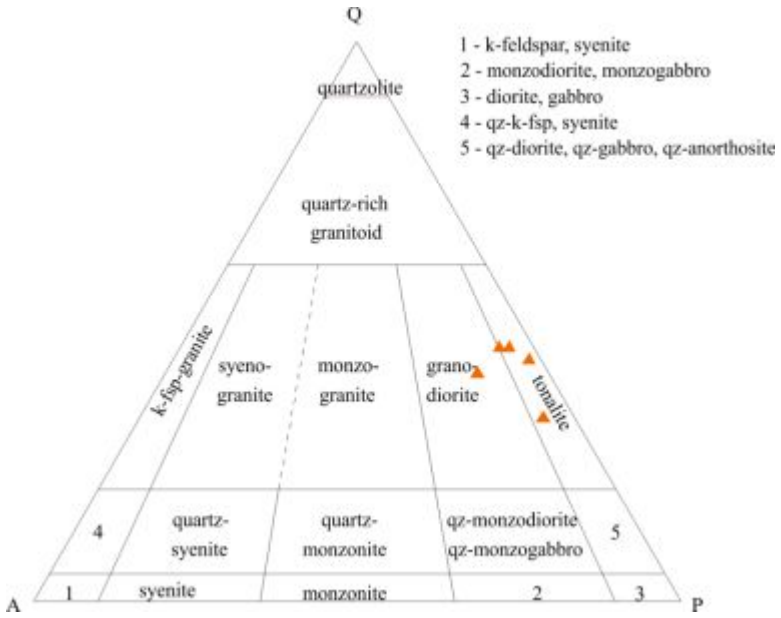

Figure 35 QAP diagram after Streckeisen, 1974. Four samples of tonalitic layer plot in the field of tonalite, sample 14SW42 can be classified as granodiorite. Q = quartz, A = K-Fsp, P = plagioclase.

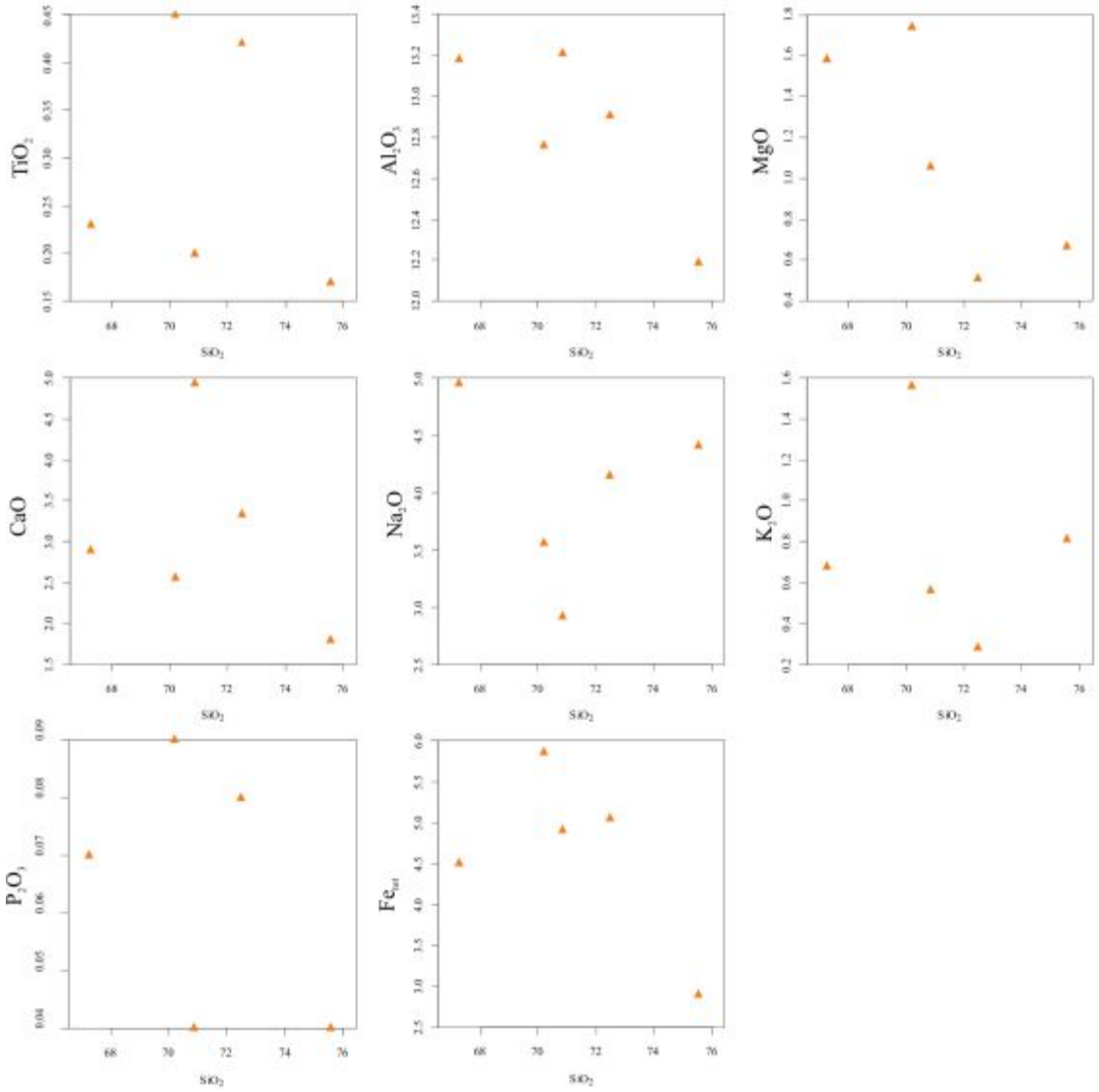

Figure 36 Binary plots of SiO_2 vs major elements (both axes in wt%) of tonalitic layer of Surna Nappes. No fractionation trends can be observed, due to small number of sample.

CONVENTIONAL GEOTHERMOBAROMETRY

THEORETICAL BACKGROUND

A fundamental condition for any geothermobarometric calculation is the chemical equilibrium of involved phases (Gibbs free energy at minimum), and a closed system (dV = 0). The implementation of the thermodynamic laws in thermobarometric calculations results in the following relationship

$$\Delta G \; = \; 0 \; = \Delta H - T\Delta S + \; \Delta V(P-1) + \; \; RTln(K)$$

G… Gibbs free enthalpy, ΔH… difference in enthalpy of reaction, T… temperature [°K], ΔS… difference in entropy of reaction, ΔV… difference in molvolumes of reaction, P… pressure [bar], R… gas constant (8.31 [J/molK]), K… equilibrium constant of reaction

By determining thermodynamic parameters like H, S, V and choosing the proper activity model, the equilibrium constant K generates a line with a certain slope in the P/T space. Different equilibria produce different slopes, and intersecting those results in a point in the P/T space. Proper geothermometers have a small reaction volume (and a high change in entropy) and plot therefore as steep line in the P/T space. Reverse behavior is observed for geobarometers.

GEOTHERMOMETRY

Ionic exchange geothermometers are based on the exchange of isomorphic elements (elements with similar valence and ionic radius) between coexisting minerals, and are mainly determined by the following parameters:

- electronegativity
- crystal class
- H_2O-content of minerals

The higher the difference of these parameters between mineral phases is, the higher is the ionic exchange process. Biggest differences occur between hydrated and non-hydrated minerals (Franz L., 2016).

Garnet – Biotite Thermometry

Because of the reasons mentioned above, Fe^{2+}/Mg exchange between garnet and biotite is appropriate for evaluating temperature (significant difference in electronegativity, Mg = 1.31 and of Fe^{2+} = 1.83). At low temperatures, phlogopite and almandine rich compositions are dominant and with rising temperature the bonding of Mg to garnet increases, whereas the bonding of Fe^{2+} decreases.

$$KMg_3[(OH)_2Si_3AlO_{10}] + Fe_3Al_2Si_3O_{12} \rightarrow KFe_3[(OH)_2Si_3AlO_{10}] + Mg_3Al_2Si_3O_{12}$$

phlogopite + almandine → annite + pyrope

In more accurate thermometer equations the non-ideal mixing of garnet and biotite, the effects of Ca and Mn content in natural garnet, and Ti & Al of natural biotite are also considered (Dachs E. 2015).

For this study the calibration after Holdaway, 2000 was used, by determining the temperature following the equation

$$T\,[K] = \frac{40198 + 0.295P + G + B}{7.802 - 3RlnK_D}$$

G & B... Margules Parameter.

Garnet – Hornblende Thermometry

This thermometer is based on the Fe^{2+}/Mg exchange between garnet and hornblende endmembers. Calculations in PET were performed with calibration after Dale et al., 2000, following the reaction

$$Ca_2Fe_5Si_8O_{22}(OH)_2 + \frac{5}{3}Mg_3Al_2[Si_3O_{12}] \rightarrow Ca_2Mg_5Si_8O_{22}(OH)_2 + \frac{5}{3}Fe_3Al_2[Si_3O_{12}]$$

ferroactinolite + $\frac{5}{3}$ pyrope → tremolite + $\frac{5}{3}$ almandine

Limitations for this thermometer arise in the composition of amphiboles: (per formula unit) Ti = 0.25, Mn = 0.12, K = 0.4 and Na_{M4} = 1.0, and values for X_{Mg}^{M2}, X_{Mg}^{M4} and X_{Na}^{A}< 0.015 should be avoided (Dale et al., 2000), (Fe^{3+} calculated after to Blundy & Holland, 1990).

For calculations in winTWQ the endmembers of the calibration after Graham & Powell, 1984 were selected, following the reaction

$\frac{1}{3}Mg_3Al_2[Si_3O_{12}] + \frac{1}{4}NaCa_2Fe_4Al[Al_2Si_6O_{22}(OH)_2] \rightarrow \frac{1}{3}Fe_3Al_2[Si_3O_{12}] + \frac{1}{4}NaCa_2Mg_4Al[Al_2Si_6O_{22}(OH)_2]$

$\frac{1}{3}$ pyrope + $\frac{1}{4}$ ferropargasite → $\frac{1}{3}$ almandine + $\frac{1}{4}$ pargasite

and temperature is calculated in the form

$$T\ [°C] = \frac{2880+3280X_{Ca,Grt}}{lnK_D+2.426} - 273$$

Uncertainties arise from the Fe^{3+} estimation of amphiboles and application of the latter calibration is restricted to Mn-poor systems (Franz L., 2016).

Plagioclase– Hornblende Thermometry

Blundy & Holland, 1994 introduced a semi-empirical thermometer based on the Al^{IV} content in amphibole coexisting with plagioclase in Si-saturated rocks, and calibrated the following thermodynamic reactions

$NaCa_2Mg_5Si_7AlO_{22}(OH)_2 + 4\ SiO_2 \rightarrow Ca_2Mg_5Si_8O_{22}(OH)_2 + NaAlSi_3O_8$

edenite + 4 quartz → tremolite + albite

$NaCa_2Mg_4AlAl_2Si_6O_{22}(OH)_2 + 4\ SiO2 \rightarrow Ca_2Mg_4Al_2Si_7O_{22}(OH)_2 + NaAlSi_3O_8$

pargasite + 4 quartz → hornblende + albite

(Fe^{3+} calculated after to Blundy & Holland, 1994).

Garnet – Clinopyroxene Thermometry

This thermometer is again based on the Mg/Fe^{2+} exchange of garnet and clinopyroxene following the reaction

$\frac{1}{3}\ Mg_3Al_2[Si_3O_{12}] + CaFe[Si_2O_6] \rightarrow \frac{1}{3}\ Fe_3Al_2[Si_3O_{12}] + CaMg[Si_2O_6]$

$\frac{1}{3}$ pyrope + hedenbergite → $\frac{1}{3}$ almandine + diopside

and temperature determination by the equation

$$T\ [°C] = [(1939.9 + 3270\ X_{Ca}^{Grt} - 1396\ (X_{Ca}^{Grt})^2 + 3318\ X_{Mn}^{Grt} - 353\ (X_{Ca}^{Grt})^2 + 1105\ X_{Mg\#}^{Grt} - 3561\ (X_{Mg\#}^{Grt})^2 + 2324\ (X_{Mg\#}^{Grt})^3 + 169.4P/(lnK_D + 1.223)] - 273$$

where K_D = $(Fe^{2+}/Mg)^{Grt}/(Fe^{2+}/Mg)^{Cpx}$, X_{Ca}^{Grt} = Ca/(Ca+Mn+Fe^{2+}Mg) in garnet, X_{Mn}^{Grt} = Mn/(Mn+Mn+Fe^{2+}+Mg) in garnet and $X_{Mg\#}^{Grt}$ = Mg/(Mg+Fe^{2+}) in garnet

after Krogh Ravna, 2000. Errors of $\pm$ 50°C are common for nearly all calibrations, mainly because of the non-ideality of additional elements in clinopyroxene like MnO and Cr_2O_3. The Fe^{3+} content in clinopyroxene is another source of imprecision. (Franz L., 2016)

Zr in Rutile Thermometry

Empirical studies, for instance of Zack et al., 2004, Ferry & Watson, 2007, and Tomkins et al., 2007, show that the Zr-content in rutile is temperature dependent. Tomkins et al., 2007 considers also a pressure dependent equation. Since rutile is part of the stable assemblage in amphibolites and garnet-hornblende mica schists, this thermometer was applied to three samples with calibration by all previously mentioned authors. See Table 27, Table 28 and Table 29 for equations, results and errors.

GEOBAROMETRY

Net – transfer mineral reactions accompany a significantly higher mole volume of at least one involved phase. The phase with smaller mole volume is the one which is stable at lower pressures. The volume change of almost all net-transfer reactions is high, resulting in the suitability as geobarometer (Franz L., 2016).

Garnet – Hornblende – Plagioclase Barometry

The following reactions by Dale et al., 2000 were considered

$$Ca_2Mg_3Al_4Si_6O_{22}(OH)_2+\frac{4}{3}Ca_3Al_2Si_3O_{12}+\frac{2}{3}Mg_3Al_2Si_3O_{12}+4SiO_2 \rightarrow Ca_2Mg_5Si_8O_{22}(OH)_2+4CaAl_2Si_2O_8$$

tschermakite + $\frac{4}{3}$ grossular + $\frac{2}{3}$ pyrope + 4 quartz → tremolite + 4 anorthite

and

$$NaCaMg_4Al_3Si_6O_{22}(OH)_2 + \frac{2}{3}Ca_3Al_2Si_3O_{12} + \frac{1}{3}Mg_3Al_2Si_3O_{12} + 6SiO_2 \rightarrow Ca_2Mg_5Si_8O_{22}(OH)_2 + 4CaAl_2Si_2O_8 + NaAlSi_3O_8$$

$$\text{pargasite} + \frac{2}{3}\text{grossular} + \frac{1}{3}\text{pyrope} + 6\text{ quartz} \rightarrow 2\text{ anorthite} + \text{albite}$$

Limiting parameters are the same as for garnet – hornblende thermometer (Fe^{3+} calculated according to Blundy & Holland, 1994).

Garnet – Plagioclase – Biotite – Quartz Barometry

This barometry was introduced due to the common missing of Al_2SiO_5 phases in metapelites. Hoisch, 1990 used 43 natural samples for calibrating the following reactions

$$\frac{1}{3}Mg_3Al_2Si_3O_{12} + \frac{2}{3}Ca_3Al_2Si_3O_{12} + K(Mg_2Al)(Si_2Al_2)O_{10}(OH) + 2SiO_2 \rightarrow 2CaAl_2Si_2O_8 + KMg_3(AlSi_3)O_{10}(OH)_2$$

$$\frac{1}{3}\text{ pyrope} + \frac{2}{3}\text{ grossular} + \text{ eastonite} + 2\text{ quartz} \rightarrow 2\text{ anorthite} + \text{ phlogopite}$$

and the following calibrated geobarometric expression

$$P\,[bar] = \frac{-31830.6 + 79.0281T - RTlnK_{R1} - 26968.7\left(X_{Al}^{Bt} - X_{Mg}^{Bt}\right) + 32604.5\,X_{Fe}^{Bt} + 42855.4\,X_{Ti}^{Bt}}{3.8145 - \frac{2}{3}\Delta V_{Grs}}$$

and

$$Fe_3Al_2Si_3O_{12} + \frac{2}{3}Ca_3Al_2Si_3O_{12} + K(Fe_2Al)(Si_2Al_2)O_{10}(OH)_2 + 2SiO_2 \rightarrow 2CaAl_2Si_2O_8 + KFe_3AlSi_3O_{10}(OH)_2$$

$$\frac{1}{3}\text{ almandine} + \frac{2}{3}\text{ grossular} + \text{ siderophylitte} + 2\text{ quartz} \rightarrow 2\text{ anorthite} + \text{ annite}$$

and the following calibrated geobarometric expression

$$P\,[bar] = \frac{-46707.2 + 85.5824T - RTlnK_{R2} - 30960.2\left(X_{Al}^{Bt} - X_{Fe}^{Bt}\right) + 24289.6\,X_{Mg}^{Bt} + 37265.6\,X_{Ti}^{Bt}}{3.8986 - \frac{2}{3}\Delta V_{Grs}}$$

Reliable results can be obtained if mineral compositions are in the range which was used by the author (for instance Xan > 0.18, since values below don't ensure Ca-exchange with

garnet). Although muscovite is part of the peak mineral assemblage it is ignored for geothermobarometric calculations due to uncertainties in thermodynamic data and solution models of white mica.

Garnet – Clinopyroxene – Plagioclase – Quartz Barometry

Eckert et al., 1991 provided a useful barometer of the above mentioned mineral assemblage, resulting in the reaction

$$CaAl_2Si_2O_8 + CaMgSi_2O_6 \rightarrow \frac{2}{3} Ca_3Al_2Si_3O_{12} + \frac{1}{3} Mg_3Al_2Si_3O_{12} + SiO_2$$

$$\text{anorthite} + \text{diopside} \rightarrow \frac{2}{3}\,\text{grossular} + \frac{1}{3}\,\text{pyrope} + \text{quartz}$$

with the resulting geobarometric equation

$$P[kbar] = 2.60 + 0.01718T + 0.003596T \ln K$$

The error of $\pm$ 1.9 kbar should be rather added than subtracted (Newton & Perkins, 1982).

Garnet – Rutile – Ilmenite – Plagioclase – Quartz Barometry (GRIPS)

Bohlen & Liotta, 1986 calibrated this barometer for garnet-bearing amphibolites. The breakdown of ilmenite with increasing pressure results in the coexistence of rutile and garnet. The barometer is based on the equilibrium

$$CaFe_2Al_2Si_3O_{12} + 6\,TiO_2 \rightarrow 6\,FeTiO_3 + 3\,CaAl_2Si_2O_8 + 3\,SiO_2$$

$$\text{garnet } (Grs_1Alm_2) + 6\,\text{rutile} \rightarrow 6\,\text{ilmenite} + 3\,\text{anorthite} + 3\,\text{quartz}$$

Errors and uncertainties arise from the often unknown position of rutile (relict of high-pressure metamorphism) and the relationship between rutile and ilmenite (Franz L., 2016). For amphibolite samples of this study rutile occurs often as inclusion in amphibole rims and shows exsolution of ilmenite. In garnet – hornblende mica schist rutile is found in the matrix and as enclave in garnet or amphibole.

GEOTHERMOBAROMETRIC MULTIEQULIBRIUM CALCULATIONS

All the above mentioned thermobarometry methods have the disadvantage that applied equilibria equations are not internally consistent with each other, i.e. each incorporates a particular set of thermodynamic data for each mineral. Multiequilibrium calculations with programs like winTWQ have the benefit that all possible reactions between phases are considered (database by Berman, 1988, Berman, 2007 & Holland & Powell 1998). Used solution models are indicated in the individual P/T plots (see digital Appendix).

RESULTS

Folders in the digital appendix include

- positions of mineral chemical analysis (mineral chemical data used for geothermobarometric calculations are indicated in appropriate colors)
- the corresponding results presented as P/T plots (clarification of the abbreviations used in the titles of the P/T plots is shown in Table 25
- tables of mineral compositions of all measurement points

Table 25 Description of used abbreviations in P/T plot of geothermobarometric calculations, see also digital Appendix.

abbreviation	geothermometer	geobarometer	calibration
gtbt	garnet-biotite		Holdaway, 2000
gtbtpl		garnet-biotite-plagioclase	Hoisch, 1990 Mg-reaction (R1)
gtbtpl2		garnet-biotite-plagioclase	Hoisch, 1990 Fe-reaction (R2)
gtam	garnet-hornblende		Dale et al., 2000 & Graham & Powell, 1984
gtampl	garnet-hornblende-plagioclase		Dale et al., 2000 reaction 1 & Graham & Powell, 1984
gtampl2	garnet-hornblende-plagioclase		Dale et al., 2000 reaction 2 & Graham & Powell, 1984
ampl		amphibole-plagioclase	Blundy&Holland, 1990 reaction 1
ampl2		amphibole-plagioclase	Blundy&Holland, 1990 reaction 2
gtcpxpl	garnet-clinopyroxene-plagioclase		Eckert et al., 1991 Mg-reaction
gtcpx		garnet-clinopyroxene	Krogh Ravna, 2000
GRIPS		garnet-rutile-ilmenite-plagioclase	Bohlen & Liotta, 1986

Table 26 shows the summary of geothermobarometric calculations from the different lithologies of the Surna Nappe. Selected samples are plotted in Figure 37, resulting in four P/T windows. In general, all results, regardless of the lithology, obtained by the garnet-biotite-plagioclase-quartz thermo- and barometer yield higher P/T conditions than results of the garnet-amphibole-plagioclase system.

The main focus of geothermobarometric studies was on garnet – hornblende mica schists. In total 12 samples have been investigated. As mentioned before, the garnet-biotite-plagioclase-quartz geobarometer and garnet-biotite geothermometer yield higher P/T conditions than the garnet-amphibole-plagioclase geobarometer and garnet-plagioclase geothermometer. Garnet – biotite geothermometer is constant between 600-700 °C, and garnet-biotite-plagioclase-quartz geobarometer varies in the range of 9 – 20 kbar. Samples which yield low pressure and temperature (14SW27 & 14SW29) are from the northern part of the Surna Nappe, approximately 40 km NW from the other sample localities. Garnet – hornblende – plagioclase geobarometry shows more invariable pressures around 9 kbar and temperature varying from 400 – 600 °C.

For garnet – quartz mica schists the application of garnet-biotite-plagioclase-quartz geobarometer and garnet-biotite geothermometer were the only possibilty of evaluating P/T conditions. Sample 14SW06 yields ~ 650 °C with garnet – biotite geothermometry. Sample 14SW28, taken from the northern part of the Surna Nappe, shows a more retrogressed and highly deformed fabric which is reflected in P/T calculations (~5 kbar/500 °C respectively 3 kbar/500 °C with considering amphibole).

The usage of appropriate geobarometer in amphibolites is challenging, but for sample 14SW22, the garnet-biotite-plagioclase-quartz and garnet-amphibole-plagioclase geobarometer could be applied. Pressure results vary from 6 – 12 kbar, temperatures are consistent at approximately 650 °C. Minimum pressure is given by the GRIPS barometer with 7kbar.

The peak assemblage in tonalitic layers consists of garnet, plagioclase, biotite, white mica $\pm$ amphibole. For geothermobarometric calculations with the garnet-biotite-plagioclase-quartz geobarometer and the garnet-biotite geothermometer (sample 14SW12 and 14SW42) P/T conditions of 20 kbar/700 °C were obtained. Sample 14SW42 contains amphibole what results in lower P/T conditions of 13 kbar/640 °C (PET) and again 20 kbar/780 °C with winTWQ.

Since calc-silicate rocks comprise the peak paragenesis clinopyroxene – garnet – plagioclase the application of the corresponding geothermobarometer yield for all investigated samples ~ 17 kbar/650 °C. The garnet-amphibole thermometry gives similar temperatures of 620 °C.

One pegmatite sample (14SW32), which contains garnet, plagioclase, amphibole and clinozoisite, was used for multiequilibrium calculations with winTWQ. Activity for clinozoisite, evaluated with AXwin, is 0.74. H_2O activity was set to 1.0 and results give 12

kbar/550 °C. More reliable seem the activity – corrected P/T grid of endmembers with the program Perplex_X (Connolly, 2005), where the same solution models and thermodynamic parameters are used (all activities considered have prior been calculated with AXwin and are denoted at univariant reactions, see Figure 38A&B).

Si (p.f.u.) in white mica can be used as an indicator for pressure estimations. Si is replacing tetrahedral Al with a linear relation with rising pressure (Deer et al., 1971, and Massonne & Schreyer, 1987). The highest phengite content is found in tonalitic layers with 3.28 Si p.f.u., garnet – hornblende mica schists comprise 3.25 Si p.f.u., garnet – quartz mica schists 3.22 Si p.f.u. and amphibolite 3.18 Si p.f.u.. Figure 39 illustrates the linear correlation of increasing Si in phengite with increasing pressure of different lithologies in the Surna Nappe. Pressure results are obtained by conventional geothermbarometry and plotted against the Si content in white mica of the same sample.

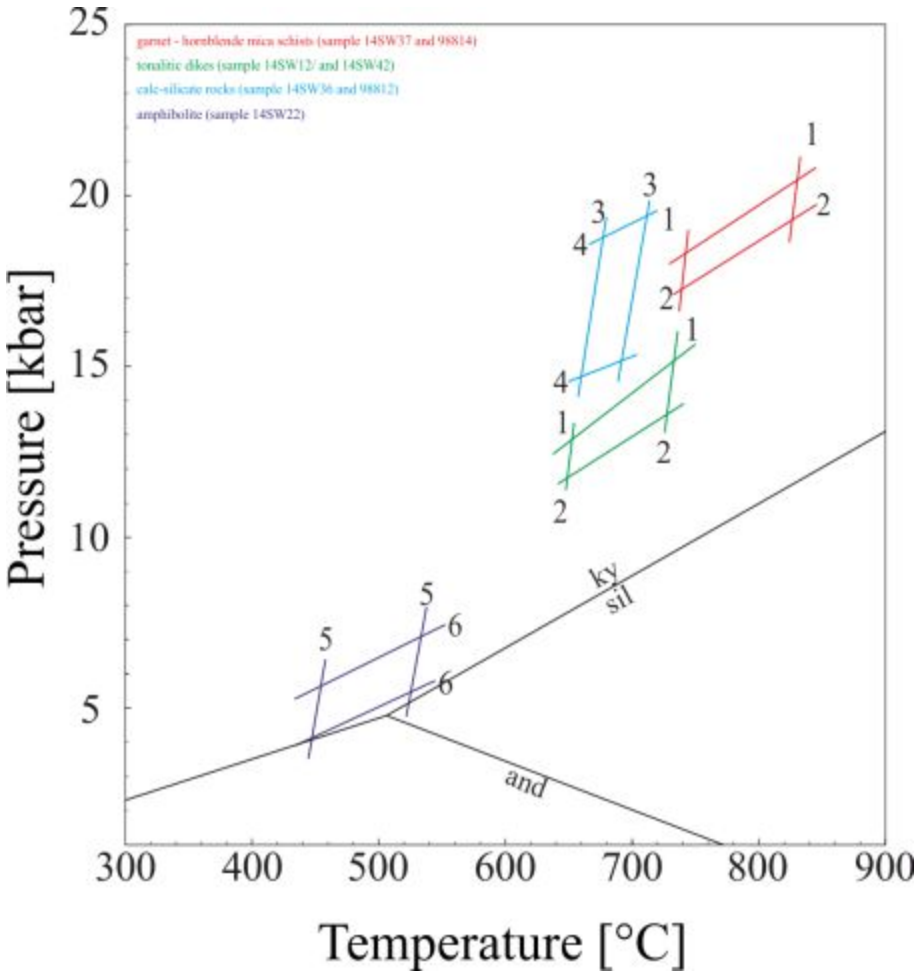

Figure 37 P/T plot of selected lithologies and sample of Surna Nappe resulted by different geothermobarometric calculations. Garnet-hornblende mica schists yield highest P/T conditions of ~ 18 kbar/750 °C. Calc-silicate rocks yield similar pressures but slightly lower temperature (~17kbar/700°C). Tonalitic layers, calculated with the same geothermbarometers as garnet-hornblende mica schist plot in the range of 640 – 720 °C and 13 kbar. Lowest P/T conditions are obtained from amphibolites, with 6 kbar and 500 °C. 1 garnet-biotite geothermometer, 2 garnet-biotite-plagioclase-quartz geobarometer, 3 garnet-clinopyroxene geothermometer, 4 garnet-clinopyroxene-plagioclase-quartz geobarometer, 5 garnet-amphibole geothermometer, 6 garnet-amphibole-plagioclase-quartz geobarometer. Aluminum silicates stability fields after Holdaway & Mukhopadhyay, 1993.

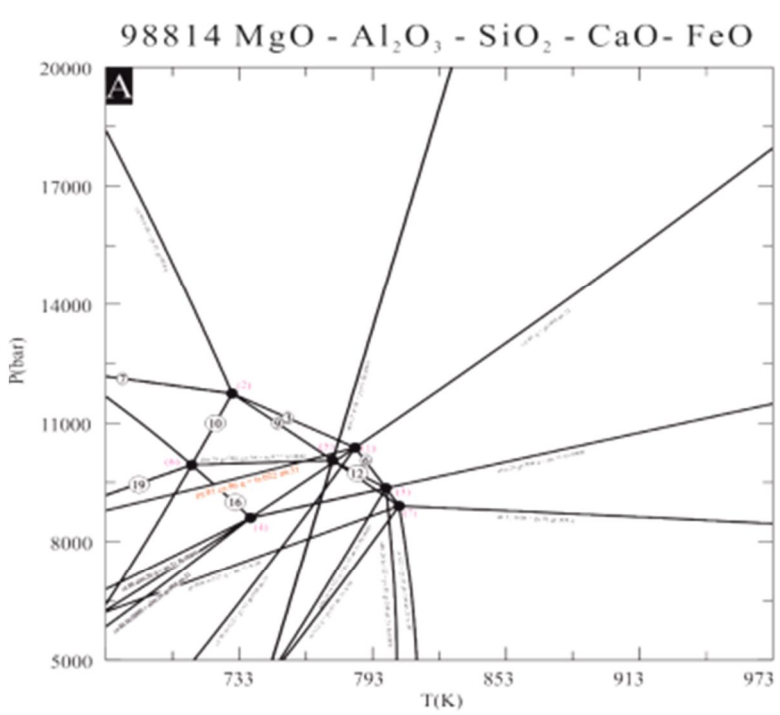

(pseudo-) invariant points are summarized below:

(1-0) py.01 cz.86 alm.26 gr.004 ts.022 an.31 q
(2-0) py.01 cz.86 alm.26 gr.004 ts.022 q tr.08
(3-0) py.01 alm.26 gr.004 ts.022 an.31 q ftr.0000
(4-0) cz.86 alm.26 gr.004 ts.022 an.31 q ftr.0000
(5-0) py.01 alm.26 gr.004 ts.022 q tr.08 ftr.0000
(6-0) cz.86 alm.26 gr.004 ts.022 q tr.08 ftr.0000
(7-0) py.01 gr.004 ts.022 an.31 ftr.0000 q tr.08

(pseudo-) univariant equilibria are summarized below:

(1-1) alm.26 tr.08 = py.01 ftr.0000
(2-1) cz.86 ts.022 = py.01 gr.004 an.31
(3-1) ts.022 = py.01 cz.86 gr.004 q
(4-1) cz.86 q = gr.004 an.31
(5-1) py.01 cz.86 q = ts.022 an.31
(6-1) ts.022 = py.01 gr.004 an.31 q
(7-1) ts.022 = py.01 cz.86 tr.08
(8-1) cz.86 tr.08 = py.01 gr.004 q
(9-1) ts.022 tr.08 = py.01 gr.004 q
(10-1) cz.86 tr.08 = gr.004 ts.022 q
(11-1) alm.26 ts.022 = py.01 gr.004 an.31 ftr.0000
(12-1) ts.022 ftr.0000 = py.01 alm.26 gr.004 q
(13-1) alm.26 gr.004 q = an.31 ftr.0000
(14-1) alm.26 ts.022 q = py.01 an.31 ftr.0000
(15-1) cz.86 ftr.0000 = alm.26 gr.004 an.31
(16-1) cz.86 ftr.0000 = alm.26 gr.004 q
(17-1) cz.86 alm.26 q = an.31 ftr.0000
(18-1) alm.26 gr.004 q tr.08 = ts.022 ftr.0000
(19-1) cz.86 alm.26 tr.08 = ts.022 ftr.0000
(20-1) ts.022 = py.01 gr.004 an.31 tr.08
(21-1) an.31 tr.08 = py.01 gr.004 q
(22-1) ts.022 q = py.01 an.31 tr.08
(23-1) gr.004 ts.022 q = an.31 tr.08

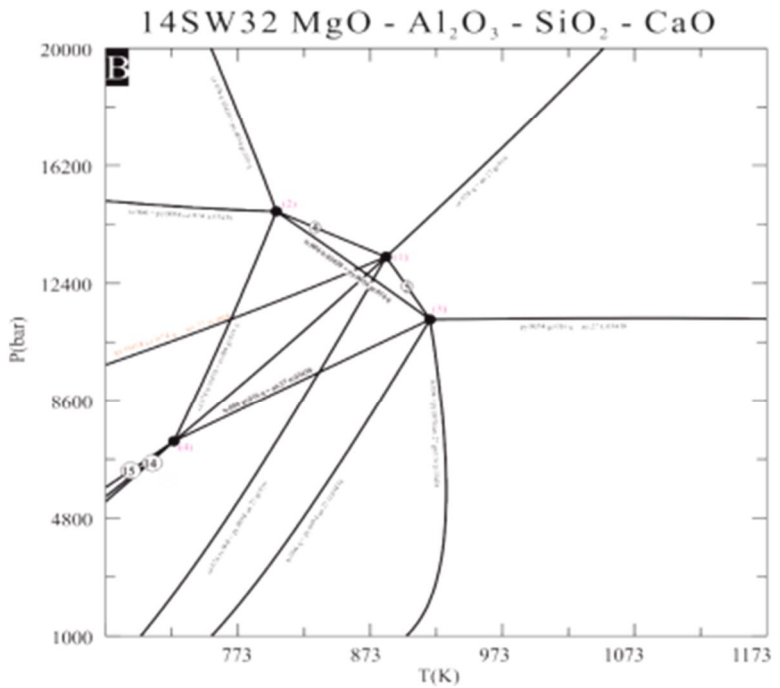

(pseudo-) invariant points are summarized below:

(1-0) py.0054 cz.074 an.27 ts.004 gr.016 q
(2-0) py.0054 cz.074 ts.004 gr.016 q tr.03438
(3-0) py.0054 an.27 ts.004 gr.016 q tr.03438
(4-0) cz.074 an.27 ts.004 gr.016 q tr.03438

(pseudo-) univariant equilibria are summarized below:

(1-1) cz.074 ts.004 = py.0054 an.27 gr.016
(2-1) py.0054 cz.074 q = an.27 ts.004
(3-1) cz.074 q = an.27 gr.016
(4-1) ts.004 = py.0054 cz.074 gr.016 q
(5-1) ts.004 = py.0054 an.27 gr.016 q
(6-1) ts.004 = py.0054 cz.074 tr.03438
(7-1) cz.074 tr.03438 = py.0054 gr.016 q
(8-1) ts.004 tr.03438 = py.0054 gr.016 q
(9-1) cz.074 tr.03438 = ts.004 gr.016 q
(10-1) ts.004 = py.0054 an.27 gr.016 tr.03438
(11-1) ts.004 q = py.0054 an.27 tr.03438
(12-1) py.0054 gr.016 q = an.27 tr.03438
(13-1) ts.004 gr.016 q = an.27 tr.03438
(14-1) cz.074 tr.03438 = an.27 ts.004 gr.016
(15-1) cz.074 ts.004 q = an.27 tr.03438

Figure 38 Activity corrected P/T grid calculated with Perplex_X software package, H_2O = saturated and activity of latter is 1.0. Reaction equations are written such as that the high temperature assemblage is on the right of the = sign. (A) Sample 98814 garnet – hornblende mica schist in the selected MgO-Al_2O_3-SiO_2-FeO system. (B) Sample 14SW32, pegmatite, in the simplified MgO – Al_2O_3 – SiO_2 – CaO system. Reaction lines which are exceeded are highlighted red.

Table 26 Summary of results obtained by geothermobarometric calculations for garnet – hornblende mica schist, garnet – quartz mica schist, amphibolite, tonalitic layer, calc-silicate rock and pegmatite. For abbreviations see **Table 25**. First row indicates applied program. * stand for GRIPS vs. garnet-biotite geothermometer and # for GRIPS vs. garnet-amphibole geothermometer.

sample	lithology	PET										winTWQ										Freudy		Zr in Rt		
		grbt		grbpl		grbpl2		ampl		gtam		gtampl		gtampl2		gtcpx		gtcpxpl		grbpl		gtampl		gtcpxpl		GRIPS		Grt-Amp-Pl-Cz		Grt-Pl-Amp-Cz		Tomkins et al., 2007	Zack et al., 2004	Ferry et al., 2007
		T [°C]	P [kbar]	P [kbar]		T [°C]	P [kbar]	T [°C]		T [°C]	P [kbar]	P [kbar]		T [°C]	P [kbar]	T [°C]	P [kbar]	P [kbar]		T [°C]	P [kbar]	T [°C]	P [kbar]	P [kbar]		T [°C]	P [kbar]	T [°C]	P [kbar]	T [°C]	P [kbar]	T [°C]	T [°C]	T [°C]
14SW18	grt-hb- mica schist																															~ 610	~ 720	~ 630
14SW27	grt-hb- mica schist	520	9	10																500	8					500	8*					~ 550	~ 610	~ 570
14SW29	grt-hb- mica schist	500	9	10						450	3	5								480	8					550	8#							
14SW34	grt-hb- mica schist	700	12	12						430	5	8								650	11	550	8			520	7#							
14SW37	grt-hb- mica schist	800	20	20						660	12	12								750	19	750	16			760	13#							
14SW52	grt-hb- mica schist	650	15	15																670	14													
14SW66	grt-hb- mica schist	750	20	19						650	15	14								750	19	800	20											
98806	grt-hb- mica schist	700	14	13						410	7	9								700	12					570	9#							
98811	grt-hb- mica schist	600																																
98814	grt-hb- mica schist	740	17	17						430	7	8								700	17	600	10					380	13	520	11			
98817	grt-hb- mica schist	700				600		480		8		9								650		720	15											
98820	grt-hb- mica schist	650	9	9				600		7		7								630	9	800	11			620	7*							
14SW06	grt-qz- mica schist	660																		630														
14SW28	grt-qz- mica schist	500	5	6																500	3													
14SW03	amphibolite					~ 600																												
14SW22	amphibolite	660	12	12						450	6	6								620	10	560	8			560	7							
14SW62	amphibolite					~ 600																										~ 650	~ 700	~600
14SW12	tonalitic layers	700	20	21																700	19													
14SW41	tonalitic layers	760	20	20						640	13	13								750	20	780	20											
14SW42	tonalitic layers	680	17	18																650	15													
14SW36	calc-silicate rock															650	15							650	15									
98812	calc-silicate rock															680	19							570	18									
98848	calc-silicate rock									620												630												
98850	calc-silicate rock															700	15							680	15									
14SW32	pegmatite									550																		550	12	600	14				

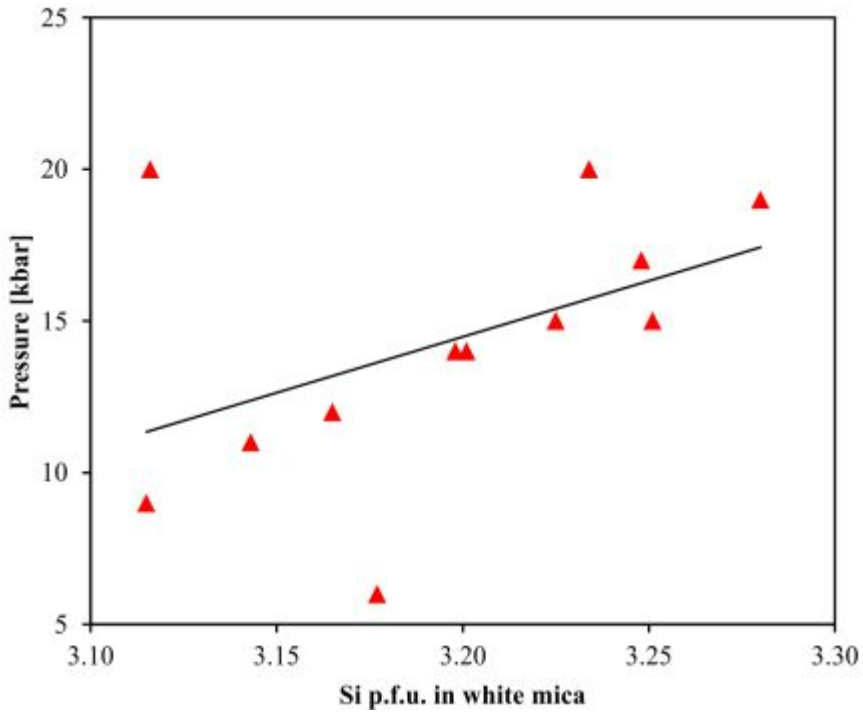

Figure 39 Binary plot of Si p.f.u. in white mica vs. corresponding pressure results obtained by conventional geothermobarometry, indicating the linear increase of phengite with increasing pressure. Illustrated are results from different lithologies.

Table 27 Temperature estimation with Zr-in-rutile thermometry of sample 14SW18, garnet – hornblende mica schist, after Tomkins et al, 2007, Zack et al., 2004 & Ferry et al., 2007.

sample & location		14SW18_amp_rt1	14SW18_amp_rt2	14SW18_amp_rt3	14SW18_amp_rt4	14SW18_amp_rt5	14SW18_amp_rt6	14SW18_amp_rt7	14SW18_amp_rt8		
		core, inclusion in amp, adjacent to bt	rim, inclusion in amp, adjacent to bt	core, inclusion in amp	rim, inclusion in amp	core, inclusion in amp	core, adjacent to amp	core, inclusion in amp	rim, inclusion in amp		
TiO2		100.41	100.02	100.54	100.36	100.4	97.84	100.6	100.23		
ZrO2		0.0261	0.0388	0.0275	0.0515	0.0394	0.0254	0.0529	0.0458		
Total		100.4361	100.0588	100.5674	100.4112	100.4293	97.8653	100.6328	100.2757		
Zr [wt%]		0.019	0.029	0.020	0.038	0.029	0.019	0.024	0.034		
Zr [ppm]		193	287	204	380	292	188	244	339		
Tomkins et al., 2007, T [°C] =(83.9+0.4*P)/(0.1428-R*ln(Zr in ppm))-273											
α-Quartz - field										average T [°C]	±1σ [°C]	±2σ [°C]
8	kbar	585	615	589	637	616	584	608	628	607	19	38
9	kbar	587	617	591	639	618	585	608	630	609	19	38
10	kbar	588	618	592	640	619	586	609	631	610	19	38
11	kbar	590	619	594	642	621	588	607	633	612	19	38
12	kbar	591	621	595	643	622	589	608	634	613	19	38
13	kbar	593	622	596	645	624	591	610	635	614	19	38
14	kbar	594	624	598	646	625	592	611	637	616	19	38
15	kbar	595	625	599	648	626	593	613	638	617	19	38
16	kbar	597	627	601	649	628	595	614	640	619	19	38
17	kbar	598	628	602	651	629	596	615	641	620	19	38
18	kbar	600	630	603	652	63	598	617	643	622	19	38
Zack et al., 2004, T [°C] = 134.7*ln(Zr in ppm) -25												
		684	737	691	775	740	680	715	760	228	34	68
Ferry et al., 2007, T [°C] = (-4630/(log Zr in ppm) -7.420))-273												
		609	640	613	663	641	607	627	653	632	20	40

Table 28 Temperature estimation with Zr-in-rutile thermometry of sample 14SW27, garnet – hornblende mica schist, after Tomkins et al, 2007, Zack et al., 2004 & Ferry et al., 2007.

sample & location		14SW27_grt3_rt1	14SW27_grt3_rt2	14SW27_grt3_rt3	14SW27_grt3_rt4	14SW27_grt3_rt5			
		rim, adjacent to grt	core, adjacent to bt	rim, matrix	core, matrix	core, adjacent to grt			
TiO2		99.59	100.13	99.88	100.56	101.14			
ZrO2		0.0094	0.0225	0.0234	0.0109	0.0143			
Total		99.5994	100.1524	99.9035	100.5708	101.1542			
Zr [wt%]		0.007	0.017	0.017	0.008	0.011			
Zr [ppm]		70	167	173	81	106			
Tomkins et al., 2007, T [°C] =(83.9+0.4*P)/(0.1428-R*ln(Zr in ppm))-273									
α-Quartz - field							average T [°C]	±1σ [°C]	±2σ [°C]
8	kbar	518	575	578	527	544	548	24	49
9	kbar	519	576	579	528	546	550	24	49
10	kbar	520	578	580	529	547	551	25	49
11	kbar	522	579	582	531	548	552	25	49
12	kbar	523	581	583	532	550	554	25	49
13	kbar	524	582	585	533	551	555	25	49
14	kbar	526	583	586	535	552	556	25	49
15	kbar	527	585	587	536	554	558	25	49
16	kbar	528	586	589	537	555	559	25	50
17	kbar	529	587	590	539	556	560	25	50
18	kbar	531	589	592	540	558	562	25	50
Zack et al., 2004, T [°C] = 134.7*ln(Zr in ppm) -25									
		546	664	669	566	603	610	50	100
Ferry et al., 2007, T [°C] = (-4530/(log Zr in ppm) -7.420))-273									
		539	598	601	549	567	571	25	51

Table 29 Temperature estimation with Zr-in-rutile thermometry of sample 14SW62, amphibolite, after Tomkins et al, 2007, Zack et al., 2004 & Ferry et al., 2007.

sample & location	14_SW_62 amp1 r1 core, inclusion in amp	14_SW_62 amp1 r2 core, inclusion in amp	14_SW_62 amp1 r3 rim, inclusion in amp	14_SW_62 amp1 r4 core, inclusion in amp	14_SW_62 amp1 r5 core, inclusion in amp	14_SW_62 amp2 r1 rim, inclusion in amp	14_SW_62 amp3 r2 rim, inclusion in amp	14_SW_62 amp3 r3 rim, inclusion in amp	14_SW_62 amp3 r4 core, inclusion in amp	14_SW_62 amp3 r5 core, inclusion in amp
TiO2	100.00	100.53	100.12	99.82	100.31	99.58	99.82	100.02	100.50	99.84
ZrO2	0.002	0.0047	0.0046	0.0090	0.0062	0.0027	0.0035	0.0011	0.0036	0.0042
Total	100.02	100.58	100.17	99.87	100.33	99.61	99.86	100.03	100.54	99.92
Zr [wt%]	0.0013	0.0039	0.0039	0.0068	0.0161	0.0159	0.0261	0.0081	0.0263	0.0240
Zr [ppm]	163	349	339	368	161	159	261	81	263	240

Tomkins et al., 2007: T [°C] = (83.9+0.410*P(GPa)+0.428 R*ln(Zr in ppm)) 273

α-Quartz - Field											average T [°C]	±1σ [°C]	±2σ [°C]
8	sbar	596	653	651	658	544	610	630	547	631	624	619	32	64
9	sbar	600	658	655	662	548	614	634	551	635	628	623	32	64
10	sbar	604	662	660	666	552	618	639	555	639	632	628	33	65
11	sbar	608	666	661	671	506	622	643	559	643	636	632	33	65
12	sbar	612	671	668	675	510	626	647	563	648	640	636	33	66
13	sbar	616	675	673	680	514	630	651	566	652	645	640	33	66
14	sbar	620	679	677	684	518	634	656	570	656	649	644	33	66
15	sbar	624	683	681	688	522	639	660	574	660	653	649	33	67
16	sbar	629	688	686	693	526	643	664	578	665	657	653	33	67
17	sbar	633	692	690	697	531	647	668	583	669	662	657	34	67
18	sbar	637	697	694	701	535	651	673	586	673	666	661	34	67

Zack et al., 2004: T [°C] = 134.3*ln(Zr in ppm) -23

	664	764	760	771	699	688	725	566	725	718	708	59	118

Ferry et al., 2007: T [°C] = (4550/(-ln(Zr in ppm) -7.4350))-273

	598	656	653	660	596	612	632	548	633	626	621	33	65

THERMODYNAMIC MODELLING

Thermodynamic modelling based on Gibbs free energy minimization and fixed chemical compositions is a powerful tool for not only to recover PT conditions but to interpret mineral textures, predict mineral assemblages and mineral compositions at specific PT conditions and determine the PT evolution of a rock. Calculations have been performed with the software package Perplex_X (Connolly, 2005) using the thermodynamic data file hp04ver.dat of Holland & Powell, 1998 and updates.

GARNET-HORNBLENDE MICA SCHIST

Sample 14SW52 was chosen because it is one of a few samples which does not contain epidote or clinozoisite, and thermodynamic calculations can be performed without considering Fe_2O_3 as a separate component. The mineral assemblage consists of calcic amphibole, almandine-rich garnet, white mica, quartz, biotite, plagioclase (Xab 0.77 – 0.84), rutile and retrograde chlorite. Whole rock analysis yields a composition of SiO_2 = 68.84 wt%, TiO_2 = 0.76 wt%, Al_2O_3 = 13.44 wt%, Fe_{tot} = 7.20 wt%, MnO = 0.085 wt%, MgO = 2.66 wt%, CaO = 1.21 wt%, Na_2O = 1.70 wt%, K_2O = 2.62 wt%, P_2O_5 = 0.099 wt% and LOI = 0.95, resulting in the ten component system NCKFMATSHMn. 10% Fe_2O_3 is assumed. The following solution models were used: garnet: Ganguly et al., 1996, amphibole: White et al., 2003 & Wei et al., 2003, biotite: Tajcmanova et al., 2009, clinopyroxene: Holland & Powell, 1996, chlorite: Holland et al., 1998, plagioclase: Newton et al., 1980, white mica: Pheng(HP), cordierite: hCrd, ilmenite: ideal ilmenite-geikielite-pyrophanite solution and K-Fsp: Waldbaum & Robie, 1971. For the corresponding garnet profile of sample 14SW52 see digital Appendix. Figure 40 illustrates the P/T pseudosection of sample 14SW52. The molar bulk composition is indicated on the top of Figure 40. The stability field of biotite, amphibole, white mica, plagioclase, garnet, quartz, rutile and H_2O is highlighted in red. For a more accurate P/T estimation the isopleths of Xgrs (rim) and Xmg(rim) in garnet have been added. They intersect at approximately 14 kbar and 640°C, corresponding to lower eclogite facies.

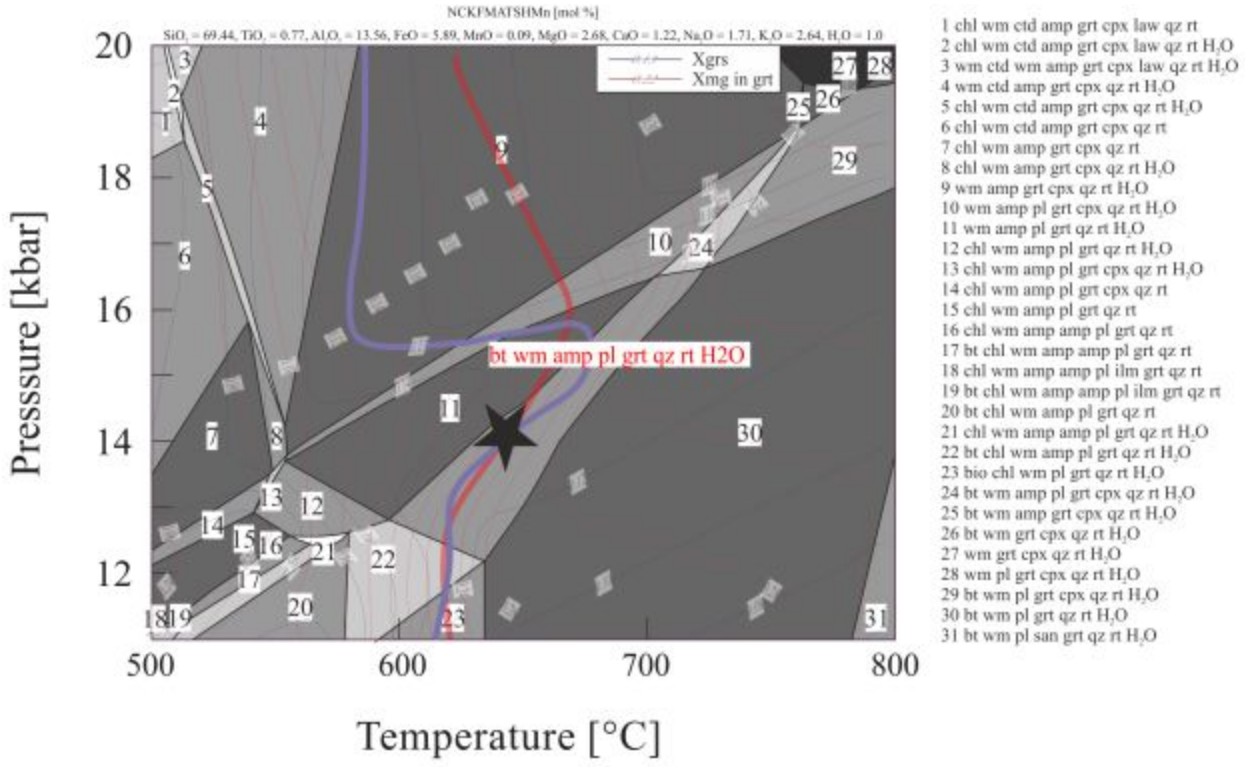

Figure 40 P/T pseudosection of sample 14SW52, garnet-hornblende mica schist. The various mineral assemblages (1-31) over the P/T window are indicated on the right. The red highlighted paragenesis represents the minerals found in the sample. Isopleths of Xgrs (rim, violet) and Xmg (rim, red) in garnet intersect at approximately 14 kbar and 640°C, corresponding to lower eclogite facies.

AMPHIBOLITE

Sample 14SW22 is classified as amphibolite and was choosen due to its well equilibrated mineral assemblage consisting of calcic amphibole (tschermakite), almandine-rich garnet, quartz, biotite, plagioclase (Xab 0.63 – 0.93), rutile and retrograde chlorite. The whole rock analysis yields a composition of SiO_2 = 52.97 wt%, TiO_2 = 1.64 wt%, Al_2O_3 = 17.25 wt%, Fe_{tot} = 9.12 wt%, MnO = 0.074 wt%, MgO = 5.54 wt%, CaO = 9.16 wt%, Na_2O = 2.70 wt%, K_2O = 0.26 wt%, P_2O_5 = 0.560 wt% and LOI = 0.4, resulting in the ten component system NCKFMATSHMn. 20% Fe_2O_3 is assumed and no ferric iron is considered as component. The following solution models were used: garnet: Ganguly et al., 1996, amphibole: Diener et al., 2011, biotite: Tajcmanova et al., 2009, clinopyroxene: Green et al., 2007, chlorite: Holland et al., 1998, plagioclase: Newton et al., 1980 and white mica: Chatterjee & Froese, 1975. First, for an estimation of the water content a P/X pseudosection at a fixed temperature (600 °C, gained by garnet-amphibolite thermometry, see Table 26) and varying water content on the x-axis was calculated. The observed paragenesis in the thin section was found in the calculated diagram at approximately 2.0 wt% H_2O and 8 kbar. Figure 41 illustrates the pseudosection of sample 14SW22. The molar bulk composition is indicated on the top of Figure 41. The stability field of biotite, amphibole, plagioclase, garnet, quartz, rutile and H_2O is highlighted red. Since this stability covers a large PT area the isopleths of Xan (matrix) and Xalm (rim) have been added. They intersect at approximately 8.5 kbar and 660 °C, which corresponds to upper amphibolite facies.

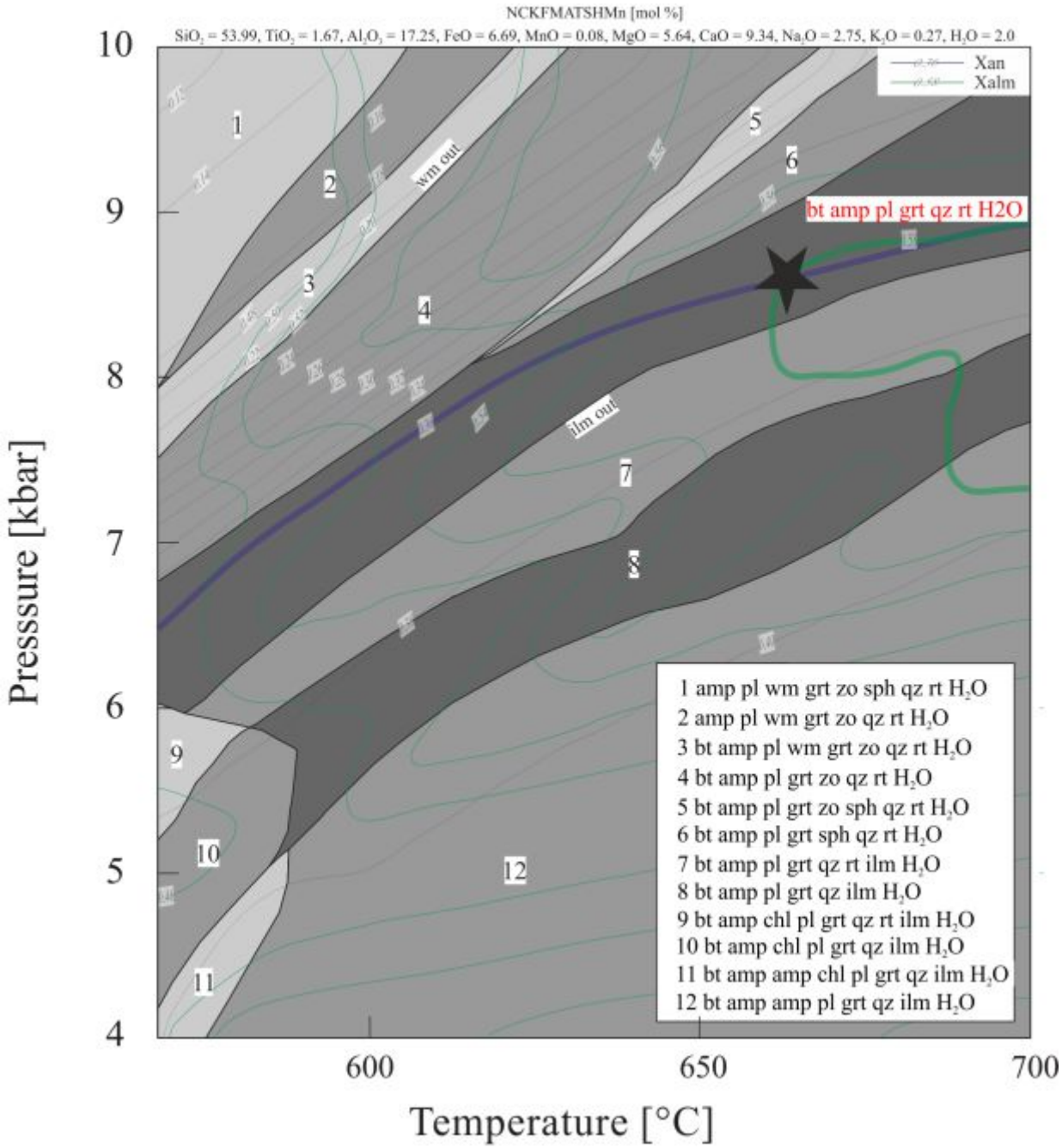

Figure 41 P/T pseudosection for amphibolite (sample 14SW22). Mineral assemblages of the various fields (1-12) are indicated in the right box. The stable paragenesis found in the thin section is highlighted in red. This stability field has a great extent on the temperature axis, therefore the isopleths of Xalm (rim, green) and Xan (matrix, violet) confine a P/T estimation. Isopleths intersect at approximately 8.5kbar and 660°C, corresponding to upper amphibolite facies. The composition of the system is indicated above the figure.

DISCUSSION

The results in the previous chapters are summarized and discussed here. The Surna Nappe is characterized by a variety of lithologies. It is dominated by calcic - metasedimentary rocks, primary garnet - hornblende mica schist with subordinate amphibole - lacking garnet - quartz mica schist and calc - silicate rocks. They are interbedded with amphibolites, interpreted based on geochemistry as tholeiitic basalts. Tonalitic layers are intercalated with the amphibolites. The origin (volcanic or intrusive) of these tonalitic layers within the tholeiitic basalts cannot be decided based on this dataset alone. Pegmatites are a common feature in all lithologies.

Garnet zoning

Garnet is present in all lithologies and represents a proper mineral for interpreting the metamorphic history these rocks have experienced. Based on compositional profiles and 2D element distribution mapping of selected elements, several different types of garnets can be distinguished in the different lithologies of the Surna Nappe. One frequent zoning pattern observed in all lithologies, except in the tonalitic layers, is an almandine-rich idiomorphic garnet showing a complete homogenous profile. This indicates that garnet grow occurred either within a small PT window, or diffusion obscured the previous developed zoning pattern (see Figure 8C & D). The element distribution map of yttrium (chosen due to its slow diffusivity, after Pyle & Spear, 1999) and also the BSE image show various bands and annuli of high yttrium concentrations (see Figure 8F & Figure 12D). A second profile type found in garnet - hornblende mica schist and garnet - quartz mica schist displays typical prograde zoning pattern. Spessartine and the $Fe/(Fe^{2+}+Mg)$ ratio show a rimward decrease and corresponding increase in the pyrope and grossular content (see Figure 8B & Figure 12B & F), suggesting growth during heating (Möller, 1998). This kind of compositional profile in garnet is commonly known from average pelitic compositions metamorphosed up to the staurolite isograd in the prograde Barrovian sequence in Scotland (Chakraborty & Ganguly, 1991). In many cases, the outermost rim compositions reflect reequilibration during decompression and adjustment to reactions taking place in the matrix (Möller, 1998). The inclusions of plagioclase, amphibole and rutile suggest early growth of garnet under amphibolite facies conditions (Möller, 1998). Compositional profiles of garnet in the tonalitic layers indicate a significant increase in grossular from core to rim and a decrease in almandine (see Fig. 16). This may either reflect a

significant change in PT conditions, or the breakdown of plagioclase and building of biotite/epidote.

Quantitative PT estimations

The focus of the conventional geothermbarometry was the determination of the metamorphic peak conditions. In total, eight different geothermo - and barometers have been used to investigate the PT conditions in six different lithologies of the Surna Nappe (see Table 26). The garnet-biotite geothermometer combined with the garnet-biotite plagioclase - quartz geobarometer yields higher PT values compared to other systems. The pressure results of sample 14SW37 and 14SW66 (garnet - hornblende mica schists) with 20 kbar seem not to be realistic, although those two samples also yield the highest pressure values with garnet-amphibole-plagioclase - quartz geobarometry (12 kbar and 15 kbar, respectively), maybe due to disequilibrium of involved phases. In calc-silicate rocks the garnet – clinopyroxene Fe – Mg exchange thermometer combined with the net – transfer reaction anorthite + diopsoide → grossular + pyrope + quartz geobarometer yield consistently high pressures of 15 - 18 kbar. These results are associated with eclogite facies condition, and present a robust estimation of ultimate PT conditions.

Temperature estimations have been evaluated mainly by garnet-biotite and garnet-amphibole geothermometers. Former gives temperatures between 500 - 700 °C, except sample 14SW37, 14SW66 and 98814, which give values above 700 °C. Garnet - amphibole geothermometer yields an average temperature around 450 °C, and hence significantly lower than the garnet-biotite geothermometer. The Zr - in-rutile geothermometer reveals consistent temperatures around 600 °C, and could therefore be seen as the peak temperature since rutile is part of the stable peak paragenesis.

The significant lower PT conditions gained by amphibolite samples (see Figure 37) may represent a re-equilibration of the mineral assemblage in this lithology at lower amphibolite facies conditions.

Thermodynamic modelling

The garnet-hornblende mica schist sample 14SW52, representing the major lithology in the Surna Nappe, yields 15 kbar and 650 °C by conventional geothermbarometry (garnet –

biotite – plagioclase - quartz barometry and garnet - biotite thermometry). The thermodynamic modelling and plot of Xgrs (rim) and Xmg (rim) isopleths gave similar results, with 14 kbar and 640 °C (see Figure 40), confirming eclogite facies peak metamorphic conditions for this lithology.

The PT conditions gained by conventional geothermobarometry of the amphibolite sample 14SW22 yield 8 kbar and ~ 600 °C calculated with garnet-amphibolite-plagioclase-quartz barometry and garnet-amphibole thermometry. These results are confirmed by thermodynamic modelling of the same sample (see Figure 41) yielding 8.5 kbar and slightly higher temperatures of 650 °C. These results again point to a re-equilibration of the amphibolite lithologies during retrograde conditions with clearly lower pressures, but still relatively high temperatures.

Regional correlation with the Seve Nappe Complex

The above mentioned results indicate a prograde clockwise PT path with metamorphic peak conditions of at least 15 kbar and 650 °C. Similar temperature estimations, but significantly lower pressure conditions of 9 kbar and 625 °C, have been calculated by Hacker & Gans, 2005 near Orkanger. However, they did not specify the lithology from which the PT conditions were derived, and since they are similar to our results from the amphibolites, their results could represent re-equilibration during retrograde metamorphism. Hacker & Gans, 2005 concluded furthermore, that formation pressures and temperatures of the Seve Nappe Complex range from 645 °C and 10 kbar to 745 °C and 13 kbar. The PT path Hacker & Gans, 2005 suggested implies an early regional metamorphism (> 445 - 432 Ma) followed by contact metamorphism at 3 kbar (445 – 432 Ma) and a second regional metamorphism at 9 – 12 kbar (< 432 – 443 Ma). Root & Corfu, 2012 dated eclogites from Jämtland, Sweden at 446 $\pm$ 1 Ma, with corresponding PT conditions of 16.5 kbar and 650 – 680 °C (Litjens, 2002 quoted by Brueckner & van Roermund, 2007) and 25 – 26 kbar at 650 – 700 °C by Majka et al., 2013.

CONCLUSION

Evolutionary model for the Surna Nappe

Based on the results from this study and the comparison with the literature, the following evolutionary reconstruction for the Surna Nappe can be derived. The following tectonometamorphic events can be interpreted:

(1) HP to UHP metamorphism occurred around 445 my (Root & Corfu, 2012 & Hacker & Gans, 2005) in the Seve Nappe Complex at Jämtland (Sweden), which corresponds to the evaluated peak conditions of the here present work.

(2) HP metamorphism is followed by decompression and melting of amphibolites as dated by Ladenberger et al., 2014 to 442 – 436 my, resulting in the formation of tonalitic layers within the amphibolites of the Surna Nappe. Recent U - Pb dating of the tonalitic layers in the northern part of the study area by Hestnes, 2016 reveals an age of 438 Ma which correlates with the results by Ladenberger et al., 2014.

(3) Pegmatites in the Surna Nappe dated to 431 Ma (Tucker et al., 2004) cut an older amphibolite foliation which was produced within an overall convergent plate tectonic setting, and which must therefore be slightly older than 431 Ma.

(4) Extensional shear fabrics of lower amphibolite to greenschist facies conditions cut the older main fabric, and hence pegmatites must by younger than 400 my and are associated with the MTFC and the Høybakken detachment. A white mica cooling age of 404 Ma by Hacker & Gans, 2005 indicates the cooling of the Surna Nappe below 500 °C at this time.

REFERENCES

Andréasson P.-G., Gee D.G. & Sukotji S, 1985: “Seve eclogites in the Norrbotton Caledonides, Sweden”. The Caledonide Orogen – Scandinavia and Related Areas, John Wiley and Sons Ltd

Andréasson P.-G., 1994: “The Baltocandian margin in Neoproterozoic-early Palaeozoic times; some constraints on terrane derivation and accretion in the Arctic Scandinavian Caledonides”. GFF, Vol. 120, p. 159-172

Andréasson P. & Gee D.G., 2008": The Baltica- Iapetus boundary in the Scandinavian Caledonides and a revision of the Middle and Upper Allochthons (abstract)". 33rd International Geological Congress, Oslo, Norway

Beckman V., Möller C., Söderlund U., Corfu F., Pallon J. & Chamerlain K.R., 2014: “Metamorphic zircon formation at the transition from gabbro to eclogite in Trollheim-Surnadalen, Norwegian Caledonides”. In: Corfu F., Gasser D. & Chew D.M. (eds) “New Perspectives on the Caledonides of Scandinavia and Related Areas”. Geological Society London, Special Publications 390

Berman R.G., 1988: “Internally-consistent thermodynamic data for minerals in the system Na2O-K2O-MgO-FeO-Fe2O3-Al2O3-SiO2-TiO2-H2O-CO2.” Journal of Petrology, Vol. 29, p. 445-522

Berman R.G., 1991: “Thermobarometry using multi-equilibrium calculations: a new technique, with petrological applications”. In Quantitative methods in petrology: an issue in honor of Hugh J. Greenwood, Eds. Gordon T.M., Martin R.F., Canadian Mineralogist, Vol. 29, p. 833-855

Berman R.G., 2007: “winTWQ (version 2.3): a software package for performing internally-consistent thermobarometric calculations”. Geological Survey of Canada, Open File 5463, (ed. 2.32)

Blundy J.D. & Holland T.J.B., 1990: “Calcic amphibole equilibria and a new amphibole-plagioclase geothermometer”. Contributions to Mineralogy and Petrology, Vol. 104, p. 208-224

Bohlen S.R. & Liotta J.J., 1986: “A Barometer for Garnet Amphibolites and Garnet Granulites”. Journal of Petrology, Vol. 27, Part 5, p. 1025-1034

Brueckner H.K., Van Roermund H.L.M. & Pearson N.J., 2004: “An Archean (?) to Paleozoic evolution of a garnet peridotite lens with sub-Baltic Shield affinity within the Seve Nappe Complex of Jämtland, Sweden, central Scandinavian Caledonides, Journal of Petrology, Vol. 45, p. 415-437

Brueckner H.K. & Van Roermund H.L.M., 2007: “Current HP metamorphism on both margins of Iapetus: Ordovician ages for eclogites and garnet pyroxenites from the Seve Nappe Complex, Swedish Caledonides”. Journal of Geological Society, Vol. 164, p. 117-128, London

Chatterjee N.D. & Froese E., 1975: "A thermodynamic study of the pseudobinary join muscovite-paragonite in the system $KAlSi_3O_8$-$NaAlSi_3O_8$-Al_2O_3-SiO_2-H2O". American Mineralogist, Vol. 60, p. 89-114

Claesson S., 1982: "Caledonian metamorphism of Proterozoic Seve rocks in Mt. Åreskutan, southern Swedish Caledonides". Geologiska Föreningens i Stockholm Förhandlingar, Vol. 103, Pt. 3, p. 291-304

Cocks L.R.M. & Torsvik T.H., 2002: "Earth geography from 500 to 400 million years ago: a faunal and palaeomagnetic review". Journal of Geological Society, Vol. 159, p. 631-644, London

Connolly J.A.D., 2005: "Computation of phase equilibria by linear programming: A tool for geodynamic modeling and its application to subduction zones decarbonation". Earth and Planetary Science Letters, Vol. 236, p. 524-514

Corfu F., Andersen T.B. & Gasser D., 2014: "The Scandinavian Caledoindes: main features, conceptual advances and critical questions". In: Corfu F., Gasser D. & Chew D.M. (eds) "New Perspectives on the Caledonides of Scandinavia and Related Areas". Geological Society London, Special Publications 390

Cox K.G., Bell P.J. & Pankhurst R.J., 1979: "The interpretation of igneous rocks. George Allen & Unwin, p. 1-450

Dachs E., 1998: "PET: Petrological Elementary Tools for Mathematica". Computers & Geosciences, Vol. 24, No. 3, p. 219-235

Dachs E., 2015: "Theoretische Petrologie script", unpublished

Dale J., Holland T. & Powell R., 2000: "Hornblende-garnet-plagioclase thermobarometry: a natural assemblage calibration of the thermodynamics of hornblende". Contributions to Mineralogy and Petrology, Vol. 140, p. 353 – 362

Deer W.A., Howie R.A. & Zussman J., 1971: "Rock Forming Minerals, Vol. 3, Sheet Silicates". Longman Group Limited, London

Diener J.F.A., Powell R., White R.W. and Holland T.J.B., 2007: "A new thermodynamic model for clino- and orthoamphiboles in the system Na_2O-CaO-FeO-MgO-Al_2O_3-SiO_2-H_2O-O". Journal of Metamorphic Geology, Vol. 25, Issue 6, p. 631-656

Droop G.T.R., 1987: "A general equation for estimating Fe^{3+} concentration in ferromagnesian silicates and oxides from microprobe analyses, using stoichiometric criteria". Mineralogical Magazine, Vol. 51, p. 431-5

Eckert J.O., Newton R.C. & Kleppa O.J., 1991: "The ΔH of reaction and recalibration of garnet-pyroxene-plagioclase-quartz geobarometers in the CMAS system by solution calorimetry". American Mineralogist, Vol. 76, p. 148-160

Ferry J.M. & Watson E.B., 2007: "New thermodynamic models and revised calibrations for the Ti-in-zircon and Zr-in-rutile thermometers". Contributions to Mineralogy and Petrology, Vol. 154, p. 429-437

Franz L., 2016: "Geothermobarometrie - Vorlesungsunterlagen". Mineralogisch-Petrographisches Institut, Universität Basel

Ganguly J. & Chakraborty S., 1991: “Compositional Zoning and Cation Diffusion in Garnets”. In: Ganguly J. (eds) “Diffusion, Atomic Ordering, and Mass Transport, Selected Topics in Geochemistry”, Advances in Physical Geochemistry, Vol. 8, Springer Verlag

Ganguly J., Cheng W. and Tirone M., 1996: “Thermodynamics of aluminosilicate garnet solid solution: new experimental data, an optimized model, and thermometric applications”. Contributions to Mineralogy and Petrology, Vol. 126, Issue 1, p. 137-151

Gasser D., Svendby A.K., Solli A. & Slagstad T., 2016: “Berggrunnskart Orkanger 1:50 000”. Norges Geologiske Undersøkelse

Gee D.G., Guezou J.-C., Roberts D. & Wolff F.C., 1985: “The central southern part of the Scandinavian Caledonides”. The Caledonide Orogen – Scandinavia and Related Areas, John Wiley and Sons Ltd

Gee D. G., Juhlin C., Pascal C. & Robinson P., 2010: “Collisional Orogeny in the Scandinavian Caledonides (COSC)”. GFF, Vol. 132, p.29-44

Graham C.M. & Powell R., 1984: “A garnet-hornblende geothermometer: calibration, testing, and application to the Pelona Schist, Southern California”. Journal of Metamorphic Geology, Vol. 2, Issue 1, p. 13-31

Green E.C.R., Holland T.J.B & Powell R., 2007: “An order-disorder model for omphacitic pyroxenes in the system jadeite-diopside-hedenbergite-acmite, with applications to eclogite rocks”. American Mineralogist, Vol. 92, p. 1181-1189

Grimmer J.C., Glodny J., Drüppel K., Greiling R.O. & Kontny A., 2015: “Early – to mid-Silurian extrusion wedge tectonics in the central Scandinavian Caledonides“. Geology, Vol. 43, No. 4, p. 347-350

Hacker B.R. & Gans P.B., 2005: “Continental collision and the creation of ultrahigh-pressure terranes: Petrology and thermochronology of nappes in the central Scandinavian Caledonides”. Geological Society of America Bulletin 117, No. 1-2, p. 117-134

Hestnes Å, 2016: “Lithological and structural analysis of the Rødbergt-Rørvika-Varpneset transect, Mid-Norwegian Caledonides”. Unpublished MSc thesis, Norwegian University of Science and Technology, Trondheim

Hoisch T.D., 1990: “Empirical calibration of six geobarometers for the mineral assemblage quartz + muscovite + biotite + plagioclase + garnet”. Contributions to Mineralogy and Petrology, Vol. 104, p. 225-234

Holdaway M.J., 2000: “Application of new experimental and garnet Margules data to the garnet-biotite geothermometer”. American Mineralogist, Vol. 85, p. 881-892

Holdaway M.J. & Mukhopadhyay B., 1993:” A reevaluation of the stability relations of andalusite: Thermochemical data and phase diagram for the aluminum silicates”. American Mineralogist, Vol. 78, p. 298-315

Holland T.J.B. & Powell R., 1996: “Thermodynamics of order-disorder in minerals: II Symmetric formalism applied to solid solutions”. American Mineralogist, Vol. 81, p. 1425-1437

Holland T.J.B., Baker J. & Powell R., 1998: “Mixing properties and activity-compositions and relationships of chlorite in the system MgO-FeO-Al_2O_3-SiO_2-H_2O”. European Journal of Mineralogy, Vol. 10, Issue 3, p. 395-406

Holland T.J.B. & Powell R., 1998: “An internally consistent thermodynamic data set for phase of petrological interest”. Journal of Metamorphic Geology, Vol. 16, Issue 3, p. 309-343

Irvine T. & Baragar W., 1971: “A guide to the chemical classification of the common volcanic rocks”. Canadian Journal of Earth Sciences, Vol. 8, p.523-548

Janoušek V., Farrow C.M. & Erban V., 2006: “Interpretation of Whole-rock Geochemical Data in Igneous Geochemistry: Introducing Geochemical Data Toolkit (GCDkit)”. Journal of Petrology, Vol. 47, No. 6, p. 1255-1259

Johnsen S. O., 1979: "Geology of the area west and north west of Orkdalsfjorden, Sør-Trøndelag". Norges geol. Unders., 348, p. 33-46

Klonowska I., Majka J., Janák M. Gee D.G. & Ladenberger A., 2013: Pressure – temperature evolution of a kyanite – garnet politic gneiss from Åreskutan: evidence of ultra – high – pressure metamorphism of the Seve Nappe Complex, west – central Jämtland, Swedish Caledonides”. In: Corfu F., Gasser D. & Chew D.M. (eds) “New Perspectives on the Caledonides of Scandinavia and Related Areas”. Geological Society London, Special Publications 390

Kollung S., 1990: “The Surna, Rinna and Orkla Nappes of the Surnadal-Orkdal district, southwestern Trondheim Region”. Nor. Geol. Unders.. Bulletin 418, p. 9-17

Kontny A., Engelmann R., Grimmer J.C., Greiling R.O. & Hirt A., 2012: “Magnetic fabric development in a highly anisotropic magnetite bearing ductile shear zone (Seve Nappe Complex, Scandinavian Caledonides)”. International Journal of Earthscience, Vol. 101, Issue 3, p. 671-692

Krill A.G., 1985: “Relationships between the Western Gneiss Region and the Trondheim Region: Stockwerk-tectonics reconsidered”. The Caledonide Orogen – Scandinavia and Related Areas, John Wiley and Sons Ltd

Krill A.G. & Röshoff K., 1981: “Basement-cover Relationships in the Central Scandinavian Caledonides". Excursion B-5, Uppsala Caledonide Symposium

Krogh Ravna E.J., 2000: “The garnet-clinopyroxene Fe^{2+}-Mg geothermometer: an updated calibration”. Journal of Metamorphic Geology, Vol. 18, Issue 2, p. 211-219

Lapadu-Hargues P., 1960: “Sur I’existence et la Nature de l’apport Chimique dans certains series Chriallophylliennes”. Bulletin de la Societe Geologique de France, Vol. 5, Issue 15, p. 255

Leake B.E., Woolley A.R., Apps C.E.S., Birch W.D., Gilbert M.C., Grice J.D., Hawthorne F.C., Kato A., Kisch H.J., Krivovichev V.G., Linthout K., Laird J., Mandarino J.A., Maresch W.V., Nickel E.H., Rock N.M.S., Schumacher J.C., Smith D.C., Stephenson N.C.N., Ungaretti L., Whittaker E.J.W. & Youzhi G., 1997: “Nomenclature of amphiboles: Report of the subcommittee on amphiboles of the international mineralogical association, commission on the new minerals and mineral names”. The Canadian Mineralogist, Vol. 35, p. 219-246

Leake B.E., 1964: “The Chemical Distinction Between Ortho- and Para-amphibolites”. Journal of Petrology, Vol. 5, Part 2, p. 238-254.

Litjens A., 2002: “PT estimation of high-pressure metamorphic rocks from the Seve Nappe Complex, Jämtland, Central Scandinavian Caledonides”. MSc thesis, University of Utrecht

Majka J., Janák M., Andersson B, Klonowska I., Gee D.G., Rosen Å. & Kośmińska K., 2013: “Pressure – temperature estiamtions on the Tjeliken eclogite: new insights into the (ultra)-high pressure evolution of the Seve Nappe Complex in the Scandinavian Caledonides”. In: Corfu F., Gasser D. & Chew D.M. (eds) “New Perspectives on the Caledonides of Scandinavia and Related Areas”. Geological Society London, Special Publications 390

Majka J., Rosén Å., Janák M., Froitzheim N., Klonowska I., Menecki M., Sasinková V. & Yoshida K., 2014: “Microdiamond discovered in the Seve Nappe (Scandinavian Caledonides) and its exhumation by the “vacuum-cleaner” mechanism”. Geology, Vol. 42, No. 12, p.1107-1110

Massonne H.-J. & Schreyer W., 1987: “Phengite geobarometry based on the limiting assemblage with K-feldspar, phlogopite and quartz”. Contributions to Mineralogy and Petrology, Vol. 95, Issue 2, p. 212-224

Miyashiro A., 1973: “Metamorphism and Metamorphic belts”. George Allen & Unwin Ltd., London, Great Britain

Morimoto N., Fabries J., Ferguson A.K., Ginzburg I.V:, Ross M., Seifert F.A., Zussman J., Aoki K. & Gottardi G., 1988: “Nomenclature of pyroxenes”. Subcommittee on Pyroxenes, Commission on New Minerals and Minerals Names, International Mineralogical Association. American Mineralogist, Volume 73, p. 1123-1133

Möller C., 1998: “Decompressed eclogites in the Sveconorwegian (-Greenvillian) orogeny of SW Sweden: petrology and tectonic implications”. Journal of Metamorphic Geology, Vol. 16, p. 641-656

Newton E.C., Charlu T.V. & Kleppa O.J., 1980: “Thermochemistry of high structural state plagioclase”. Geochimica et Cosmochimica Acta, Vol. 44, Issue 7, p. 933-941

Newton R.C. & Perkins D., 1982: “Thermodynamic calibrating of geobarometers based on the assemblage garnet-plagioclase-orthopyroxene (clinopyroxene) - quartz”. American Mineralogist, Vol 67, p. 203-222

Osmundsen P.T., Eide E.A., Haabesland N.E., Roberts D., Andersen T.B., Kendrick M., Bingen B., Braathen A. & Redfield T.F., 2006: "Kinematics of the Høybakken detachment zone and the Møre-Trøndelag Fault Complex, central Norway". Journal of the Geological Society, Vol. 163, p. 303-318

Peacey J.S., 1963: “Deformation in the Gangåsvann Area”. Norges geol. Unders. 223, p. 275-293

Poldervaart A., 1955: “Chemistry of the earth’s crust”. Geological Society of America, Special Paper 62, p. 119-144

Pyle J.M. & Spear F.S., 1999: "Yttrium zoning in garnet: Coupling of major and accessory phase during metamorphic reactions". Mineralogical Society of America, Vol. 1, Pt. 6, p. 1-49

Reymer A.P.S., Boelrijk N.A.I.M., Hebeda E.H., Priem H.N.A., Verdurmen E.A.Th. & Verschure R.H., 1980: "A note on Rb-Sr whole-rock ages in the Seve Nappe of the central Scandinavian Caledonides". Norsk geologisk Tidsskrift 2, p. 139-147

Roberts D., 2003: "The Scandinavian Caledonides: event chronology, palaeogeographic setting and likely modern analogues". Tectonophysics, Vol. 365, p. 283-299

Roberts D., Nordgulen Ø. & Melezhik V., 2007: "The Uppermost Allochthon on the Scandinavian Caledonides: From a Laurentian ancestry through Tactonian orogeny to Scanfian crustal growth on Baltica", The Geological Society of America, Memoir 200, p. 357-377

Roberts D. & Gee D.G., 1985: "An introduction to the structure of the Scandinavian Caledonides". The Caledonide Orogen – Scandinavia and Related Areas, John Wiley and Sons Ltd.

Roberts D. & Stephens M., 2000: "Caledonian Orogenic Belt". In: Lundqvist T. and Autio S. (eds), Description to the Bedrock Map of Central Fennoscandia (Mid-Norden), Geological Survey of Finland, Special Paper 228., p 79-104

Robinson P. & Roberts, 2008: "A tectonostratigraphic transect across the central Scandinavian Caledonides, Storlien-Trondheim-Lepsøy. Part II: Excursion guide in Norway". Guidebook for the Norwegian part of Excursion #34 of the 33nd International Geological Congress, Oslo, Norway, August 2008

Root D. & Corfu F, 2012: U-Pb geochronology of two Ordovician high-pressure metamorphic events in the Seve Nappe Complex, Scandinavian Caledonides". Contributions to Mineralogy and Petrology, Vol. 163, p. 769-788

Seranne M., 1992: "Late Paleozoic kinematics of the Møre-Trøndelag Fault Zone and adjacent areas, central Norway". Norsk Geologisk Tidsskrift 72, 141-158

Spear F.S., 1993: "Metamorphic Phase Equilibria and Pressure-Temperature-Time Paths". Mineralogical Society of America, Monograph, Washington, D.C., USA

Spear F.S. & Cheney J.T., 1989: "A petrogenetic grid for pelitic schists in the system SiO_2 - Al_2O_3 – FeO – MgO - K_2O – H_2O". Contributions to Mineralogy and Petrology, Vol. 101, p. 149-164

Stephens M.B. & Gee D.G., 1985: "A tectonic model for the evolution of the eugeoclinal terranes on the central Scandinavian Caledonides". The Caledonide Orogen – Scandinavia and Related Areas, John Wiley and Sons Ltd

Streckeisen A.L., 1974: "Classification and nomenclature of Plutonic rocks". Geol. Rundschau, Vol. 63, p. 773-786

Tajčmanová L., Connolly J.A.D & Cesare B, 2009: "A thermodynamic model for titanium and ferric iron solution in biotite". Journal of Metamorphic Geology, Vol. 27, Issue 2, p. 153-165

Tomkins H.S., Powell R. & Ellis D.J., 2007: “The pressure dependence of the zirconium-in-rutile thermometer”: Journal of Metamorphic Geology, Vol. 25, p. 703-713

Trucker R.D., Robinson P., Solli A., Gee D.G., Thorsnes T., Krogh T.E., Nordgulen Ö. & Bickford M.E., 2004: “Thrusting and extension in the Scandian Hinterland, Norway: New U-Pb ages and tectonostratigraphic evidence”. American Journal of Science Vol. 304, p. 477-532

Waldbaum D.R., & Robie R.A., 1971: “Calorimetric investigation of Na-K mixing and polymorphism in the alkali feldspars”. Zeitschrift für Kristallograhie, Vol. 134, p. 381-420

Wei C.J., Powell R. & Zhang L.F., 2003: “Eclogites from the south Tianshan, NW China: petrological and characteristics and calculated mineral equilibria in the Na_2O-CaO-FeO-MgO-Al_2O_3-SiO_2-H_2O system”. Journal of Metamorphic Geology, Vol. 21, Issue 21, p. 163-179

Werner C.-D., 1987: “Saxonian Granulites – Igneous or Lithogenous. A contribution to the geochemical diagnosis of the original rocks in high-metamorphic complexes”. ZfI-Mittelungen, Vol. 133, p. 221-250

White R.W., Powell R. & Phillips G.N., 2003: “A mineral equilibria study of the hydrothermal alteration in mafic greenschist facies rocks at Kalgoorlie, Western Australia”. Journal of Metamorphic Geology, Vol. 21, Issue 5, p. 455-468

Whitney D.L. & Evans B.W., 2010: “Abbreviations for names of rock-forming minerals”. American Mineralogist, Vol. 95, p. 185-187

Zack T., Moraes R. & Kronz A., 2004: “Temperature dependence of Zr in rutile: empirical calibration of a rutile thermometer”. Contributions to Mineralogy and Petrology, Vol. 148, p.471-488

APPENDIX

Appendix A Geological map after Gasser et al., 2016 with all sample notifications.

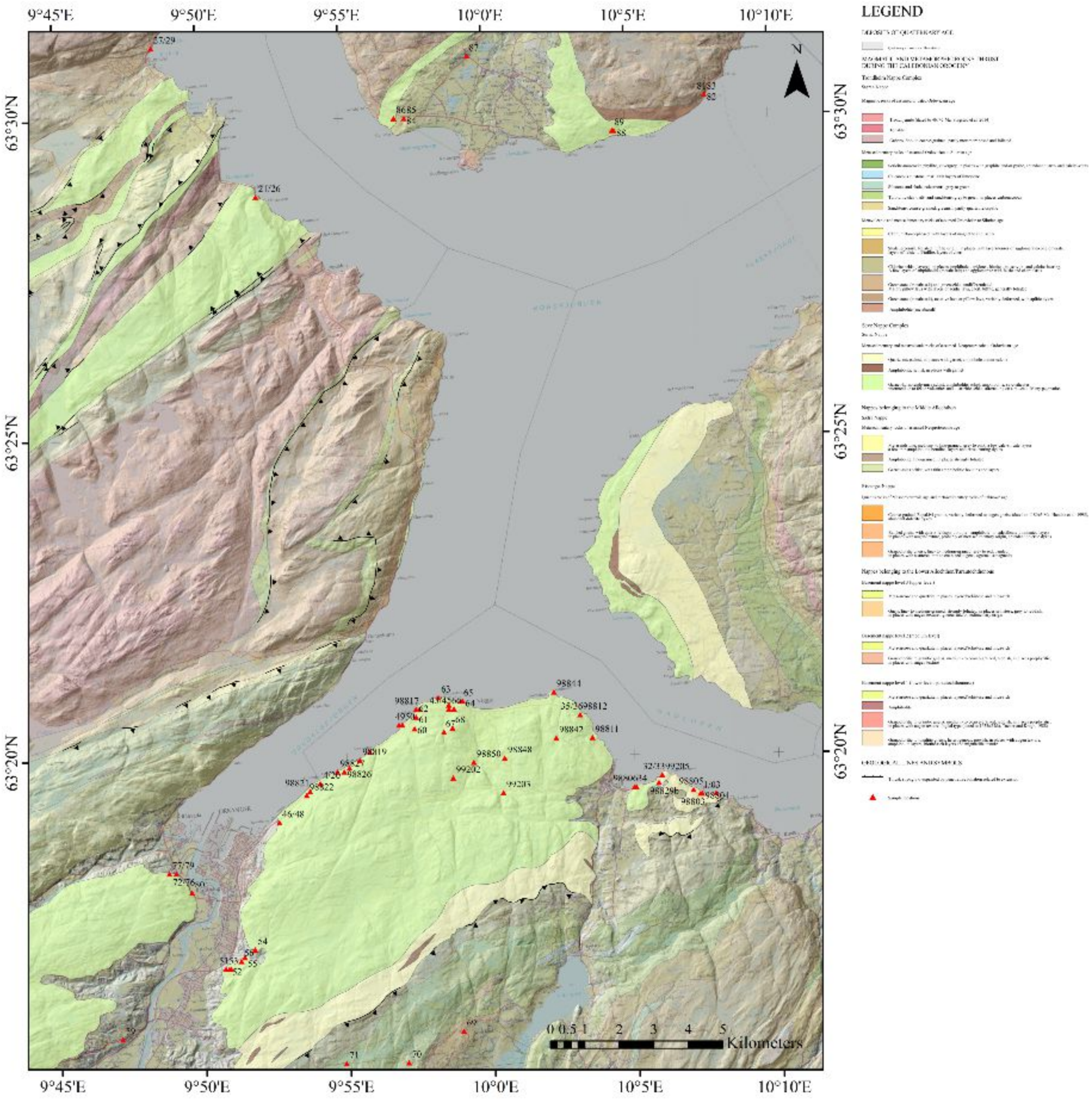

Appendix B Sample list with GPS coordinates, fields description, mineralogy and processing. Abbreviation for groups: (1) garnet - hornblende mica schist, (2) garnet - quartz -mica schist, (3) amphibolite, (4) tonalitic layer, (5) calc-silicate rock, (6) pegmatite. Mineral abbreviation after Whitney & Evans, 2010.

Appendix C Geological map after Gasser et al., 2016 with samples indicated which are included in the whole rock data set, see **Appendix D.**

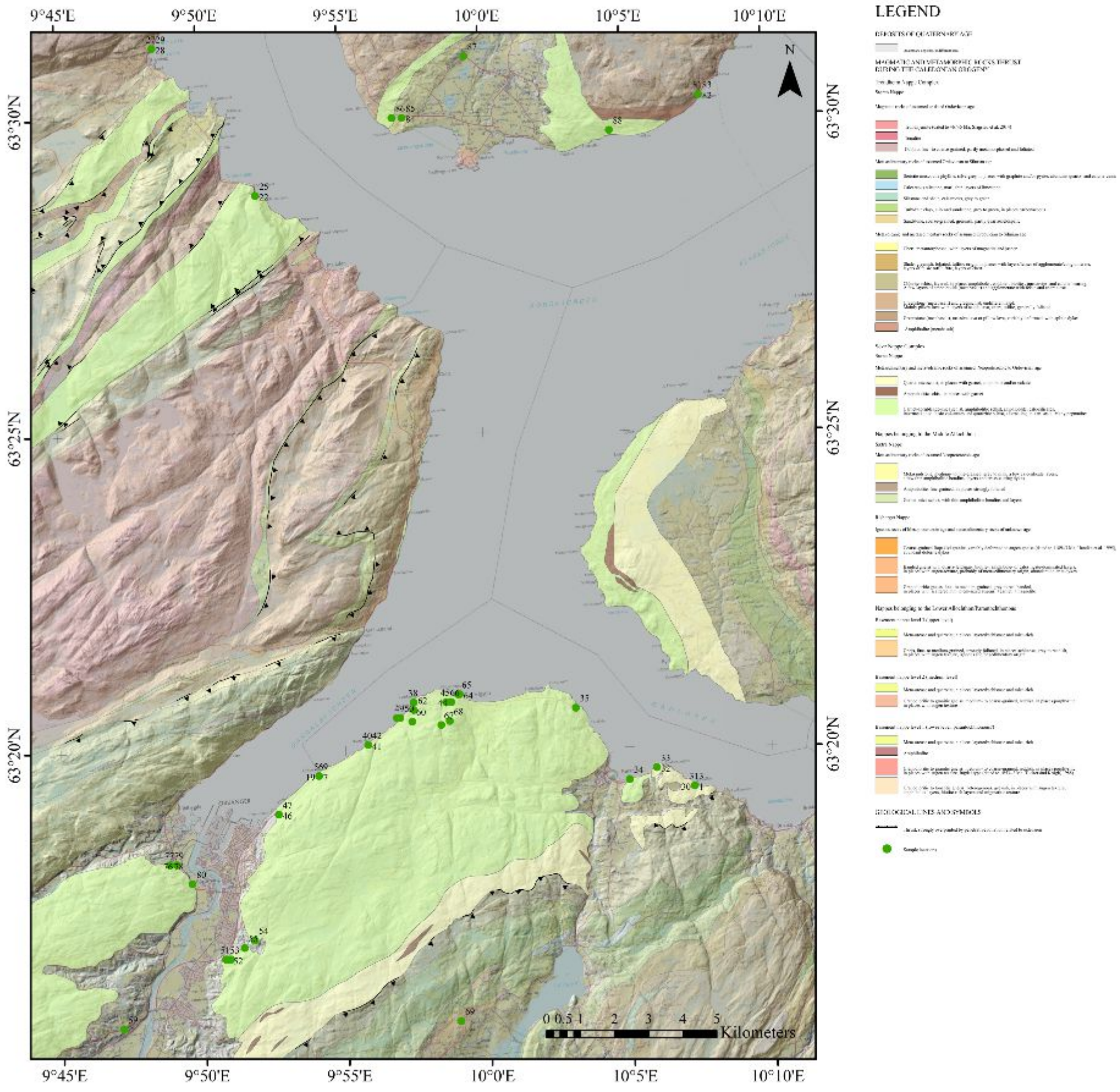

Appendix D Summary of major and trace element analysis of the different lithologies of the Surna Nappe.

sample	lithology	SiO_2 [wt%]	TiO_2 [wt%]	Al_2O_3 [wt%	Fe_2O_3 _wt%	MnO [wt%]	MgO [wt%]	CaO [wt%]	Na_2O [wt%]	K_2O [wt%]	P_2O_5 [wt%]	LOI _wt%	sum [wt%]	Ba (PPM)	Ce (PPM)	Cr (PPM)	Cs (PPM)	Cu (PPM)	Ga (PPM)	Nb (PPM)	Nd (PPM)	Ni (PPM)	Pb (PPM)	Rb (PPM)	Sc (PPM)	Sr (PPM)	Th (PPM)	U (PPM)	V (PPM)	Y (PPM)	Zn (PPM)	Zr (PPM)
14SW01	grt-bt-mica schist	81.43	0.40	8.11	3.58	0.100	1.32	0.40	0.79	2.08	0.070	0.84	99.11	349	47	73	<20	45	<15	<20	<20	<20	<20	75	<20	25	<20	<20	51	<20	42	70
14SW18	grt-bt-mica schist	55.96	0.86	18.28	9.44	0.160	3.36	4.48	2.22	3.03	0.060	1.49	99.34	33	19	814	<20	120	15	<20	<20	344	<20	<10	37	201	<20	<20	168	<20	62	39
14SW19	grt-bt-mica schist	65.88	0.67	14.98	6.03	0.110	2.88	1.80	4.45	2.45	0.090	0.51	99.84	426	122	127	<20	27	25	29	58	43	<20	77	26	27	<20	<20	236	61	156	319
14SW25	grt-bt-mica schist	66.73	0.84	12.59	6.44	0.071	3.61	3.25	2.11	1.60	0.151	1.00	100.37	439	69	193	<20	182	18	36	37	78	<20	106	25	33	<20	<20	223	76	115	289
14SW27	grt-bt-mica schist	75.65	0.60	10.51	4.71	0.079	1.73	1.64	2.73	1.38	0.187	0.80	100.01	42	58	43	<20	22	22	48	31	20	<20	<10	28	346	<20	<20	248	24	86	133
14SW29	grt-bt-mica schist	52.81	2.65	13.84	12.19	0.228	3.17	6.91	4.08	1.16	1.202	0.95	99.19	8	20	527	<20	<20	16	<20	<20	120	<20	<10	39	230	<20	<20	244	<20	70	40
14SW30	grt-bt-mica schist	63.19	0.69	12.67	5.79	0.090	3.29	7.44	1.89	1.31	0.170	4.13	99.51	16	20	84	<20	<20	22	<20	33	<20	<20	<10	39	394	<20	<20	559	36	94	88
14SW31	grt-bt-mica schist	70.28	0.68	10.15	5.14	0.070	2.94	4.41	2.04	1.08	0.090	2.16	99.15	259	42	73	<20	<20	<15	<20	33	<20	<20	54	<20	281	<20	<20	69	21	49	144
14SW33	grt-bt-mica schist	63.05	0.83	14.68	7.06	0.070	4.24	3.74	2.31	3.43	0.150	1.73	99.29	43	20	<20	<20	<20	<15	<20	<20	<20	<20	17	<20	93	<20	<20	32	22	61	58
14SW34	grt-bt-mica schist	62.79	1.04	14.93	7.41	0.070	3.98	2.41	2.72	2.66	0.150	0.77	98.94	154	20	<20	<20	60	<15	<20	24	<20	<20	19	<20	91	<20	<20	<20	35	75	71
14SW37	grt-bt-mica schist	58.56	0.88	16.94	7.98	0.110	4.79	3.10	2.70	2.71	0.190	1.10	99.04	44	36	13	<20	<20	<15	<20	<20	<20	<20	11	21	48	<20	<20	24	24	110	85
14SW38	grt-bt-mica schist	57.35	0.86	16.96	8.44	0.110	4.85	3.49	1.22	3.92	0.160	1.84	98.98	132	20	25	30	62	<15	<20	22	<20	<20	22	<20	183	<20	<20	52	28	55	59
14SW42	grt-bt-mica schist	62.49	0.71	15.72	6.13	0.070	3.75	4.55	2.02	2.61	0.130	0.90	99.08	51	107	46	<20	42	<15	<20	46	<20	<20	17	<20	24	<20	<20	50	48	115	109
14SW44	grt-bt-mica schist	67.03	0.70	11.84	4.55	0.090	2.56	8.24	2.98	0.16	0.150	0.33	99.10	356	76	136	<20	112	<15	<20	55	38	<20	70	<20	96	<20	<20	96	52	84	118
14SW45	grt-bt-mica schist	58.45	0.84	15.86	7.52	0.100	4.45	5.42	1.82	3.17	0.170	0.76	98.55	310	20	411	<20	21	15	<20	<20	242	<20	87	37	170	<20	<20	98	<20	74	74
14SW49	grt-bt-mica schist	57.06	0.85	16.94	7.97	0.100	4.66	3.59	3.43	2.98	0.160	1.00	98.74	516	48	141	29	31	17	<20	<20	87	<20	92	<20	381	<20	<20	92	<20	95	115
14SW50	grt-bt-mica schist	58.47	0.83	17.80	8.18	0.100	4.93	1.96	1.38	3.60	0.150	1.87	99.05	26	109	191	<20	<20	26	23	52	99	<20	<10	27	190	<20	<20	194	29	112	369
14SW51	grt-bt-mica schist	75.07	0.71	10.33	4.78	0.070	2.14	2.84	1.87	1.15	0.140	0.42	99.50	207	59	212	<20	35	16	<20	32	87	<20	61	21	133	<20	<20	110	23	80	196
14SW52	grt-bt-mica schist	68.84	0.76	13.44	7.20	0.090	2.66	1.21	1.70	2.62	0.100	0.95	99.56	343	75	44	<20	154	<15	<20	30	<20	<20	47	<20	70	<20	<20	67	<20	76	206
14SW53	grt-bt-mica schist	70.48	0.75	9.78	5.57	0.060	2.40	1.78	1.29	1.88	0.130	0.71	94.82	678	70	53	<20	69	19	21	35	<20	<20	82	<20	131	<20	<20	62	23	204	191
14SW54	grt-bt-mica schist	69.34	0.79	12.72	6.16	0.070	3.01	2.11	1.97	3.01	0.130	1.06	99.37	381	136	19	<20	44	22	69	67	<20	<20	32	37	195	<20	<20	168	60	176	280
14SW55	grt-bt-mica schist	64.91	0.65	15.15	5.16	0.070	2.40	4.48	3.38	1.81	0.150	0.82	98.97	152	61	110	<20	29	15	<20	31	44	21	46	20	244	<20	<20	105	28	72	148
14SW59	grt-bt-mica schist	74.31	0.27	12.98	2.93	0.050	0.70	3.03	4.67	0.15	0.050	0.20	99.36	188	72	138	<20	21	<15	<20	<20	32	<20	49	<20	137	<20	<20	94	25	55	187
14SW64	grt-bt-mica schist	65.16	0.76	13.73	5.66	0.070	2.53	5.91	2.18	1.94	0.150	1.13	99.22	129	32	<20	<20	<20	19	<20	<20	<20	<20	11	<20	571	<20	<20	31	<20	36	49
14SW65	grt-bt-mica schist	71.04	0.59	12.40	4.30	0.080	1.63	3.10	3.25	1.27	0.120	0.66	98.45	310	48	177	<20	116	17	<20	24	59	<20	100	22	134	<20	<20	134	<20	87	187
14SW66	grt-bt-mica schist	60.88	0.81	16.25	6.65	0.070	4.10	4.00	2.27	2.61	0.190	1.41	99.22	354	75	234	<20	<20	19	<20	37	86	<20	110	22	186	<20	<20	132	29	94	248
14SW67	grt-bt-mica schist	68.61	1.45	7.49	8.60	0.110	4.32	6.17	0.88	0.51	0.390	0.93	99.45	414	20	<20	25.0	<20	<15	<20	<20	<20	<20	<10	<20	650	<20	<20	<20	<20	<20	150
14SW68	grt-bt-mica schist	59.36	1.29	14.08	11.24	0.210	2.72	6.58	3.06	0.23	0.240	0.28	99.49	37	56	95	<20	80	15	<20	39	38	<20	<10	22	298	<20	<20	102	28	45	181
14SW74	grt-bt-mica schist	73.68	0.21	13.64	3.74	0.079	1.35	1.39	5.11	1.03	0.074	0.45	99.59	342	110	130	<20	70	21	<20	50	66	<20	101	20	235	<20	<20	155	22	93	140
14SW75	grt-bt-mica schist	73.05	0.23	12.84	3.71	0.047	1.37	3.00	4.48	0.62	0.022	0.22	99.60	540	48	127	<20	42	23	<20	37	66	<20	134	29	133	<20	<20	146	30	101	150
14SW76	grt-bt-mica schist	67.23	0.23	13.73	6.06	0.094	2.24	4.84	3.91	0.67	0.035	0.40	99.44	226	20	22	<20	159	21	<20	<20	<20	<20	20	46	228	<20	<20	391	<20	100	36
14SW77	grt-bt-mica schist	73.82	0.37	12.39	4.55	0.055	0.89	2.05	5.21	0.22	0.068	0.24	99.86	131	20	<20	<20	38	16	<20	<20	<20	<20	<10	<20	155	<20	<20	<20	23	34	58
14SW78	grt-bt-mica schist	65.93	0.43	13.69	7.15	0.094	2.79	3.96	5.22	0.35	0.072	0.27	99.96	556	20	<20	<20	36	<15	<20	<20	<20	<20	34	<20	275	<20	<20	55	<20	65	68
14SW79	grt-bt-mica schist	51.89	1.95	14.70	12.43	0.155	4.68	8.01	4.38	0.17	0.180	0.73	99.25	317	79	99	<20	24	19	<20	32	46	22	102	22	203	<20	<20	110	28	79	122
14SW84	grt-bt-mica schist	62.88	0.66	11.91	5.11	0.087	3.11	6.63	1.78	2.07	0.142	1.52	99.88	92	52	150	<20	86	<15	<20	42	30	<20	<10	<20	373	<20	<20	73	23	49	257
14SW85	grt-bt-mica schist	65.36	0.73	14.98	5.91	0.082	3.13	3.46	2.75	2.70	0.155	1.03	100.26	419	47	118	<20	<20	21	<20	35	59	<20	121	23	369	<20	<20	135	27	96	170
14SW05	grt qz mica schist	43.23	1.55	16.38	29.17	1.160	3.33	2.29	0.04	1.50	0.460	1.45	100.57	43	20	107	<20	63	21	<20	20	<20	<20	<10	34	150	<20	<20	339	47	263	121
14SW06	grt-qz-mica schist	41.26	1.53	17.91	25.55	0.630	4.71	3.08	0.17	2.65	0.590	0.94	99.01	16	34	26	27	27	21	<20	<20	<20	<20	<10	38	175	<20	<20	281	26	32	71
14SW16	grt qz mica schist	56.74	0.23	13.06	22.45	1.120	2.44	3.00	0.06	0.27	0.310	0.23	99.91	724	65	123	<20	<20	24	<20	41	53	<20	148	<20	386	<20	<20	151	26	118	150
14SW17	grt-qz-mica schist	51.96	0.64	14.14	23.04	1.180	3.36	2.92	0.03	1.75	0.230	0.52	99.76	434	55	126	<20	39	24	<20	39	63	<20	134	25	129	<20	<20	155	27	102	151
14SW28	grt-qz-mica schist	67.69	0.70	13.09	5.19	0.100	2.31	3.32	2.63	2.34	0.430	1.44	99.24	116	65	127	<20	21	<15	<20	<20	35	<20	52	22	104	<20	<20	84	27	50	264
14SW58	grt-qz-mica schist	63.50	0.85	13.76	6.76	0.080	4.01	3.73	1.91	2.15	0.110	2.03	98.89	314	51	135	<20	65	18	<20	24	86	<20	107	<20	99	<20	<20	113	27	80	176
14SW86	grt-qz-mica schist	70.07	0.67	12.94	4.88	0.070	3.15	4.04	1.59	1.86	0.150	0.91	99.35	235	65	206	28	35	<15	<20	<20	59	<20	79	<20	76	<20	<20	86	25	59	239
14SW87	grt qz mica schist	61.52	0.84	15.97	7.23	0.080	3.94	3.45	2.39	2.98	0.140	1.13	100.10	269	32	154	<20	27	15	<20	<20	53	<20	77	<20	128	<20	<20	115	22	99	183
14SW88	grt-qz-mica schist	58.53	0.87	15.99	7.51	0.100	4.56	6.05	1.76	2.51	0.190	1.66	99.72	319	84	54	<20	85	15	<20	29	<20	<20	67	<20	222	<20	<20	89	24	55	190
14SW09	amphibolite	48.08	0.79	15.27	9.52	0.140	12.39	10.93	1.91	0.21	0.060	5.67	97.96	300	78	188	<20	43	19	<20	<20	62	<20	66	<20	163	<20	<20	123	27	80	209
14SW07	amphibolite	50.78	1.98	16.75	9.81	0.180	3.45	14.31	0.44	0.31	0.250	0.34	98.60	81	56	<20	<20	<20	15	<20	<20	<20	<20	<10	<20	140	<20	<20	43	<20	22	81
14SW09	amphibolite	49.04	0.40	14.38	9.02	0.160	8.20	15.46	0.51	0.35	0.050	0.56	98.12	87	46	84	<20	73	19	<20	23	<20	<20	<10	29	216	<20	<20	308	46	52	174
14SW10	amphibolite	50.62	1.89	14.81	12.05	0.110	4.98	10.23	2.82	0.44	0.160	0.39	98.52	157	139	166	<20	77	22	<20	48	94	<20	29	22	522	<20	<20	179	22	182	289
14SW33	amphibolite	52.97	1.64	17.25	9.12	0.074	5.54	9.16	2.70	0.26	0.560	0.40	99.67	325	86	105	26	<20	19	<20	54	28	<20	75	21	265	<20	<20	111	27	70	182
14SW40	amphibolite	47.16	0.68	17.39	15.02	0.140	5.86	7.28	3.45	0.87	0.010	0.83	98.69	330	69	125	<20	93	20	<20	57	55	<20	98	24	216	<20	<20	118	29	98	168
14SW46	amphibolite	50.25	1.49	14.74	12.55	0.290	5.93	7.88	4.19	0.27	0.140	0.87	98.58	70	116	98	<20	<20	19	<20	87	20	<20	15	29	154	31	<20	179	71	121	487
14SW47	amphibolite	56.72	1.13	14.26	12.30	0.170	4.27	6.47	3.51	0.10	0.080	0.34	99.34	48	20	44	<20	<20	17	<20	28	<20	<20	<10	27	188	<20	<20	137	74	49	179
14SW60	amphibolite	53.09	2.17	14.14	11.46	0.180	4.66	8.67	3.20	0.38	0.240	0.50	98.89	58	20	345	<20	<20	19	<20	21	137	<20	<10	35	139	<20	<20	316	32	86	107
14SW62	amphibolite	49.84	1.02	16.19	10.23	0.120	6.29	7.24	4.44	1.22	0.130	1.38	98.09	94	122	<20	<20	25	<15	<20	51	<20	<20	<10	<20	354	25	<20	35	34	<20	87
14SW80	amphibolite	47.83	1.85	19.37	9.06	0.162	3.08	11.68	3.88	1.31	0.495	0.49	99.10	111	37	35	<20	104	<15	<20	<20	<20	<20	50	<20	114	<20	<20	68	<20	37	66
14SW11	tonalitic layer	70.12	0.18	10.02	3.66	0.070	0.74	2.74	3.34	0.64	0.040	0.35	92.03	117	39	23	<20	<20	<15	<20	<20	<20	<20	15	21	162	<20	<20	55	<20	42	68
14SW13	tonalitic layer	75.55	0.17	13.19	3.90	0.060	0.67	1.79	4.41	0.81	0.040	0.39	98.87	118	20	17	<20	36	<15	<20	<20	<20	<20	12	23	106	<20	<20	122	<20	21	57
14SW12	tonalitic layer	70.85	0.20	13.21	4.91	0.060	1.06	4.93	2.92	0.56	0.040	0.21	98.95	49	38	<20	<20	<20	<15	<20	<20	<20	<20	<10	20	162	<20	<20	27	28	<20	66
14SW14	tonalitic layer	67.27	0.23	13.18	4.51	0.080	1.58	2.89	4.95	0.68	0.070	0.52	96.27	48	20	93	<20	<20	15	<20	25	<20	<20	<10	28	185	<20	<20	101	25	47	57
14SW41	tonalitic layer	72.48	0.42	12.91	5.05	0.110	0.51	3.34	4.15	0.28	0.080	0.33	99.65	80	20	45	<20	135	21	<20	<20	<20	<20	<10	35	172	<20	<20	407	41	87	121
14SW42	tonalitic layer	70.19	0.45	12.76	5.86	0.070	1.74	2.55	3.56	1.56	0.090	0.54	99.36	206	70	39	<20	22	18	38	32	<20	<20	19	<20	575	<20	<20	241	22	74	157
14SW32	calc-silicate rock	70.44	0.27	16.46	1.44	0.010	0.65	3.53	5.15	0.64	0.070	0.71	99.38	41	52	<20	<20	<20	16	<20	43	<20	<20	<10	<20	115	<20	<20	<20	72	25	287
14SW35	calc-silicate rock	73.70	0.09	15.24	0.72	0.070	0.13	1.93	6.01	0.74	0.020	0.63	99.27	13	36	53	<20	33	16	<20	<20	<20	<20	<10	33	291	<20	<20	294	31	96	74
14SW73	calc-silicate rock	72.19	0.22	14.33	2.94	0.132	0.65	3.23	5.41	0.23	0.216	0.31	99.87	268	95	112	<20	36	<15	<20	25	34	<20	78	<20	184	<20	<20	85	21	57	170
14SW26	pegmatite	62.10	0.21	10.94	5.08	0.140	4.08	14.86	0.88	0.34	0.230	0.29	99.55	23	55	20	<20	51	26	<20	28	<20	<20	<10	23	367	<20	<20	173	62	55	217